ENHANCED PRODUCTION OF NEGATIVE IONS IN A PULSED VOLUME ION SOURCE

A thesis for the degree of

PHILOSOPHIAE DOCTOR

Presented to

DUBLIN CITY UNIVERISITY

By

KEVIN NOEL MELLON B.Sc

School of Physical Sciences

DUBLIN CITY UNIVERSITY

Research Supervisor

Dr. Michael B Hopkins

January 1993

ACKNOWLEDGEMENTS

I would like to thank all those who helped throughout the duration of this work. Special thanks must go to my research supervisor Mike Hopkins for his help and guidance over the last three and a bit years. Also thanks to my family, friends and fellow post grads, the lads and Michéle, the numerous other members of staff who helped.

I would also like to acknowledge the financial support given by Euratom to this project.

DECLARATION

I hereby certify that this material, which I now submit for assessment on the programme of study leading to the award of Philosophiae Doctor is entirely my own work and has not been taken from the work of others save and to the extent that such work has been cited and acknowledged within the text of my work.

Signed: Kevin Mellon

Kevin N Mellon

Date: Jan '93

CONTENTS

Table of Figures

ABSTRACT

The need for high brightness neutral beams for neutral beam heating systems has lead to extensive research into low pressure, high power negative ion sources. Negative ion sources at present have low gas and power efficiencies and to realise the current densities for the future H^-/D^- based neutral injectors needed for the next generation of fusion tokamaks will necessitate continued efforts into improving the design of negative ion sources.

In this thesis a new approach to the production of negative ions in volume ion sources is investigated. For effective negative ion production large densities of vibrationally excited molecules, $v \geq 5$, are required. These vibrationally excited molecules are effectively produced in volume ion sources by high energy electron collisions, $\varepsilon > 20eV$, with the background gas. The negative ions are subsequently produced by dissociative attachment of electrons to these vibrationally excited levels. However a major loss mechanism for negative ions is collisional detachment by fast electrons. Tandem sources divide the source into driver and extraction regions by a magnetic filter. When a plasma is switched off the fast electron density decays away in less the 1μs , while the electron density and vibrationally excited states can survive well into the post discharge. Thus by pulsing the discharge current there results two distinct plasma regimes, similar to the driver and extraction regions of a tandem source. Here we use such a temporal filter to separate the driver and extraction regions in time rather than in space. High frequency modulation of the source can result in an increase by a factor of four in the time averaged negative ion density with a simultaneous reduction in the extracted electron current. Temporally and spatially resolved photodetachment and langmuir probe measurements are presented which show the enhancements in the H^- density to be consistent with modulation of a source in which E-V/DA production and CD loss mechanisms are dominant.

TABLE OF IMPORTANT SYMBOLS

AD Associative Detachment

CD Collisional Detachment

DA Dissociative Attachment

EEDF Electron Energy Distribution Function

E-V Vibrational excitation via an electronic singlet state

f_{mod} Modulation frequency

kT_e Electron temperature

MN Mutual Neutralisation

n_e Electron density

n_{ef} Fast electron density

n_h Atomic density

n_+ Ion density

n_- Negative ion density

n" Density of vibrationally excited states

PE Plasma Electrode

PSU Power supply unit

RCIP Ionisation of $H_2(v")$ by primary electrons

σ Cross section

$<\sigma\ v>$ Reaction rate

τ_e Electron density characteristic decay time

τ_{H^-} Negative ion characteristic decay time

ΔI^- Photodetachment signal current

Chapter 1. Introduction to negative ion sources.

1.0. Introduction.

Negative ion research is driven by the need for high power density neutral beams for use in proposed nuclear fusion reactors. These reactors will require the neutralisation of charged particle beams of currents up to several amps and energies of 1MeV. Positive ion beams have proven to be inefficiently neutralised at high energies and thus the sources for future reactors will have to be negative hydrogen or deuterium ion sources. Negative ions have been shown to play an important role not only in electrical discharges but also in the ionosphere and in the fusion reactions in the sun and other stars, Massey 1950 [1]. The presence of negative ions in such reactions has been used to explain the absorbtion spectra of stars. In this chapter a brief over view of nuclear fusion and the need for negative ions as primary particles for neutral beam injection heating is given. An introduction to the sources currently under investigation for the production of negative ions, i.e the volume ion source, the surface conversion source and caesiated sources is presented.

1.1. Nuclear fusion.

Since the middle of this century vast resources have been applied towards the development of a viable nuclear fusion reactor [2]. The reactions ,

$$D + T \rightarrow 4H_e\ (3.52MeV) + n\ (14.06MeV) \qquad \text{Eqn. 1.1}$$

$$D + D \rightarrow T(1.01MeV) + p(3.02MeV) \qquad \text{Eqn. 1.2}$$

have cross sections large enough to make it possible that they may be sustained in a terrestrial reactor. About 1 tonne of deuterium could theoretically produce one gigawatt-year of electricity compared to two million tonnes of carbon for a coal fired generator. This comparison shows the enormous benefits that would be available from an economical fusion powered generating plant. Fusion, unlike it's fission counterpart, produces no long lived radioactive isotopes. The intense neutron fluxes from a fusion reactor would leave the blanket and support structures becoming radioactive, but this

effect would be much less of a problem than the large amounts of radioactive waste currently produced in fission reactors [2].

Two main approaches are being followed, they are inertial confinement fusion and magnetically confined fusion. Inertial confinement fusion is based on the heating of a pellet made of a mixture of deuterium and tritium which has been solidified at low temperatures [2], this pellet is then heated to high temperatures by an intense laser beam which causes the pellet to implode, releasing energy as the fusion occurs over a very short time scale.

The second approach relies on the confinement of an extremely hot and dense plasma in a donut shaped ring by strong magnetic fields, the tokamak [3]. Most of the fusion programme research is based on magnetically confined fusion plasmas. A tokamak is in simplest terms a large scale transformer in which the fusion plasma becomes the secondary winding.

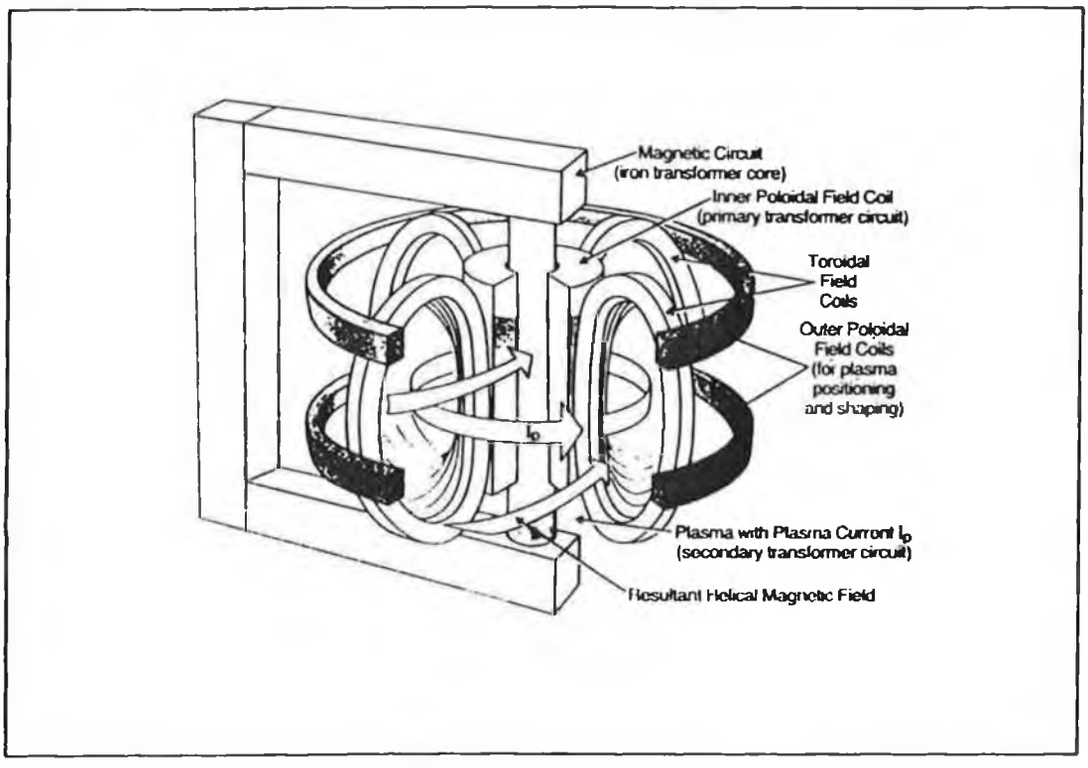

Figure 1.1. Representation of a tokamak reactor.

The plasma is confined in the tokamak by two magnetic fields, a polodial field and toroidal field, and the plasma current is inductively driven by a current in the primary coils. Figure 1.1 shows a representation of a tokamak, it consists of a large

vacuum chamber shaped like a doughnut, the torus, surrounded by a large iron yoke. The vacuum chamber is surrounded by magnetic coils that provide the toroidal confining field. The plasma current is increased by maintaining a change of primary magnetic flux in the primary coil. Once the primary flux change ceases, the plasma current starts to decay and eventually the plasma is extinguished. Thus the tokamak operation is pulsed. The plasma is heated by the Joule dissipation of the current flowing through it [4]. Other heating mechanisms may also be used to raise the temperature inside the plasma, in fact in larger tokamaks the ohmic heating will cease to be dominant and will become additional to other heating systems. The methods developed for additional heating are wave heating and neutral beam injection heating [5]. The most common forms of wave heating are,

(1) Electron Cyclotron Resonance Heating. (ECRH).

In this method an electromagnetic wave with frequency similar to the frequency of the electron cyclotron resonance is coupled into the plasma. Because of the high frequency involved, (100GHz), the electromagnetic waves propagate freely into the centre of the plasma and can raise the plasma temperature and with the development of the gyrotron source [6] ECRH heating at high powers has become practical.

(2) Lower Hybrid Resonance Heating. (LHRH).

An electromagnetic wave, (1GHz), is coupled into the outer regions of the plasma and this can be used to control the profile of the fusion plasma.

(3) Ion Cyclotron Resonance Heating. (ICRH).

Again an E/M wave is coupled in to the plasma, this time with a frequency equal to the ion cyclotron resonance frequency, (50MHz), and this helps to raise the ion temperature of the plasma.

1.2. Neutral beam injection heating.

The basis of neutral beam injection heating is that fast, high energy, neutrals are injected into the magnetically confined plasma. These neutrals, being unaffected

by the magnetic fields, can penetrate into the plasma and deposit their energy in the plasma through collisions with the ionised gas. This energy transfer then helps to raise the temperature of the plasma. Neutral beams with the energy, power and collimation required for injection systems are only achievable from the neutralisation of high energy positive or negative ion beams [7]. Ion beams are generally produced at low energy by attachment to, or ionisation of, a source gas and are then extracted and accelerated in an electrostatic field. These ions are then passed through a neutraliser, usually a gas target or plasma, and the resultant neutral beam is then used to heat the fusion plasma. In general the neutrals used are either hydrogen or deuterium and thus most of the research into ion beams is based on hydrogen/deuterium ion sources.

1.3. Positive ion sources.

One of the most efficient methods of producing intense positive ion beams for neutral beam injection systems is the magnetic multipole ion source, as shown in figure 1.2.

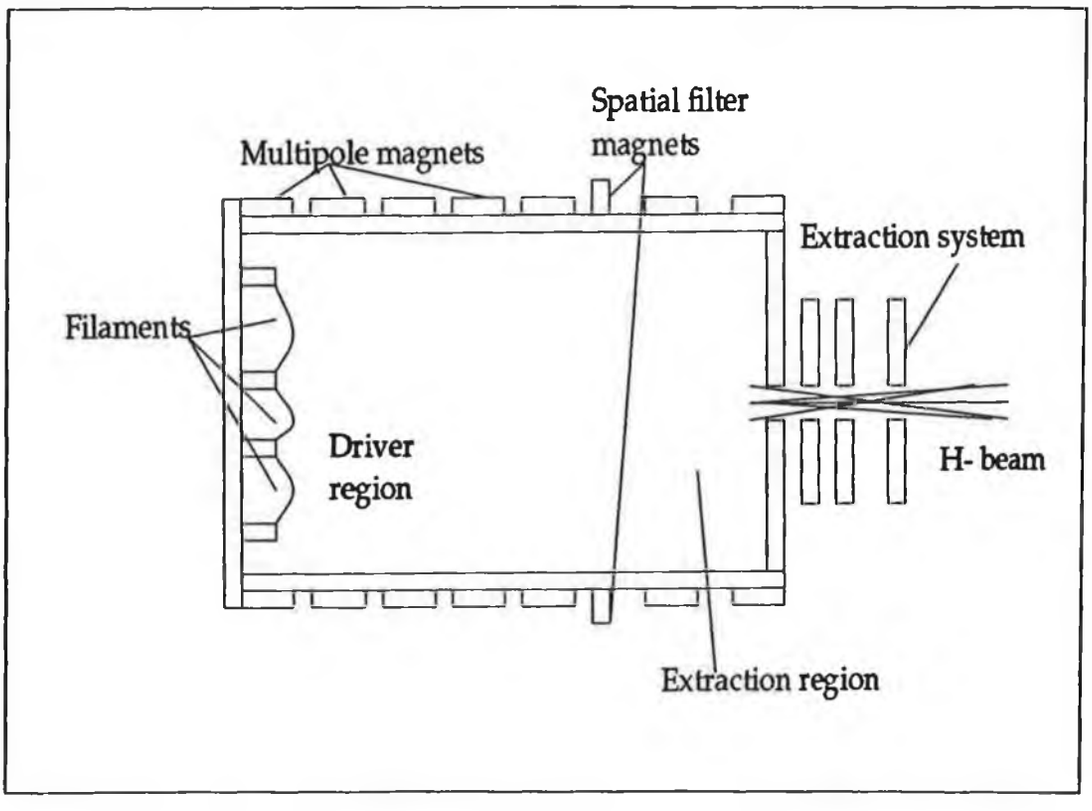

Figure 1.2. Schematic of a multipole positive ion source.

This source uses a magnetic field created by permanent magnets to help confine the high energy electrons in the centre of the discharge. An arc is struck between hot filaments and the anode wall. The fast, or hot, electrons emitted from the filaments are then accelerated towards the wall but are reflected by the confining magnetic field and they become more efficient at ionising a background gas [8]. In general there are three species created in a hydrogen volume source, H_2^+, H_3^+, H^+ [9]. The different species have different deposition profiles within the tokamak and therefore it is preferable that the extracted beam be proton dominated. Ionisation of the background gas H_2 leads to H_2^+ via,

$$e^- + H_2 \rightarrow H_2^+ + 2e^- \qquad \textbf{Eqn. 1.3}$$

and from this several other processes occur leading to H_3^+, H^+ [10],

$$H_2^+ + H_2 \rightarrow H_3^+ + H \qquad \textbf{Eqn. 1.4}$$

$$H_2^+ + H_2 \rightarrow H^+ + H_2 + H \qquad \textbf{Eqn. 1.5}$$

$$e^- + H_2^+ \rightarrow H^+ + H + e^- \qquad \textbf{Eqn. 1.6}$$

$$e^- + H \rightarrow H^+ + 2e^- \qquad \textbf{Eqn. 1.7}$$

$$e^- + H_2 \rightarrow H^+ + H + 2e^- \qquad \textbf{Eqn. 1.8}$$

The last process, the direct ionisation of the H_2 gas to H^+ will be enhanced if the hydrogen molecules are vibrationally or rotationally excited [10]. Ehlers and Leung, [11], have shown that the presence of primary ionising electrons in the vicinity of the ion extraction grid increases the number of H_2^+ ions extracted. To overcome this a permanent magnetic filter is installed across the chamber to limit the density of fast electrons near the aperture. If the magnetic field is kept low enough then ions and slow electrons will be able to drift through, this results in a more quiescent plasma near the extraction grid. Positive ion sources can operate over large pressure ranges, 1-30mTorr, and at high extracted current densities, up to $750mAcm^{-2}$, [12].

1.4. Accelerator requirements and neutralisation efficiency.

Having extracted an intense proton beam it is then necessary to convert this into a neutral beam. This is achieved by passing the ion beam through a target, neutraliser, from which the ions capture an electron. The neutraliser is normally placed immediately downstream of the extraction system. Neutralisation of H_2^+ and H_3^+ is more complex than for H^+ and results in the eventual breakup of the H_2^+ and H_3^+ to give half and one third energy H and H^+. The positive ion based neutral injector used by the Joint European Torus, JET, has eight 60A ion sources operating at 80kV per beamline. Each line is capable of delivering 8MW of neutrals to the plasma [7].

There exists a major problem with the use of positive ion based neutral systems and this can be explained using figure 1.3.

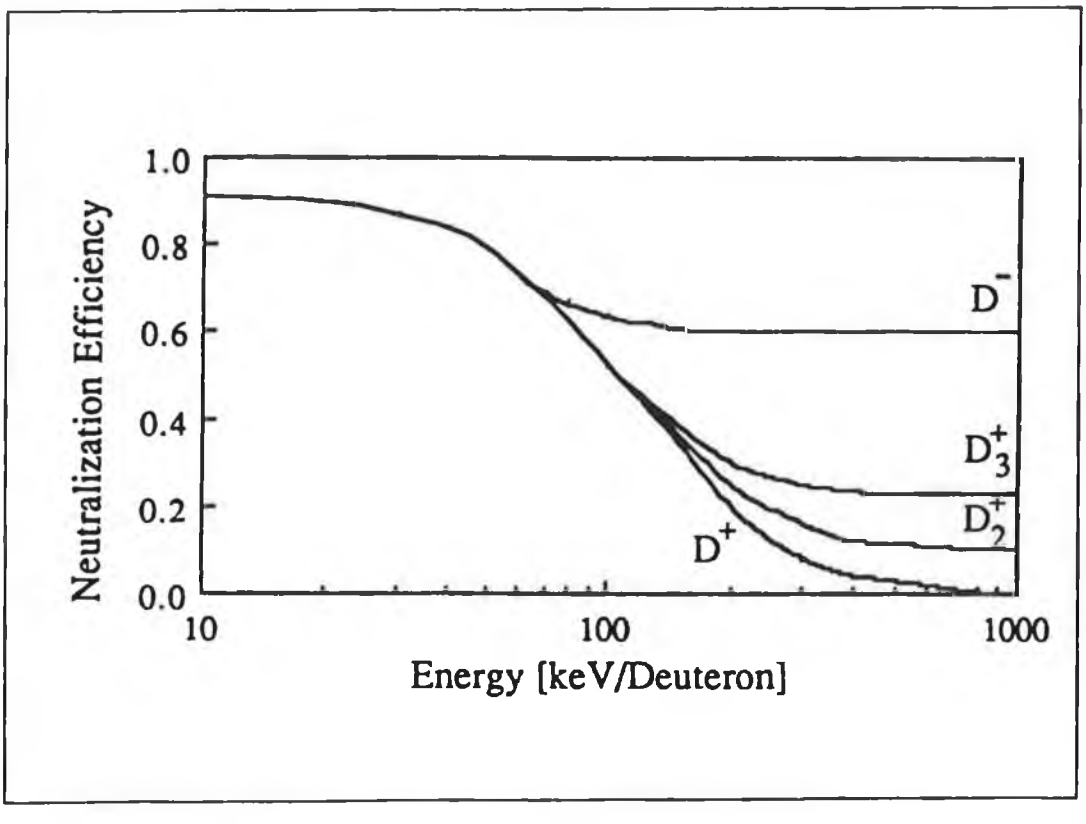

Figure 1.3. Neutralisation efficiency as a function of beam energy for positive and negative ions.

As the energy of the positive ions increases then the cross section for neutralisation decreases. For beam energies above 100keV the efficiency of neutralisation drops away dramatically and for energies of 1MeV, as is proposed for the future

experimental reactors, the positive ion neutralisation efficiency is very small. This means that positive ion based neutral systems will not be of use in the next generation of reactors. However the neutralisation cross section for negative ions is much greater at high energies, with 60% efficiency at 1MeV. Thus the need for high power, low pressure negative ion sources for NBI systems becomes apparent. It is expected that the ITER, International Thermonuclear Experimental Reactor, tokamak will require NBI powers of upto 100MWatts. This will mean negative ion currents of up to 150A if conventional neutralisers are used. This may be achieved by using several individual ion sources of lower power output. Figure 1.4 shows a representation of a possible neutral beam injector system for the ITER experiment.

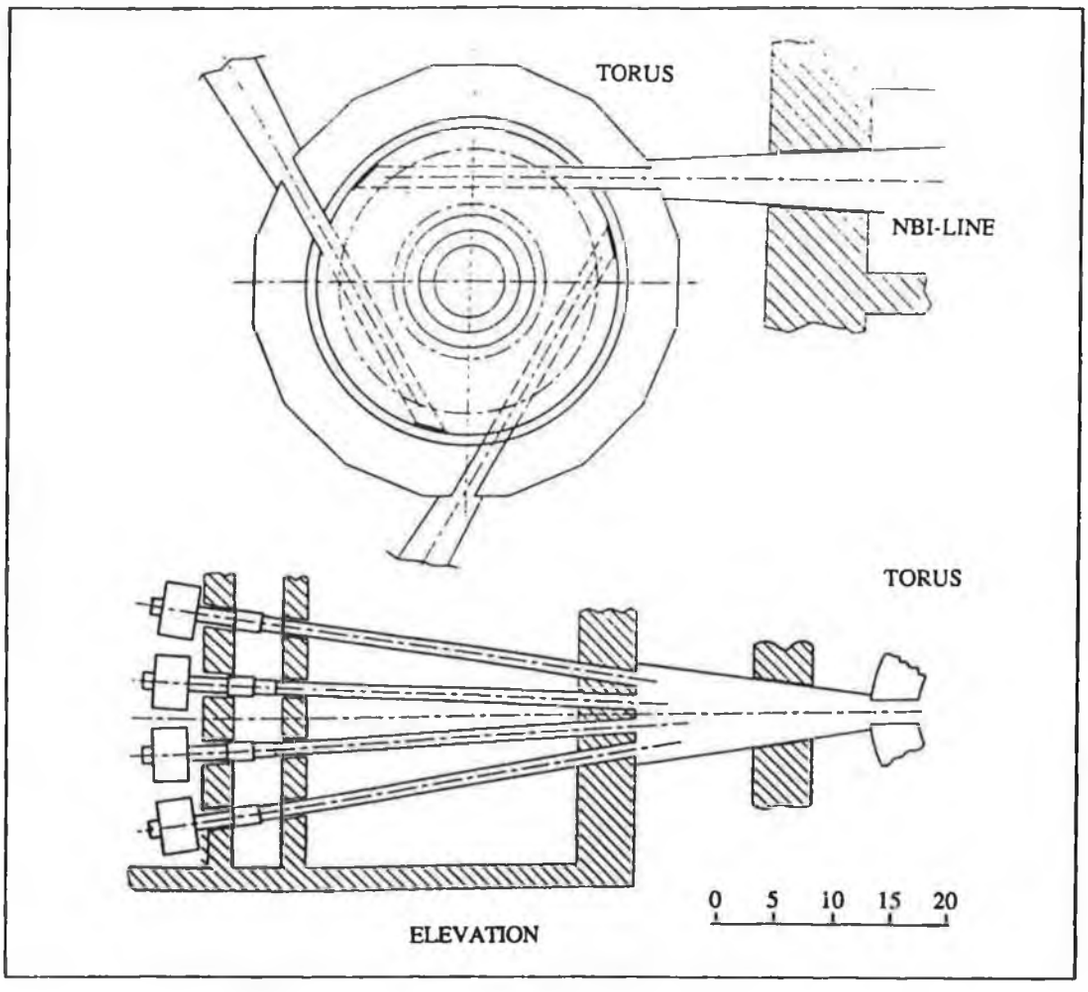

Figure 1.4. Representation of a possible NBI system for the ITER tokamak system.

In this several beam lines are focused into a single neutral beam giving a very high power beam which will enter the plasma almost tangentially, depositing their energy in the centre of the tokamak.

1.5. Volume ion sources.

One of the most successful negative ion sources to date is the pure hydrogen or volume ion source [13-16]. The volume negative ion source is similar to the positive ion source described in section 1.3. It has been known since the late 1950's that negative ions exist in significant numbers in plasma discharges [17]. Bacal et al showed that large quantities of negative ions are present in volume discharges [18]. These quantities were about 100 times larger than could be explained by the then accepted production and loss processes. It is now generally accepted that H^- production is predominantly a two stage process [13,14]. The volume process uses a H_2 molecule as an intermediate in the production of H^- and this has the limitation of requiring a high background source pressure, which this results in the gas loading of the accelerator [19]. Volume sources have low ion temperatures, tenth's of an eV, and this gives reasonable emmittance of the source making the extracted beam suitable for NBI. Extracted negative ion currents of 1.6A at $15mAcm^{-2}$ have been achieved by Japanese researchers [20] and it is hoped to increase this to a 3A neutral beam for future NBI systems.

1.6. Surface conversion sources.

Production of negative ions based on surface conversion has been under investigation for over a decade [21,22]. In surface conversion sources negative ions are produced on the surface of a metal target. In order to populate the empty affinity level of a hydrogen atom a source of electrons with an energy of -0.75eV is required. Conduction bands in metals have large quantities of such electrons, in the form of an electron gas. The bonding strength of these electrons is given by the work function of the metal, typically 2.5-5eV. When an atom is brought close to the surface of a metal the affinity level drops and broadens as the attractive interaction of the energy levels in the metal becomes stronger. At some point of approach the electronic states of the

metal are similiar to the affinity levels of the hydrogen atom and charge transfer can occur, resulting in a negative ion. Similarily a positive ion approaching the surface can be neutralised. The surface ionisation potential is a strong function of the metallic surface work function, increasing as the work function decreases. Thus for practical conversion targets low work function metals are generally used, i.e. Barium which has a work function of 2.31eV [23].

This effect is used in practical sources to generate negative ions by scattering a positive ion beam from a low work function metal target. The incident proton beam is neutralised on the incident beam and the hydrogen atom has a given probability of being ionised in the subsequently reflected beam. Small beam currents have already been shown with a negative ion formation probability of upto 60% [24].

A typical surface conversion source is shown in figure 1.5 [25,26].

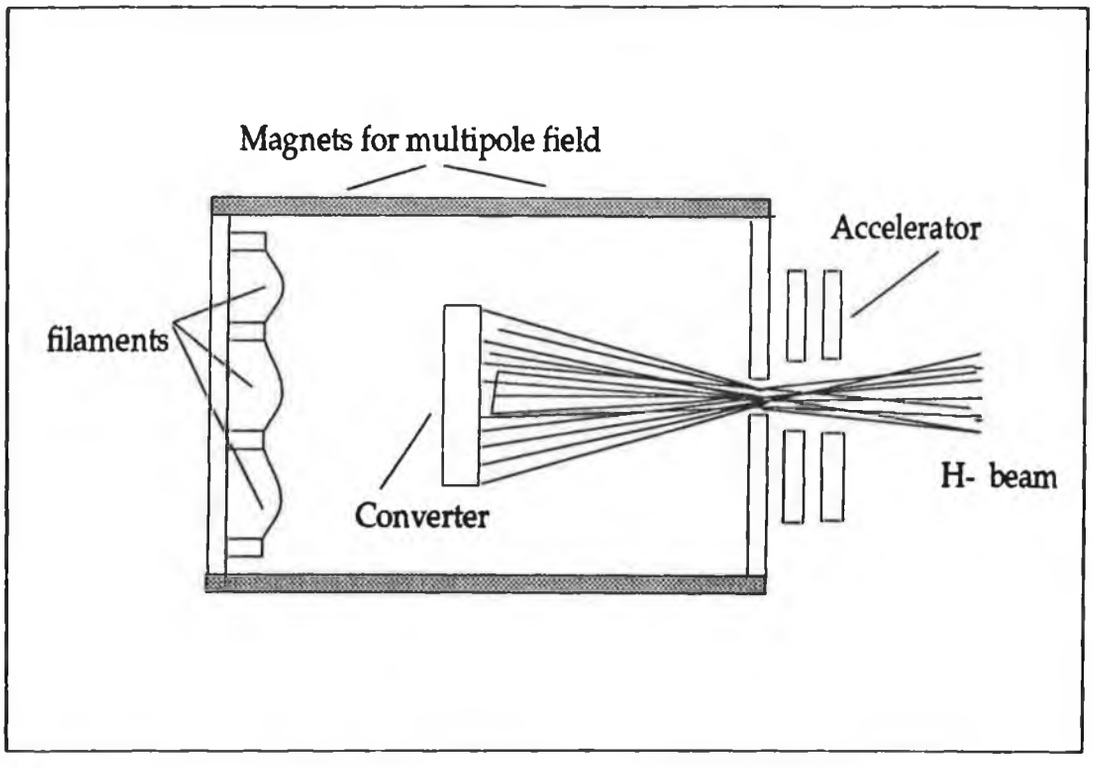

Figure 1.5. Typical surface conversion negative ion source showing the converter in the centre.

It basically consists of a plasma chamber in which the low work function metal target or converter is installed. The plasma is brought into contact with the converter which is biased negatively with respect to the plasma. Positive ions are attracted towards the

converter and are either reflected from or embedded in the surface. The incoming ions may also sputter already adsorbed particles from the surface and the flux of backscattered or sputtered atoms has a probability of being ionised to H^-. Once a negative ion is formed it is repelled away from the converter and drifts towards the extraction aperature. The conversion process is not dependent upon the density of molecules but rather the density of atoms and therefore does not have the disadvantage of needing high background pressures. However the negative ions are formed in either a sputtering or backscattering process and as the temperature is quite high, this can limit the usefulness of the extracted beam for use in NBI systems [19].

1.7. Cesiated sources.

It has been found that the addition of cesium in a negative ion source can have the effect of much improving the negative ion density [27,28]. Originally most of the work on cesiated sources was concentrated on surface production type sources, but it's effect in volume production sources has also been studied [29].

In volume ion sources, cesium is injected in to the chamber in the form of a fine powder, usually fed through a fine valve which allows control of the quantity of cesium introduced. There are numerous ways in which the introduction of cesium can enhance the H^- density [30]. Cesium has a large ionisation cross section at low electron energies compared to H_2, thus the cesium is effectively ionised in the discharge resulting in an increased plasma density. Also the cesium ions can drift more easily, than H_2, through the magnetic fields in the source to the extraction regions and this results in the electron density in this region increasing and therefore the production of H^- through dissociative attachment can be increased. In addition the cesium atoms may further cool the electrons in the extraction region through collisions and there is the possibility of cesium reacting with H_3^+ through the process,

$$Cs + H_3^+ \rightarrow Cs + H_2(v'') + H \qquad \text{Eqn. 1.9}$$

and this can enhance the density of vibrational levels available for H^- production [30].

In surface conversion sources cesium is adsorbed as a partial layer onto the target surface. This partial layer has the effect of lowering the work function of the converter which enhances the probability of the transfer of charge from the metallic

surface to the hydrogen atoms near the surface. This layer on the converter surface is achieved by injecting the cesium into the source, and it then settles on the target, or by use of a porous target in which the cesium seeps through to the surface. It has been claimed that the injection of cesium can give enhancements in the negative ion density of over a factor of four and also dramatically reduce the operating pressure of the source [31]. However cesiated sources have a disadvantage in that the cesium can gain access to the accelerator and may disrupt the extraction and acceleration of the ion beam.

1.8. Conclusion.

The use of additional heating mechanisms in fusion plasmas has lead to the development of high power neutral beam systems. These NBI systems presently use positive ion based sources but future tokamaks will necessiate the use of negative ion sources. This chapter discussed the need for low pressure negative ion sources and gave a brief insight into the more successful approaches being used to generate negative ions. This thesis is concerned with the development of a new approach to the production of H^- in volume type sources and the following chapters deal with the production and loss mechanism in volume ion sources and how the negative ion density may be improved by a technique called temporal filtering [32]. Also the possibility of using radio frequency discharges to produce large quantities of negative hydrogen ions at low pressures is discussed.

References:

[1] Massey, H. S. W.
"Negative Ions", Cambridge University Press 1950.

[2] Hunt, S.E.
"Fission, Fusion and the energy crisis"
2nd edition, Pergamon Press, Oxford, 1980.

[3] Bickerton, R.J.
Physics Bulletin, 39, 1988.

[4] Green, B.J.
"Plasma Physics and Nuclear Fusion research"
Academic Press, London, 1981.

[5] Fielding, P.J.
"Plasma Physics and Nuclear Fusion research"
Academic Press, London, 1981.

[6] Manheimer, W.M. and Granalstein, V.L.
N.R.L. memorandum, Report 3493, Washington DC, 1977.

[7] Hemsworth, R.S.
"Plasma Physics and Nuclear Fusion research"
Academic Press, London, 1981.

[8] Buzzi, J.M, Snow, J. and Hirshfield, J.L.
Physics Letters, vol 54, no.4, p344, 1975.

[9] Chan, C.F, Burrell, C.F. and Cooper, W.S.
Journal of Applied Physics, 54 (11), p6119, 1983.

[10] Holmes, A.J.T, Green, T.S. and Newman, A.F.
Rev. of Sci. Instrum, 58 (8), p1369, 1987.

[11] Ehlers, K.W. and Leung, K.N.
Rev. of Sci. Instrum, 52 (10), p1452, 1981.

[12] Striling, W.L, et al.
Rev. of Sci. Instrum. 48, p533, 1977.

[13] Bacal, M, Bruneteau, A.M and Nachman, M.
Journal of Applied Physics, 55 (1), p15, 1984.

[14] Hiskes, J.R.
"4th Int. Symp. on Production and Neutralisation of Negative Ions and Beams",
Brookhaven, NY, 1986.

[15] Leung, K.N, Ehlers, K.W. and Bacal, M.
Rev. of Sci. Instrum., 54 (1), p56, 1983.

[16] Bacal, M.
Nucl. Instrum. and Methods in Physics Research, B37/38, p28-32, 1989.

[17] Moak, C.D, et al.
Rev. of Sci. Instrum, 30, p694, 1959.

[18] Nicolopoulou, E, Bacal, M. and Doucet, H.J.
Journal of Physics, (Paris), 38, p1399, 1977.

[19] Van Os, R.
"Negative Ion Sourcery", PhD thesis 1989.

[20] Inoue, T, et al.

Proc. of the 7th Int. Conf. on Ion Implantation Technology, June 7-10, Kyoto, Japan, 1988.

[21] Van Os, R, Heeren, R.M.A. andVan Amersfoort, P.W.
Applied Physics Letters, 51 (19), p1495, 1987.

[22] Hiskes, J.R, Karo, A. and Gardner, M.
Journal of Applied Physics, 47 (9), p3888, 1976.

[23] Kaye, G.W.C. and Laby, T.H.
"Tables of Physical and Chemical Constants",
14th edition, Longman, Lndon and New York, 1973.

[24] Belchenko, Y.I, Kupriyanov, A.S.
Rev. Phys. Appl, 23, p1885, 1988.

[25] Leung, K.N. and Ehlers, K.W.
Rev. of Sci. Instrum, 53, p803, 1982.

[26] Hercovitch, A.I. and Prelec, K.
Rev. of Sci. Instrum, 52, p1459, 1981.

[27] Belchenko, Y.I. and Dudnikov, V.G.
"4th European workshop on the Production and Application of light negative ions", Mar 26-28, 1991.

[28] Hagena, O.F. and Henkes, P.R.
"4th Int. Symp. on Production and Neutralisation of Negative Ions and Beams", Brookhaven, NY, 1986.

[29] Walther, S.R, Leung, K.N. and Kunkel, W.B.
Journal of Applied Physics, 64 (7), p3424, 1988.

[30] Peterson, J.R.

"4th Int. Symp. on Production and Neutralisation of Negative Ions and Beams", Brookhaven, NY, 1986.

[31] Okumura, Y, et al.

"4th European workshop on the Production and Application of light negative ions", Mar 26-28, 1991.

[32] Hopkins, M.B. and Mellon, K.N.

Physics Review Letters, Physical Review Letters, 67, p449, 1991.

Chapter 2. Volume Negative Ion Sources and Production of Negative Ions.

2.0. Introduction

The requirement of high energy neutral beams, up to 1MeV [1], has lead to vast resources being applied over the last decades, to the development of an efficient, high power, low pressure negative ion source for use in neutral beam heating applications. Several different sources have been investigated [2], chapter 1. The most successful source to date is the volume ion source which was originally used as source of high densities of positive ions but it has been found that large quantities of negative ions are also present. In this chapter an overview of volume ion sources is presented. Volume ion production results in relatively high numbers of negative ions in the source and due to the two stage process [3] which dominates H^- production it has been found that the H^- density can be further improved by magnetically filtering the source into two regions, the tandem source [4]. It is proposed here that the volume source can be filtered in time as well as in space, this time filter is based on pulsing the discharge current on/off resulting in two discharge regions temporally seperated. A theoretical basis for the temporal filter is presented and a model based on the time dependent densities in the source is developed to predict the behaviour of the negative ion density in a modulated volume ion source.

2.1. Volume Ion Sources

Bacal et al, [5], showed that large densities of negative hydrogen ions exist in a hydrogen discharge or volume source and the possibility of extracting high densities of H^- ions from a volume ion source for neutral beam heating has been shown by Holmes et al [6], Leung et al [7], and Hiskes and Karo [8].

The volume ion source is a hot cathode discharge in which the hot filaments, usually tungsten or tantalum, constitute the cathode and the chamber walls constitute the anode. The wire filaments are heated and biased typically between 50V and 100V negative with respect to the anode. The thermionic electrons emitted from the filaments are accelerated towards the walls. The anode is surrounded by a series of

permanent magnets, leading to the name magnetic multicusp source. The magnets result in a magnetic field extending into the chamber near the anode surface. It was originally believed that the surrounding magnetic field resulted in a greater plasma density due to better ion confinement. Now it is generally accepted that the field has the effect of confining the primary electrons, emitted from the filaments, in the discharge, this effectively increases the characteristic length of the source. Buzzi et al [9] demonstrated that the plasma density increase is essentially due to the reflection of primary electrons by the magnetic wall. They also showed that without magnets on the chamber wall the average travel length of the primaries is approximately the same as the filament to wall distance, whereas with magnets on the walls the average travel length is much larger. As these high energy electrons are accelerated towards the anode they ionise the background gas. For efficient operation the mean free path of the primary electrons must be comparable to the characteristic length of the source or else the primaries may be lost to the walls. By magnetic confinement the increase in the effective source length leads to a vast improvement in efficiency of the source [10].

Several processes can result in the formation of H^- in volume ion sources, i.e, dissociative attachment of low energy electrons to metastable molecules [11],

$$H_2 + e^- \rightarrow H_2^-(^2\pi_u) \rightarrow H^- + H(2p) \qquad \text{Eqn. 2.1}$$

And polar dissociation of molecules by fast electrons,

$$H_2 + e_p \rightarrow H^- + H^+ + e^- \qquad \text{Eqn. 2.2}$$

However these two processes cannot account on their own for the high densities of negative ions found in hydrogen discharges. The dominant H^- production process is believed to be the dissociative attachment, DA, of low energy electrons to high vibrationally excited hydrogen molecules, $H_2(v'')$,

$$e^- + H_2(v''>3) \rightarrow H_2^- \rightarrow H^- + H^+ \qquad \text{Eqn. 2.3}$$

This process is a two stage process involving the initial excitation of hydrogen molecules to vibrationally excited levels and the subsequent attachment of slow electrons to form H^-.

The initial vibrational excitation may occur by several process, an example being the e-V process [12,13],

$$e^- + H_2(v'') \rightarrow H^2(v''<3) + e^- \qquad \text{Eqn. 2.4}$$

this involves the vibrational excitation of the molecule by thermal electrons in the discharge. However this process predominantly populates the lower vibrational levels, ($v''<3$), [14].

The process believed to be predominantly responsible for the population of the higher vibrational levels is the E-V process, where energetic electrons excite ground state molecules to electronically excited singlet states, as in 2.5,

$$H_2(v''=0) + e_p^- \rightarrow e^- + H_2^*(B\,^1\Sigma_u+) \qquad \text{Eqn. 2.5}$$

These electronically excited states then radiate back to a vibrationally excited state as in 2.6, [11],

$$H_2^*(B\,^1\Sigma_u^+) \rightarrow H_2(v'') + h\upsilon \qquad \text{Eqn. 2.6}$$

Other process which can lead to vibrationally excited states are recombination of atoms on the walls, equation 2.7, and Auger de-excitation of molecular ions on the walls, equation 2.8, [15].

$$H^+ + H^- \rightarrow H_2(v'') \qquad \text{Eqn. 2.7}$$

$$H_2(^3\Pi_u) \rightarrow H_2(v'') \qquad \text{Eqn. 2.8}$$

In high density regimes the excitation via the singlet state can dominate, [15], also it has been shown that the cross-section for dissociative attachment of electrons to vibrational levels to form H^- is substantially higher for the $v>3$ than for the lower levels, [16]. Thus the predominance of excitation by the E-V process is required for efficient production of negative ions via DA.

However this two stage process is limited by one major disadvantage. In the case of positive ion production, the H^+ production occurs, equation 2.9, as a direct result of energetic electrons and the positive ion density increases as a function of plasma temperature.

$$H_2 + e_f \rightarrow H_2^+ + 2e \qquad \text{Eqn. 2.9}$$

In the case of negative ion production fast electrons are required for E-V excitation of the higher vibrational levels and thus a hot plasma, kT >2eV, is required to produce sufficient densities of $H_2(v'')$. However a major loss mechanism for H^- is collisional detachment by fast electrons, [4],

$$e_f + H^- \rightarrow H + 2e \qquad \text{Eqn. 2.10}$$

Thus the presence of energetic electrons is beneficial for vibrational excitation but this is countered by the large collisional losses of the subsequently produced negative ions.

Also the requirement of a hot plasma, kT_e>2eV, for the first, E-V, stage is detrimental to the second stage, DA, as this process is more effective in cooler plasmas and reaches a maximum for electron temperatures of around 1eV, [17]. This phenomenon has serious limitations on the use of volume ion sources as a viable negative ion production mechanism. Volume negative ion sources have much lower gas and power efficiencies than their positive ion counterparts.

2.2. Magnetic filtering.

The above limitations have been overcome successfully by two methods, the tandem source, [18,19], and the hybrid source, [20]. Both of these sources enhance the volume production mechanism by having separate plasma regions. One region will contain a hot dense plasma, typically kT_e>2eV, in which the excitation of molecular vibrational levels occurs via the E-V process, and there will also be a region with a much cooler plasma, typically kT_e<1eV, in which the dissociative attachment process results in negative ion production. These regions will be seperated by a magnetic filter field. This field prevents the energetic electrons from passing into the extraction region but the vibrationally excited levels and the cooler bulk electrons and ions drift through the field, [21].

It had already been reported, [22], that the use of a transverse magnetic field enhanced the proton yield from a positive ion source by only allowing the passage of low energy electrons into an extraction region, this resulted in a more quiescent

plasma near the extraction electrode. Leung et al, [7], have also shown that the magnetic field in the chamber not only increases the extracted negative ion current but decreases the extracted electron current.

2.3. The Tandem Source.

In the tandem source a magnetic field extends across the chamber dividing the source into two separate regions, figure 2.1.(a).

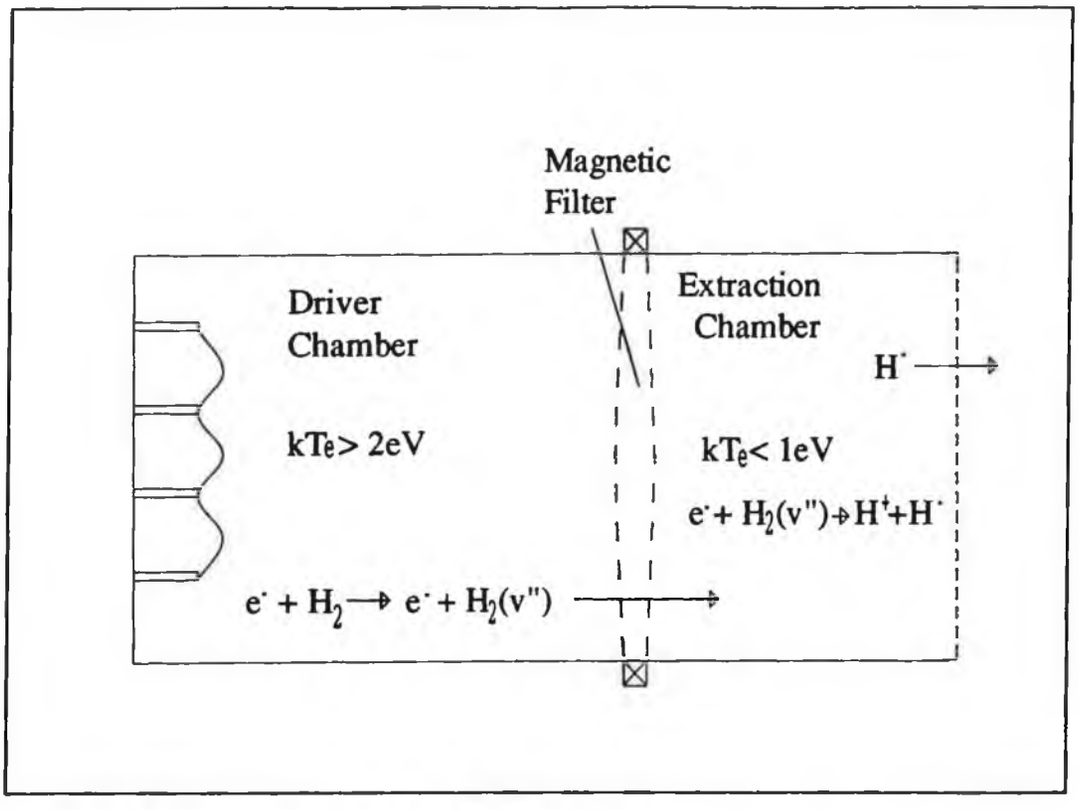

Figure 2.1.(a). Schematic of a Tandem source.

This filter field can be produced in several ways, Leung et al, [7], used a rod filter whereby the magnets are placed in rods through the chamber, Mullan and Graham, [18], used a filter field created by breaking the multipole geometry on two opposite sides of the chamber, while there may exist subtle differences in the type of field used invariably the effect is similar. The region near the front of the chamber containing the filaments is the driver region. In this region the plasma is hot, kT_e>2eV, the EEDF is non-maxwellian exhibiting a fast electron tail, Hopkins et al, [23]. Here there are high numbers of fast electrons, with fast electron densities of over 3% to 4% of

thermal electron densities being reported by Hopkins et al, [23], for a 10A, 2mTorr discharge. It is in this region that the excitation of vibrational states occurs through the E-V process. These vibrationally excited molecules then drift through the filter field into the extraction region. Production of negative ions can still occur in the driver region and these H^- can drift through the field into the extraction region. However due to the high electron temperature in the driver region the DA production rate is low and the destruction rate by CD is high and the H^- density in the driver region remains low.

In the extraction region the plasma is cooler, kT<1eV, as the fast electrons are prevented from drifting through the magnetic field. Again Hopkins et al, have shown the EEDF in the extraction region to be maxwellian with no fast electron tail. Here the negative ions are produced by dissociative attachment of low energy electrons to the vibrationally excited states. As the plasma is now cooler the DA process is enhanced and can be optimised for electron temperatures less than 1eV, the reaction rate co-efficient for DA reaches a peak of $2.8*10^{-8}$ cm^3/s at these values of kT_e whereas in the driver region the reaction rate can be as low as $1*10^{-8}$ cm^3/s for a 2eV discharge. This results in an enhancement of the production of H^-. More importantly the collisional detachment rate in this region can be an order or more lower than in the hot driver region. As it has been shown that CD can be a dominant loss process in this regime, [4], the reduction can have a dramatic effect in the H^- density in the source. Reports from Leung, Ehlers and Bacal, [24], claim an increase in the extracted negative ion current from a volume source from 2μA, without a transverse filter, to 23μA for a source with a strong filter field and a bias on the beam forming electrode of 3V.

2.4. The Hybrid Source.

The second successful attempt to optimise the negative ion density in a volume source is the hybrid source of Bacal [20], figure 2.1.(b). In such a source there is no separate filter field, but instead the filaments are placed near the walls of the source and the multicusp field, produced by mounting a series of permanent magnets with their north and south poles alternatively facing the plasma, separates the driver regions, around the filaments, from the main extraction region. It has been shown, [25], that the placing of the filaments in the multipole fields has the effect of creating

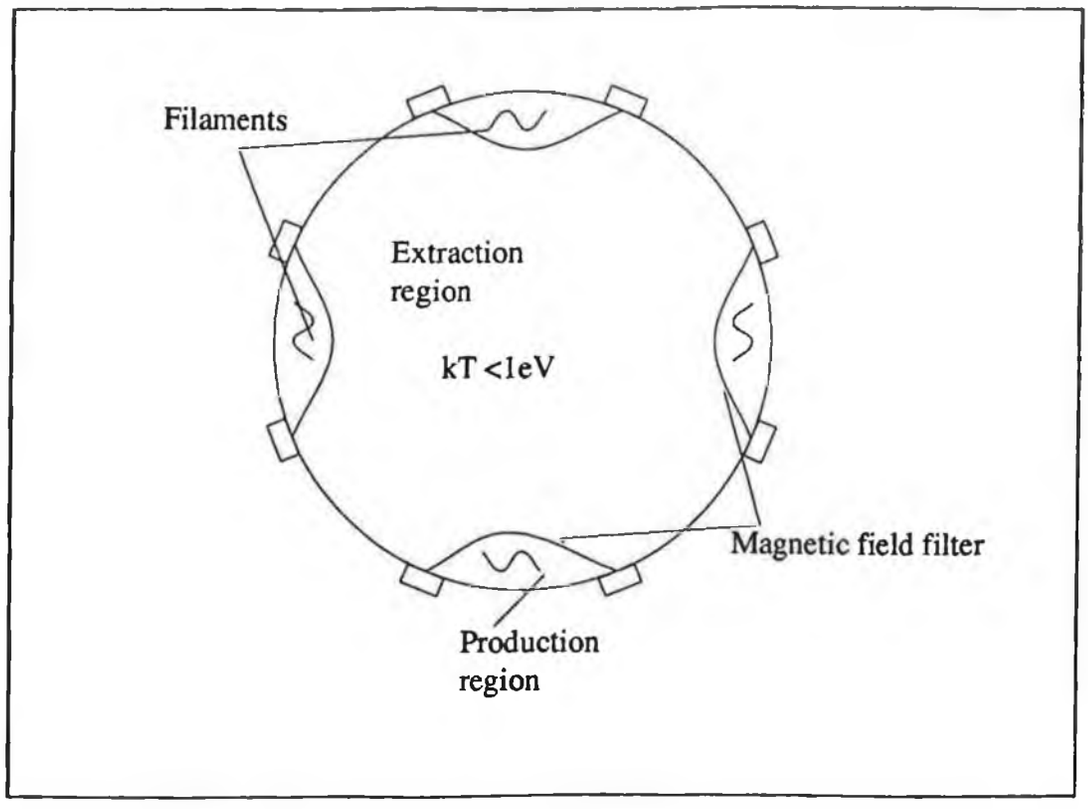

Figure 2.1.(b). Schematic of a Hybrid source.

similar driver and extraction regions as in the tandem source. The cusp fields at the wall act as strong filter fields preventing the fast electrons from entering the central region, from which the H^- ions are extracted. Again the magnetic multipole fields are used to enhance electron and ion confinement and therefore the plasma densities. Hopkins et al, [25], have further shown that the EEDF in the regions close to the filaments, which are heated, have high energy components but this hot tail disappears moving away from the filaments towards the centre of the chamber. Hence the energetic electrons are highly localised in the regions close to the filaments, with fast electron densities of 7% of the total electron density. These high densities of fast electrons were shown to alter locally, by several orders of magnitude, the rate coefficients of processes such as CD and EV. In the central region the fast electron density will have decayed away and the loss rates for CD will have dramatically reduced, and now the main destruction mechanisms will be mutual recombination, MN, of the H^- with positive ions and associative detachment of the H^- with electrons, AD. In the central region Bacal, [20], has reported high densities and a high

proportion, (≈10%), of negative ions.

In the previous two volume sources the two stage volume production process, E-V excitation followed by DA, has been optimised by the spatial segregation of the two individual processes into regions where conditions are appropriate for the specific reaction required. This relies effectively on the spatial control of the plasma parameters in the chamber. More importantly the segregation of the source by the magnetic fields produces a spatial control of the EEDF and the electron temperature, kT_e, in the source. While the EEDF and electron temperature may be controlled by varying other plasma parameters like gas density and discharge current, the magnetic field allows two distinct and different plasma regimes to co-exist in the source under the same external operating conditions, i.e a hot dense plasma whose EEDF exhibits a high energy tail is sustained alongside a cooler more maxwellian discharge. Moreover while the magnetic field produces two different plasma regimes with respect to the EEDF and the electron temperature in the chamber, the chamber is not segregated when considering other plasma parameters. The vibrationally excited molecules and the thermal electrons and ions can drift through the field from the hot regime to the cooler region and are not distinct to a particular one.

This effectiveness of separating the plasma conditions into regions optimised for a specific process while still allowing the free interchange of the appropriate species is the cornerstone of the tandem and hybrid source success. This ability to control the EEDF in two distinct regimes can also be achieved temporally, however in this instance the two regimes are seperated in time rather than in space.

2.5. The Temporal Filter Concept.

When a discharge is switched off the fast electron density has been shown to decay away in less than 1μs, [26], this is due to the short confinement time of fast electrons [27], however the relatively long lifetime of the vibrationally excited molecules, they are mainly destroyed after several wall collisions [28], means that their density remains high well into the post discharge. Also it has been shown that the lifetime of the thermal electrons, τ_e=30μs, extends into the post-discharge [27]. This ensures that H^- production can continue in the post-discharge. Similar to the tandem source the discharge can be divided into two distinct regimes with the driver

region being the cycle period when the discharge is on and the extraction region being the period when the discharge is off.

Hopkins et al, [26], have shown for a low pressure discharge, .07pa and 1A, in a source with the filter field placed very close to the plasma electrode for the purposes of maintaining a high level of primary electron confinement, that during the on period the conditions are similar to the tandem driver region. There are two groups of electrons, a low energy bulk thermal group (≈90%) and a high energy group with energy greater than 20eV (≈10%). During this period the E-V vibrational excitation occurs, the fast electron density leads to considerable collisional detachment losses, here the CD rate coefficient is given as $1.8*10^{-7}$ cm^3/s. Also due to the high electron temperature, kT≈1.44eV, the dissociative cross-section is low with the DA rate co-efficient being given as $1.3*10^{-8}$ cm^3/s. As can be seen the conditions are similar to those described in section 2.3 for the tandem driver region. In the temporal filter the on period can be termed the driver period of the cycle.

After switching off the discharge, we enter the extraction period of the cycle. During this period Hopkins et al, [26], have shown the EEDF to have cooled significantly, kT≈0.44eV, after 50μs into the post-discharge. The fast electron group has disappeared and the EEDF has become virtually maxwellian. In this temporal area the electron density has not decay significantly and assuming that the vibrational states have a long characteristic loss time, Lefebure et al, [30], has given this typically to be the order of 1ms, and the $H_2(v")$ population is similar to that of the steady state then we would expect the production of H^- to continue into the post-discharge. Also as the fast electrons have disappeared the collisional detachment losses will no longer be the dominant loss mechanism. Couple this with an increase in the cross-section for dissociative attachment as the EEDF cools after switch-off, the rate co-efficient for DA reaches a peak of $2.9*10^{-8}$ cm^3/s in the post-discharge, then we will expect to see an increase in the negative ion density in the post-discharge. Thus the temporal filter acts in a similar way to the tandem source except the filter is produced by switching on and off the discharge rather than by a magnetic field.

However the temporal filter also differs in several ways from the magnetic filter source, it can be operated more efficiently at lower pressures than the tandem source. In fact it is expected that the temporal filter will be most efficient at lower

pressures, <1mTorr, as in this region the electron temperature and fast electron density will be very high and subsequently the cooler post discharge period will result in larger enhancements in the negative ion yield. Also the temporal filter gives more control over the EEDF and it may also be possible to pump the higher vibrational levels by correct variation of the modulation duty cycle.

2.6. Control of the EEDF.

The EEDF control concept can be explained by considering the evolution of the electron temperature as in figure 2.2 [29].

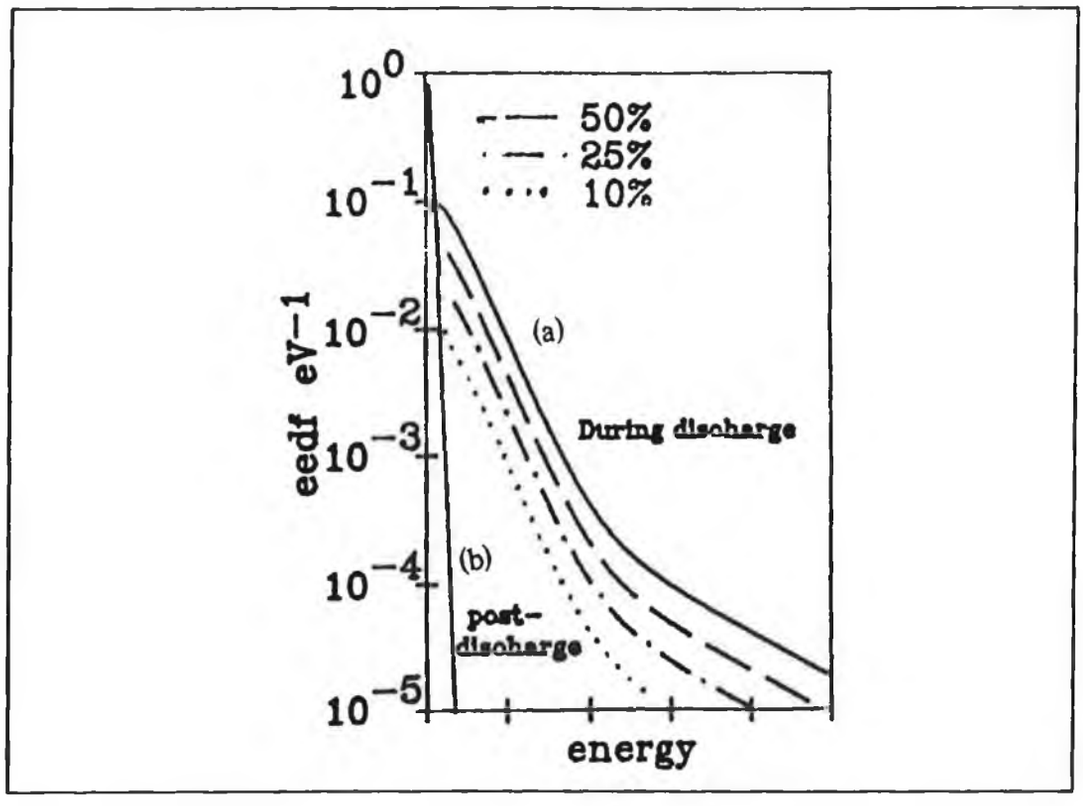

Figure 2.2. Control of the time averaged EEDF by variation of the duty cycle.

The control of the EEDF is achieved by having an "on" period of a hot plasma followed by a post discharge, "off", period of a cooler discharge, which results in a time averaged EEDF that can be changed at will simply by variation of the modulation and duty cycle of the pulse. This is parallel to controlling the EEDF in the tandem source by varying the ratio of the driver region to the extraction region, however in this case the external magnetic field must be moved which is not a simple

task. As the fast electron confinement times are less than 1μs it is possible to modulate the collisional detachment losses at high frequencies. In figure 2.2 we see the EEDF for a typical continuous discharge, driver discharge, (a), it exhibits a fast electron tail and a high electron temperature. Also shown is the EEDF 50μs into the post-discharge, extraction discharge, (b). This is a maxwellian discharge, the fast tail having decayed away, with much lower kT_e.

The time averaged EEDF is shown for various possible duty cycles, 50%, 25% and 10% at an appropriate modulation frequency. These show how the time averaged EEDF can be varied at will between the driver and production discharge conditions. As the duty cycle is decreased from driver conditions, 100% on, to lower percentage on times the high energy part of the time averaged EEDF will decay away almost linearly, while the low energy portion will increase as the bulk electrons become even more predominant. Thus by variation of the modulation frequency and duty cycle the appropriate time averaged EEDF can be chosen for the parameter regime required.

2.7. Pumping of Densities.

By appropriate modulation of the discharge current it may be possible to pump the densities of vibrational levels above that for a continuous discharge of similar power. For the production of high level vibrational states, assuming that the E-V process is the predominant mechanism for vibrational excitation, high energy electrons are necessary, eqn. 2.11,

$$H_2(v''=0) + e_f \rightarrow H_2^*(^{B'}\Sigma_u^+, {}^1C_+) \; e^- \rightarrow H_2(v'') + h\upsilon \qquad \text{Eqn 2.11}$$

however one of the $H_2(v'')$ loss mechanisms is ionisation by primary electrons, equation 2.12.

$$e_f + H_2(v'') \rightarrow H_2^+ \qquad \text{Eqn. 2.12}$$

By modulating the discharge the time averaged destruction rates are reduced, while production rates remain proportional to the discharge current.

Consider the density of $H_2(v'')$ in a continuous discharge as N_c, the discharge current is Id. The $H_2(v'')$ loss time is τ_{on} during the discharge and τ_{off} during the post-discharge. The discharge length is t_{on} and the post-discharge length is t_{off}, [29]. The

$H_2(v'')$ density during the discharge is given by,

$$n(t) = N_c\left(1-\exp(-\frac{t}{\tau_{on}})\right) \qquad \text{Eqn. 2.13}$$

n(t) approaches steady state as $t>>\tau_{on}$. In the post-discharge the density is given by,

$$n(t) = n_d \exp(-\frac{t}{\tau_{off}}) \qquad \text{Eqn. 2.14}$$

The time averaged density is determined by ,

$$<n> = \frac{1}{T}\int n(t)\,dt \qquad \text{Eqn. 2.15}$$

this is then,

$$<n> = \frac{N_c}{T}\left[t_d + \frac{(\tau_{off}-\tau_{on})\ (1-\exp(-\frac{t_{on}}{\tau_{on}}))\ (1-\exp(-\frac{t_{off}}{\tau_{off}}))}{(1-\exp(-\frac{t_{on}}{\tau_{on}}))\ \exp(-\frac{t_{off}}{\tau_{off}})}\right] \qquad \text{Eqn. 2.16}$$

For frequencies where $\tau_{on} > t_{on}$ and $\tau_{off} < t_{off}$ then,

$$<n> = N_c\left[1 + \frac{t_{off}\tau_{on}}{t_{on}\tau_{off}}\right] \qquad \text{Eqn. 2.17}$$

If the frequency is such that $t_{off}\tau_{on}/t_{on}\tau_{off}$ goes to zero then the average density approaches that of the continuous N_c, however the discharge current is given by,

$$<Id> = Id_c * \left[\frac{t_{on}}{t_{on}+t_{off}}\right] \qquad \text{Eqn. 2.18}$$

thus for the pulsed discharge the density approaches the continuous value but the discharge current is a fraction of the continuous current.

The negative ion density may also be pumped to levels above the continuous discharge of similar power, however the continued production in the post-discharge make this a more complex analysis.

2.8. Time dependent densities

2.8.1. Negative ion density.

Assuming dissociative attachment as the dominant H^- production mechanism then the negative ion density in a steady state discharge is given by;

$$n^- = n'' n_e \langle \sigma_{DA} v_e \rangle \tau_- \qquad \text{Eqn. 2.19}$$

where n_- is the negative ion density, n_e is the plasma electron density, n" is the density of vibrationally excited molecules, and τ_- is the characteristic loss time for negative ions. $\langle \sigma_{DA} v_e \rangle$ is the reaction rate coefficient for dissociative attachment of electrons to $H_2(v'')$.

The average negative ion loss time, τ_-, is given by;

$$\tau_{-on} = \frac{1}{\left(\frac{V_-}{L_-}\right) + n_p \langle \sigma_{CD} v_p \rangle + n_h \langle \sigma_{AD} v_h \rangle + n_i \langle \sigma_{MN} v_i \rangle} \qquad \text{Eqn. 2.20}$$

Where the denominator of eqn. 2.20 represents the loss terms due to wall collisions, collisions with primary electrons, collisions with atoms, collisions with ions respectively.

Eqn. 2.19 represents the negative ion density during the discharge, in the post discharge the negative ion density is given by the same eqn, however now the vibrational density, n", will be decaying and therefore the negative ion production rate will also fall. However since the fast electron density decays to zero in the order of 1μs, we set

$$n_{p_{off}} = 0 \qquad \text{Eqn. 2.21}$$

and the average loss time in the post discharge can be simplified to

$$\tau_{-off} = \frac{1}{(\frac{V_-}{L_-}) + n_h \langle \sigma_{AD} v_h \rangle + n_i \langle \sigma_{MN} v_i \rangle} \qquad \text{Eqn. 2.22}$$

To achieve an increase in the negative ion density in the post discharge, it is therefore necessary to create a situation where loss in production of H^-, due to the decay of n", is countered by an increase in the reaction rates for dissociative attachment due to lower electron energies in the post discharge and a reduction in the destruction rates due to the decay of the fast electron and ion densities.

2.8.2. Vibrationally excited density.

As stated in equation 2.19, the negative ion density is dependent upon the density of vibrationally excited molecules, assuming that the predominant H^- production process for volume negative ions is by DA. Thus we also need to determine the temporal behaviour of the vibrational density in a pulsed plasma. Again assuming that the predominant process for the vibrational excitation of molecules is by fast electron ionisation through the singlet states, other excitation processes exist, i.e. Auger relaxation of electronically excited H_2 molecules during wall collisions, auger neutralisation of H_2 molecular ions, however in the regime of interest here i.e high density discharges this assumption is valid. The density of vibrationally excited molecules, in a steady state discharge, is given by;

$$n'' = n_g n_p \langle \sigma_{EV} v_P \rangle \tau'' \qquad \text{Eqn. 2.23}$$

where, n_g is the gas density, τ" is the average loss time for vibrationally excited molecules in the discharge and $\langle \sigma_{EV} v_p \rangle$ is the reaction rate coefficient for vibrational excitation through the E-V process.

The characteristic loss time, τ", for $H_2(v")$ molecules is given by;

$$\tau''_{on} = \frac{1}{(\frac{V''}{b'' L''}) + n_g \langle \sigma_g v_g \rangle + n_p \langle \sigma_{ion} v_p \rangle + n_e \langle \sigma_{DA} v_e \rangle + n_h \langle \sigma_{VT} v_h \rangle} \qquad \text{Eqn. 2.24}$$

where the denominator represents the loss terms due to wall losses, deexcitation by

collisions with the background gas, ionization by primary electrons, loss by dissociative attachment, losses by collisions with atoms, the atomic density being given by n_h.

In the post discharge of the plasma the primary electron density will decay to zero, thus the production of vibrationally excited molecules will be set to zero, other processes may still lead to n" production but these are considered to be small compared to the E-V process. The average loss time τ'' now becomes;

$$\tau''_{off} = \frac{1}{(\frac{V''}{b''L''}) + n_g\langle\sigma_g v_g\rangle + n_e\langle\sigma_{DA} v_e\rangle + n_h\langle\sigma_{VT} v_h\rangle} \qquad \text{Eqn. 2.25}$$

Thus the vibrational density will decay in the post discharge with a loss time given by τ''_{off}, where τ''_{off} is roughly 1ms [30].

The parameters used to compute n^- and n" must also be evaluated as a function of time in a pulsed plasma. Where possible assumptions which do not dramatically change the predicted outcome but leave the calculations easier will be used.

2.8.3. The gas density n_g.

This can be computed directly from the filling pressure, where

$$n_g = 3.5*10^{13}\ molecules/cm^3\ per\ mTorr \qquad \text{Eqn. 2.26}$$

2.8.4. The primary electron density n_p.

The primary electron density is given by

$$n_p = \frac{Id}{eV}\left[\frac{1}{n_g\langle\sigma_\epsilon v_p\rangle + \frac{1}{\tau_w}}\right] \qquad \text{Eqn. 2.27}$$

where Id is the discharge current, V is the volume of the discharge, $n_g\langle\sigma_{in} v_p\rangle$, $=1/\tau_{in}$, is the loss rate due to inelastic collisions and τ_w is the characteristic loss time due to wall collisions.

For low source pressures $\tau_w<\tau_{in}$, i.e where wall losses dominate, in this region n_p is proportional to Id and can be approximated, for very low pressures to

$$n_p = \frac{Id}{eV}\tau_w \qquad \text{Eqn. 2.28}$$

Thus at low pressures we can determine the value of τ_w from a plot of n_p vs Id [26]. As the pressure is increased then τ_{in} approaches and eventually dominates over τ_w, in this region the density and the energy distribution function of the primaries are dependent upon n_g. And we can see that as n_g increases n_p decreases, and as the mean free path for collisions becomes smaller the primary electron energy becomes degraded to lower energy electrons resulting in an increase in n_e.

Thus having obtained τ_w at low pressures, we need only calculate the rate coefficient for inelastic collisions to be able to determine n_p.

2.8.5. Density of plasma electrons, n_e.

The bulk electron density is given by,

$$n_e = n_g n_p \langle \sigma_{ion} v_p \rangle \tau_e \qquad \text{Eqn. 2.29}$$

or in terms of discharge current and pressure,

$$n_e = \frac{Idn_g \langle \sigma_{ion} v_p \rangle \tau_e}{eV\left(n_g \langle \sigma_\epsilon v_p \rangle + \frac{1}{\tau_w}\right)} \qquad \text{Eqn. 2.30}$$

where τ_e is the characteristic loss time for electrons. Cronin and Sexton [34] state that for low pressures, n_e decay, in the post discharge, occurs predominantly by diffusion and attachment to atomic hydrogen.

The bulk electron density can be calculated from equation 2.30 or can be experimentally determined using langmuir probes, (see chapter 6).

2.8.6. The atomic hydrogen density n_h.

The atomic density can be expressed as,

$$n_h = (2n_g n_p \langle \sigma_{dis} v_p \rangle + \frac{n_g 2 S_m P_h A_f V_g}{V} + n_g n_{i2} \langle \sigma_{i2} v_{i2} \rangle + n_{ij} n_e \langle \sigma_{ije} v_e \rangle \qquad \text{Eqn. 2.31}$$

The first term represents the production of atoms through dissociation of molecules;

$$H_2 + e_p = H + H \qquad \text{Eqn. 2.32}$$

The second term describes the dissociation of molecules on the filaments [27], s_m is the sticking probability for molecules on the filament surface, p_h is the probability for dissociation of molecules on the filaments and a_f is the filament area. The last terms represent the production of atoms by secondary particles. t_h is the characteristic loss time for atomic hydrogen.

Since the volume recombination cross section, b, is very small, the average loss time for atoms τ_h, is dominated by recombination of atoms on the walls [28], and therefore t_h can be expressed as,

$$\tau_h = \frac{L}{\gamma v_h} \qquad \text{Eqn. 2.33}$$

where γ denotes the recombination coefficient of atoms on the walls. For chamber walls of stainless steel contaminated by the deposition of tungsten from the filaments, γ is in the region of 0.1-0.25 [32].

Depending on the dominant production process for n_h in the above equation we should be able to determine the pressure and current/voltage dependent behaviour of n_h. The density of n_h in the discharge may be extremely important in modulated plasmas as the effect of an increase in the post discharge H^- density is dependent on primary electrons being the dominant loss mechanism. In a pressure/current regime where there exist high densities of atoms and positive ions the H^- losses due to associative detachment and mutual recombination may come to dominate, here the effect of pulsing will be minimalised to an extent where it is no longer of benefit.

2.8.7. The ion density n_+.

$$n_+ = n_g n_p \langle \sigma_{ion} V_p \rangle \tau_+ \qquad \text{Eqn. 2.34}$$

This predicts that n_+ should increase as pressure at low pressures, when $1/\tau_w > n_g \langle \sigma_{ion} v_p \rangle$ and should begin to saturate when wall collisions become less dominant. Also n_+ will increase with increasing Id. For relatively low negative ion densities, where the

ratio of negative ion to electrons is small, we can assume that n_+ equals n_e. The ratio n/n_e typically has a value of between 0.01 upto 0.1, [20], in a continuous discharge and thus this assumption is valid.

2.9. Calculation of the rate coefficients.

The velocity distribution of particles in a plasma can be expressed by,

$$f(v) = 4\pi n v^2 \left(\frac{m}{2\pi kT}\right)^{\frac{3}{2}} e^{-\frac{mv^2}{2kT}} \qquad \text{Eqn. 2.35.}$$

In most instances a completely maxwellian distribution is not expected nevertheless the distributions are often very close to maxwellian , especially in the post discharge and we can then use this to calculate the collisional rates. The collisional rate coefficient <P(v)> is defined as,

$$\langle P(v)\rangle = \frac{1}{n}\int_0^{\infty} P(v)\, f(v)\, dv \qquad \text{Eqn. 2.36}$$

where p(v) is a scalar function of velocity, (i.e ((v) v).
Thus for a maxwellian distribution the collisional rate is given by,

$$\langle \sigma(v)\, v\rangle = \frac{1}{n}\int_0^{\infty} \sigma(v)\, v\, f(v)\, dv \qquad \text{Eqn. 2.37}$$

Thus,

$$\langle \sigma(v)\, v\rangle = 4\pi\left(\frac{m}{2\pi kT}\right)^{\frac{3}{2}} \int_0^{\infty} v^3\, \sigma(v)\, e^{-\frac{mv^2}{2kT}}\, dv \qquad \text{Eqn. 2.38}$$

Usually the cross sections are expressed in terms of the energy of the reacting particles rather than their velocity, so we define an energy distribution function, f(ε),

$$f(\varepsilon) = \frac{2\sqrt{\varepsilon}}{\sqrt{\pi}(kT)^{\frac{3}{2}}} e^{-\frac{\varepsilon}{kT}} \qquad \text{Eqn. 2.39}$$

Where f(ε) has been normalised such that,

$$\int_0^{\infty} f(\varepsilon)\, d\varepsilon = 1 \qquad \text{Eqn. 2.40}$$

and thus $<\sigma(v)\ V>$ becomes,

$$<\sigma(v)\ v> = 8\frac{\pi}{\sqrt{m}}\left(\frac{1}{2\pi kT}\right)^{\frac{3}{2}}\int_0^{\infty}\varepsilon\sigma(\varepsilon)e^{-\frac{\varepsilon}{kT}}d\varepsilon \qquad \text{Eqn. 2.41}$$

And using the energy distribution function and the appropriate cross section we can determine the reaction rate coefficient for the process of interest.

2.10. Model of the time dependent densities.

The time dependent densities of the plasma species can be determined from the steady state equations in section 2.8, these time dependent equations can then be used to predict the temporal behaviour of the H^- density in a discharge. Also the model can be given different dominant production and loss inputs to determine the discharge condition under which to expect an enhancement in the negative ion density.

2.10.1

From section 2.8, the time dependent densities can be written as six ordinary differential equations, in the discharge these are given by,

$$\frac{dn_p}{dt}on = \frac{Id}{eV} - n_p\left[n_g<\sigma_\epsilon v_p>+\frac{1}{\tau_w}\right] \qquad \text{Eqn. 2.42}$$

$$\frac{dn_e}{dt}on = n_g n_p<\sigma_{ion}v_p> - \frac{n_e}{\tau_e} \qquad \text{Eqn. 2.43}$$

$$\frac{dn_h}{dt}on = n_g n_p<\sigma_{dis}v_p>+n_g n_{i2}<\sigma_{i2}v_{i2}> - \frac{n_h}{\tau_h} \qquad \text{Eqn. 2.44}$$

$$\frac{dn_+}{dt}on = n_g n_p<\sigma_{ion}v_p> - \frac{n_+}{\tau_+} \qquad \text{Eqn. 2.45}$$

$$\frac{dn''}{dt}on = n_g n_p<\sigma_{EV}v_p> - \frac{n''}{\tau''} \qquad \text{Eqn. 2.46}$$

$$\frac{dn_-}{dt}on = n_e n''<\sigma_{DA}v_e> - \frac{n_-}{\tau_-} \qquad \text{Eqn. 2.47}$$

where the time dependent species are, fast electrons, bulk electrons, ions, atomic hydrogen, the vibrationally excited states and the negative ion density.

2.10.2

In the post discharge the time dependent densities can be written as,

$$\frac{dn_p}{dt}off = -n_p\left[n_g\langle\sigma_\epsilon v_p\rangle + \frac{1}{\tau_w}\right] \qquad \text{Eqn. 2.48}$$

$$\frac{dn_e}{dt}off = \frac{-n_e}{\tau_e} \qquad \text{Eqn. 2.49}$$

$$\frac{dn_h}{dt}off = n_g n_{i2}\langle\sigma_{i2}v_{i2}\rangle - \frac{n_h}{\tau_h} \qquad \text{Eqn. 2.50}$$

$$\frac{dn_+}{dt}off = -\frac{n_+}{\tau_+} \qquad \text{Eqn. 2.51}$$

$$\frac{dn''}{dt}off = -\frac{n''}{\tau''_{off}} \qquad \text{Eqn. 2.52}$$

$$\frac{dn_-}{dt}off = n_e n''\langle\sigma_{DA}v_e\rangle - \frac{n_-}{\tau_{-off}} \qquad \text{Eqn. 2.53}$$

2.11. Model of the negative ion density.

The differential equations in 2.10 can be solved for various plasma conditions to determine the temporal behaviour of the H^- densities. A more rigorous model based on the discharge parameters in the D.C.U. source is presented in chapter 6 and is used to verify the mechanisms believed responsible for the behaviour observed experimentally. Here the equations are solved for typical discharges with different dominant processes, i.e production dominated by the E-V/DA process and losses dominated by CD, MN and AD respectively.

In figure 2.3, the H^- density ,arbitrary units, is plotted as a function of time for a modelled discharge with different dominant losses, CD dominated losses (a), MN dominated losses (b) and AD dominated losses (c). A listing of the program used to model the densities is given in appendix 1. Also no enhancement of the production rate due to EEDF cooling is allowed for in this calculation.

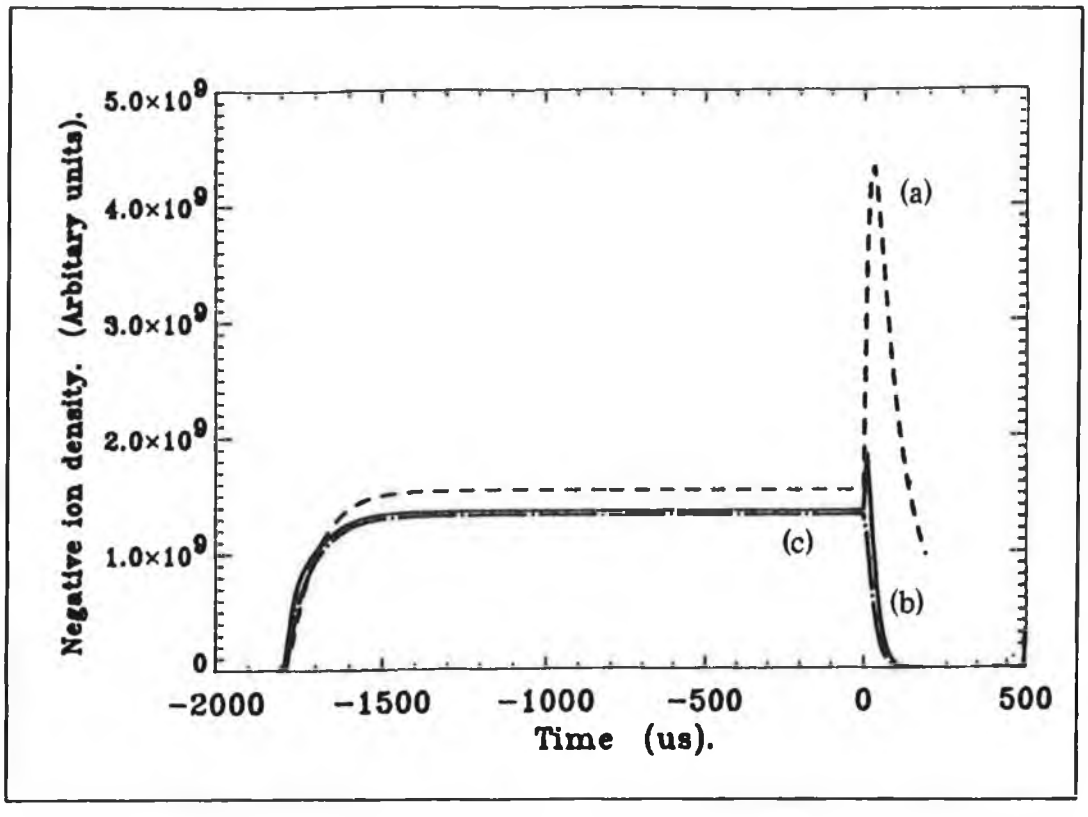

Figure 2.3. Temporal behaviour of the H^- density for various dominant loss processes.

Trace (a) shows a discharge with losses dominated by fast electron collisions with H^-, 60% of total losses. After switch off, 0μs, a rapid increase of a factor of 3 in the H^- density occurs as the fast electrons are removed form the post discharge. In trace (b) the major loss mechanism is that of mutual neutralisation with low CD losses, 10%, here a slight increase is observed in the H^- density in the post discharge. Trace c shows an AD loss dominated discharge and no increase is observed. These plots indicate that a discharge in which there exist significant fast electron densities can show enhancements in the H^- density after switch off and that such increases are not accounted for by losses such as AD and MN.

Figure 2.4 shows the predicted behaviour of a discharge dominated by CD

losses with a production mechanism of E-V and DA.

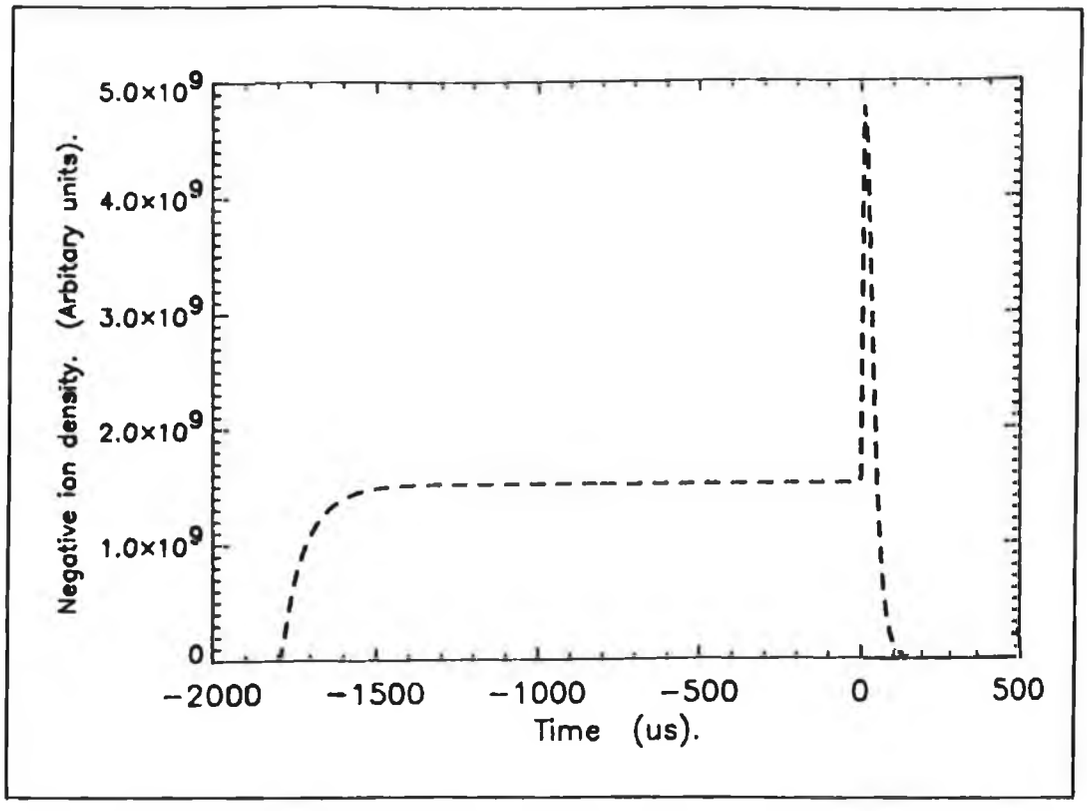

Figure 2.4. Predicted time dependency of a discharge with E-V/DA production and CD losses.

In this calculation the production rate via DA is time dependent increasing in the post as the electron temperature cools. Again a large increase in the H^- density is observed in the post discharge, this increase is a coupling of the two effects of increased production and reduced losses. A polar dissociation production mechanism will not result in any increased production after switch off, Hiskes et al [19] have given the maximum production rate for collisions with electrons of energy greater than 30eV and a threshold at 17eV, rather the production will cease almost immediately as the fast electrons are removed. This enhanced production could possibly be due to recombination of H_2^+ as this increases at lower electron temperatures [33].

However this process,

$$e^- + H_2^+ \rightarrow H^- + H^+ \qquad \text{Eqn. 2.54}$$

is not considered here to be a major production mechanism and therefore should not be the basis of large enhancements and moreover as it does not require a hot plasma

for an intermediate stage will not benefit from filtering. Figure 2.5 shows a calculated H^- density, arbitrary units, for the same conditions as in figure 2.4, pulsed at a repetition rate of 10kHz. From this it can be seen that the predicted density will have a much enhanced time averaged density.

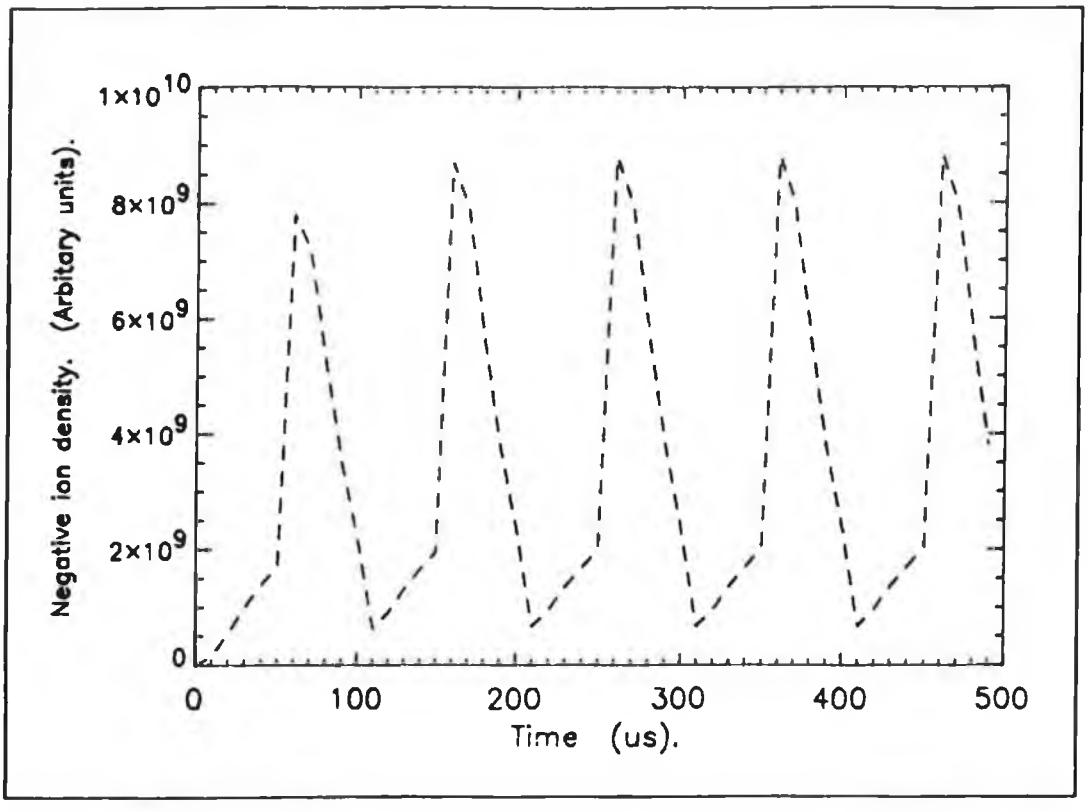

Figure 2.5. Time dependent calculated H^- density for a discharge modulated at 10kHz.

At switch off the density rapidly increases to a peak value of 2 to 3 times that during the discharge, however at switch on of the discharge again the density is rapidly depleted and decays away until after roughly 30μs it starts to increase again. While the time averaged density is improved the model predicts a highly modulated H^- density in the source.

From the above predicted densities it can expected that pulsed discharges can exhibit large enhancements over their dc counterparts when there exists either large densities of fast electrons and/or a high electron temperature during the discharge period of the cycle.

2.12. Conclusion

In this chapter an over view of volume ion sources was given, the most successful adaptations of the volume source, the tandem and the hybrid sources were discussed. The basis behind the temporal filtering concept was explained with emphasis on the pumping of densities and the control of the EEDF. It is speculated that it may be possible, under certain conditions to enhance the time averaged negative ion density in the volume source by appropriate modulation of the discharge and that this method of enhancement has several advantages over the magnetically filtered sources, i.e operation at lower pressures, ease of control over the EEDF and lower electron densities. The species densities and time dependent densities were developed for a volume ion source and these time dependent densities are then solved to give a simple model of the expected behaviour of a temporally filtered source. This model predicts that it is possible to gain large enhancements in the H^- density when pulsing discharges which have large CD losses and high electron temperatures.

References.

[1] Hemsworth, R.S, et al.
"6th International Symposium on the Production and Neutralisation of Negative Ions and Beams". November 9-13, Brookhaven, New York, 1992.

[2] Van Os.
"Negative Ion Sourcery", PhD Thesis.

[3] Bacal, M, et al.
"2nd International Symposium on the Production and Neutralisation of Negative Ions and Beams". October 6-10, Brookhaven, New York, 1980.

[4] Bacal, M.
Nuclear Instruments and Methods in Physics Research, B37/38, p28-32, 1989.

[5] Nicolopoulos, E, Bacal, M, Doucet, HJ.
J. Phys, (Paris), 38, 399, 1977.

[6] Holmes, A.J.T, Dammertz, G. and Green, T.S.
Review of Scientific Instruments, 56 (9), p1697, 1985.

[7] Leung, K.N, Ehlers, K.W. and Bacal, M.
Review of Scientific Instruments, 54 (1), p54, 1983.

[8] Hiskes, J.R. and Karo, A.M.
Journal of Applied Physics, 56 (7), p1927, 1984.

[9] Buzzi, J.M, Snow, S. and Hirshfield, J.L.
Physics Letters, 54A (4), p344, 1975.

[10] Limpeacher, R. and MacKenzie, R.
Review of Scientific Instruments, 44 (6), p726, 1973.

[11] Eenhuistra, P.J, et al.
Journal of Applied Physics, 69 (1), p85, 1990.

[12] Hiskes, J.R, et al.
Journal of Applied Physics, 53 (5), p3409, 1982.

[13] Bacal, M.
Phys. Scr, T2/2, p467, 1982.

[14] Eenhuistra, P.J, et al.
Physical Review A, 40 (7), p3613, 1989.

[15] Hiskes, J.R.
"4th International Symposium on the Production and Neutralisation of Negative Ions and Beams". Brookhaven, New York, 1986.

[16] Wadehra, J.M. and Bardsley, J.N.
Physics Review Letters, 42, p1538, 1979.

[17] Janev, R.K, Langer, W.D, Evans, K and Post, D.E.
"Elementary Processes in Hydrogen-Helium Plasmas"
Springer-Verlag, Berlin, London, New York, 1987.

[18] Mullan, A.A. and Graham, W.G.
Review of Scientific Instruments, 61 (1), p451, 1990.

[19] Holmes, A.J.T, et al.
Review of Scientific Instruments, 52 (2), p223, 1987.

[20] Bacal, M, Bruneteau, A.M. and Nachman, M.
Journal of Applied Physics, 55 (1), p15, 1984.

[21] Holmes, A.J.T.
Review of Scientific Instruments, 53 (10), p1517, 1982.

[22] Ehlers, K.W. and Leung, K.N.
Review of Scientific Instruments, 52 (10), p1452, 1981.

[23] Hopkins, M.B. and Graham, W.
Journal of Physics D, Appl. Phys, 20, p838, 1987.

[24] Leung, K.N, et al.
Review of Scientific Instruments, 54, p56, 1983.

[25] Hopkins, M.B, et al.
Journal of Physics D, Appl. Phys, 24,p268, 1991.

[26] Hopkins, M.B, et al.
Journal of Applied Physics, 70 (4), p2009, 1991.

[27] Hopkins, M.B. and Graham, W.
Journal of Applied Physics, 69 (6), p3461, 1991.

[28] Hall, R.I, Cadez, I, Landau, M, Pichou, F. and Schermann, C.
Physical Review Letters, 60 (4), p377, 1988.

[29] Hopkins, M.B.
"4th European Workshop on the Production and Applications of Light Negative Ions." March 26-28, Belfast, 1991.

[30] Lefebure, M, et al.
"Proc. Production and Application of Light Negative Ions."
Paris, 1986.

[31] Chan, C, et al.
Journal of Applied Physics, 54, p6119, 1983.

[32] Wood, B.J. and Wise, H.
Journal of Chemical Physics, 65, p1976, 1961.

[33] Towara, H, et al.
"Atomic data involving Hydrogen relevant to edge plasmas."
Report IPPJ-AM-46, Nagoya University, Japan.

Chapter 3. Extraction of negative ions from a volume ion source.

3.0. Introduction.

In this chapter we discuss the extraction of negative hydrogen ions from a pulsed and pulse modulated volume ion source. In the experiment two sources were used, the first results [1] were taken on source 1. This system was limited by two factors, it only had the capability to produce low power discharges, 10-20A, a limitation of the pulsing apparatus, and the watercooling of the source proved insufficient resulting in the possibility of damage to the wall magnets or to the source itself. The remainding experiments were carried out on source 2, the main modification here was a water jacket around the chamber walls which provided sufficient cooling of the source. However this resulted in the magnets being further away from the wall which may have affected the confinement within the source. Also the pulsing system was upgraded to allow higher power operation, discharge currents up to 250A have been pulsed. Most of the work was carried out in the discharge current range of 10 to 50A as sustained high power operation can lead to other difficulties, i.e damage to feedthroughs and filaments.The extracted current measurements presented here show a dramatic increase after the discharge is switched off, an effect of the high CD losses in the discharge. These results support the idea that the two stage process of EV and DA is a dominant mechanism for H^- production in volume ion sources. The proposed temporal filtering of volume sources is shown to be an effective means of increasing the average H^- density in the source.

3.1. The Plasma System.

A schematic of the volume ion source 2 and extraction chamber is shown in figure 3.1. The ion source is a magnetic multicusp volume ion source, consisting of a stainless steel cylindrical chamber, diameter 200mm and length 300mm. It has an outer wall allowing the chamber to be water cooled. Source 1 was cooled by a series of water channels adjacent to the magnets. A series of ports are available to facilitate the use of diagnostics on the source. The diagnostics include extraction of an ion beam, photodetachment measurements of the H^- density in the source and langmuir

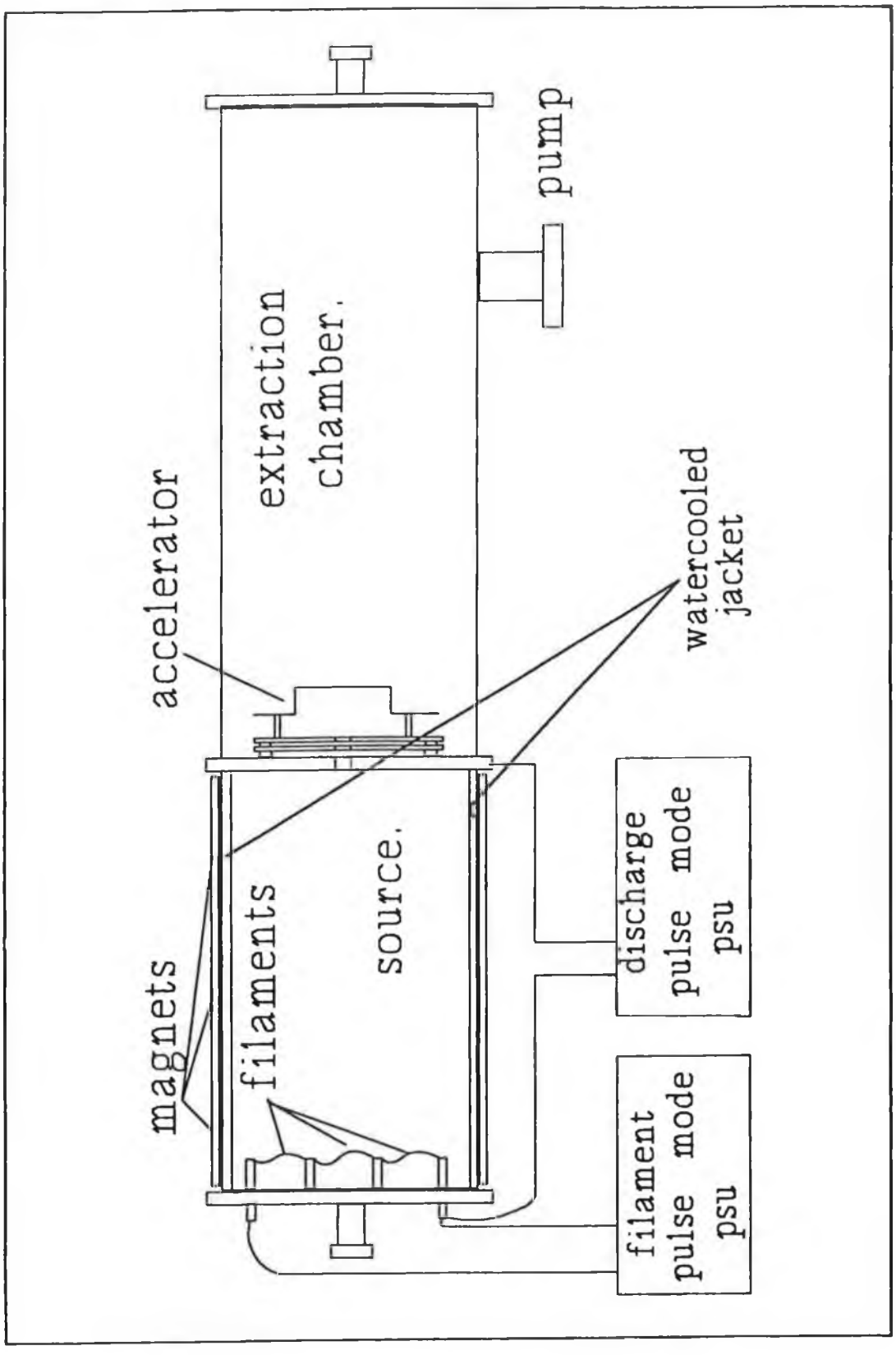

Figure 3.1. Schematic of the D.C.U. volume ion source.

probe measurements.

A magnetic multipole field on the chamber wall, the anode, is formed by rows of permanent bar magnets with north and south poles alternatively facing the plasma, four rows of magnets have also been placed on the front end wall.

An extraction chamber is separated from the source by a plasma electrode, PE, this electrode is watercooled to prevent heat damage to permanent magnets affixed. The accelerator is placed on the far side of the plasma electrode with a 5mm diameter extraction aperture.

The chamber is pumped through the extraction chamber by a 300l/s turbo molecular pump. To increase the pump rate in the source chamber holes are drilled in the plasma electrode.

The plasma is heated by a series of tungsten filaments located near the front of the source. The filaments are made of tungsten wire of diameter 1mm and are approximately 120mm in length. The filaments are connected three or four in series, and sets of filaments are connected in parallel to allow discharge currents of up to 250A. These filaments are heated by 50V dc, which is pulsed at repetition rates of 10-200Hz.

The discharge occurs between the filaments, the cathode, and the chamber walls, the anode. A discharge voltage of 60V is generally applied between the filaments and the wall. Note that the filament heating current is switched-off just before the discharge current is switched on, figure 3.2. This is to ensure the suppression of high energy electrons in the post-discharge period. An output trigger pulse, which can be moved with respect to the discharge and post-discharge periods, is available to allow time resolved diagnostic measurements to be made. Both the filament heater current and the discharge current are driven by high power pulsing units. These units are driven at a constant voltage and the power regulation is achieved by variation of the duty cycle. The units consist of high power FET's connected in parallel, each single FET is capable of effectively pulsing 25A. The continuous rating for each is higher than this, however heating caused by switching of an inductive load can be a major limitation on the actual capability. The FET's are driven by a high speed, low impedance push/pull mosFET driver circuit, which drives the current hard-on/hard-off. The FET's must be mounted on a watercooled heatsink to prevent

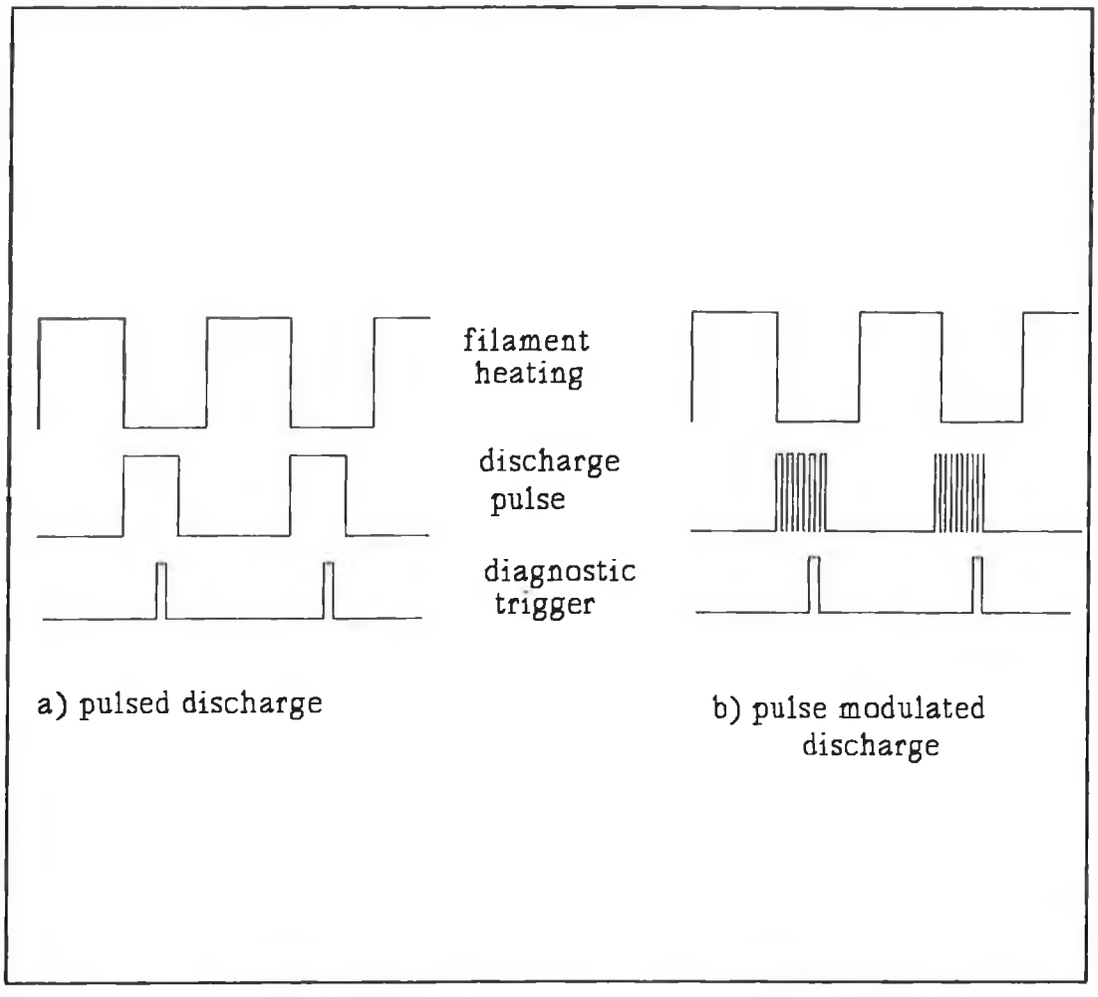

Figure 3.2. Heating current, discharge current and diagnostic trigger synchronisation.

overheating.

Due to the characteristic loss times inherent in the discharges, 10's of microseconds, the current must be switched on/off in less than 10μs. This can only be achieved by ensuring that all connecting cables are kept as short as possible, thus helping to keep the inductance of the circuit to an absolute minimum. A bank of high quality capacitors, placed close to the load will greatly reduce the effective inductance of the circuit. These are especially important if the PSU is located away from the load. The high frequency modulation of the discharge occurs on a pulsed cycle, figure 3.2. the discharge is pulsed on after the filament heater current is switched off and the high frequency modulation occurs during this 1-2ms pulse.

3.2. The extraction system.

A schematic of the extraction system is shown in figure 3.3. It consists of an aperture, diameter 5mm, in the front extraction plate, the plasma electrode. This electrode can be independently biased, but most of the experimental work was carried out with this plate at 0V. Positioned 3mm behind this plate is a second electrode, the accelerator, this has a 5mm diameter aperture and can be biased up to 6kV with respect to the anode. On this plate small magnets are mounted to form an electron trap. The magnetic field, B>500G, deflects the electrons, which are extracted along with the negative ions, on to a copper dump from which the extracted electron current may be measured. Magnets are also placed on the plasma electrode, these help to reduce the electron current collected by the first plate and so reduce the load on the power supply. The ions, being much heavier than the electrons, are only deflected slightly by the field. These ions are then accelerated on to the third plate, the faraday cup, where they are measured as a voltage across a sensing resistor. This voltage is then displayed on a fast digital oscilloscope from which it can be transferred to a personal computer.

To determine if electrons are passing through the electron trap and are being collected on the faraday cup, the accelerator is run with a helium or argon plasma. These tests have indicated that negligible electron currents are extracted on to the faraday cup.

3.3. Time dependent extracted negative ion densities.

In Chapter 2 it was proposed that when a discharge is switched off there will occur a rapid decay of fast electron density, this fast electron decay will occur in ≈ 1μs [2]. However both the vibrationally excited and bulk electron densities survive well into the post-discharge period. The decay of the fast electron density leads to a rapid reduction in the H^- losses due to collisional detachment, CD. The atomic density decays with a loss time of roughly 90μs [3], and thus the associative detachment, AD, losses may also be reduced. However this is expected to be a minor effect compared to the decrease in the collisional detachment losses. Thus in discharges where negative ion losses are dominated by fast electron and atomic interactions there exists the

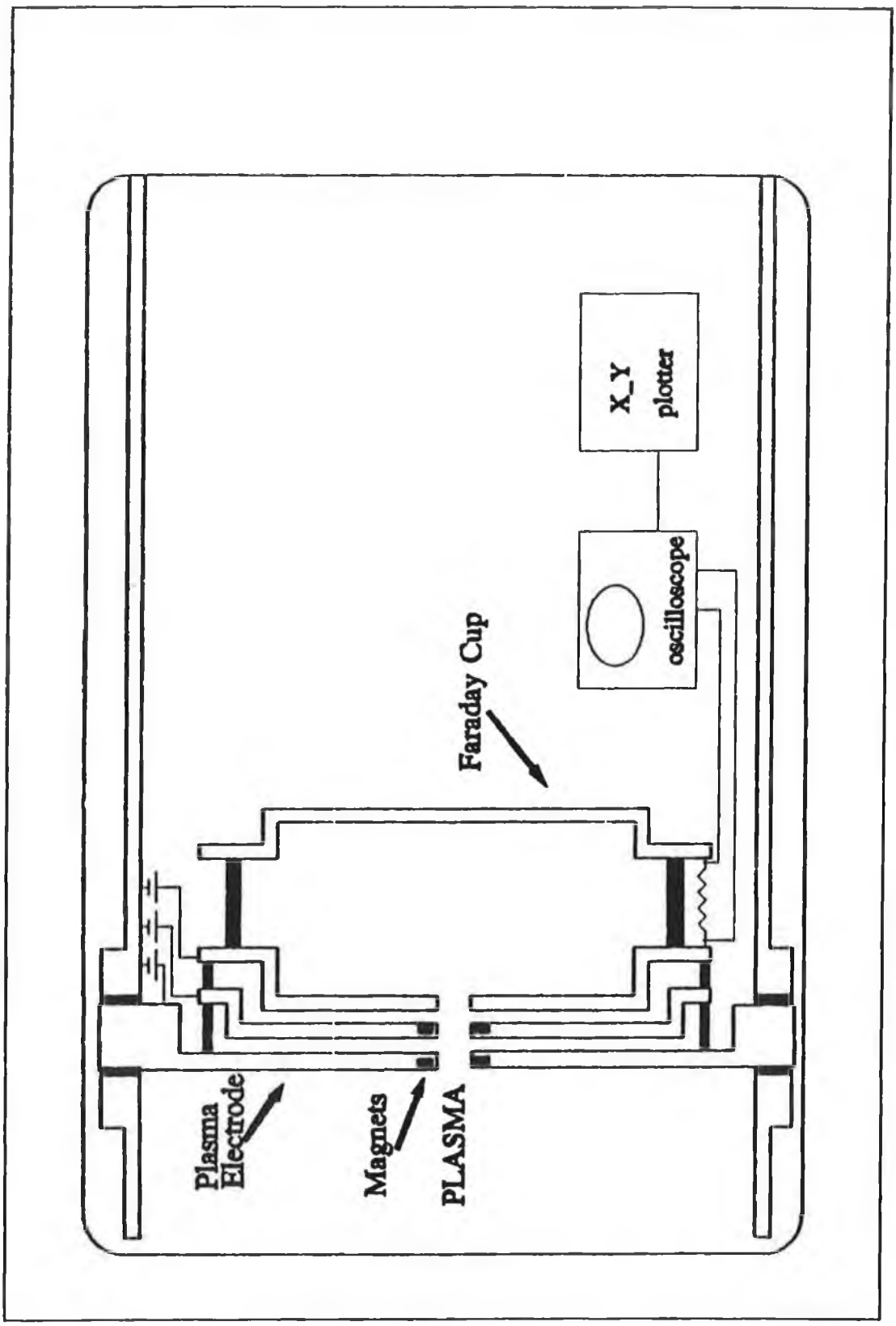

Figure 3.3. Schematic of the extraction system.

possibility of enhancement of the H^- density in the post discharge.

Further it has also been shown [2,4] that the electron temperature cools in an almost exponential manner in the post discharge. For a hot discharge, with kT_e typically larger than 2-3eV, the cooling of the EEDF in the post discharge will lead to a larger dissociative detachment cross-section as the electron temperature cools below approximately 1ev [5]. This cooling of the EEDF also leads to an enhancement of negative ion density in the post discharge. These two effects couple together and can, under the appropriate conditions, result in a dramatic increase in the negative ion density after the discharge has been switched off.

Here we present the results of extracted ion current measurements made in a pulsed and pulse modulated H_2 discharge. Figure 3.4 shows a typical time dependent extracted H^- signal. The measurements were made on source 1. The accelerator is described in section 3.1. The voltages on the electrodes are 400V, 600V and 1000V respectively. The discharge current is 15A, the repetition rate is 87Hz and discharge duration 2.7ms, the discharge voltage is 60V, and the source pressure is 2.4mTorr. The signal shows a slow increase in extracted current after switch on, increasing to a steady state value of 0.1mA after 0.8-1.0ms, this slow rise time in the signal can be attributed to the long lifetime of the vibrationally excited states, >200μs, these levels increase slowly to a steady state level and the subsequent H^- density evolves slowly with a rise time of approximately 1ms. When the discharge is switched off, 2.7ms, the H^- current density starts to increase until at approximately 90μs after switch off the extracted current has reached a peak value of 0.34mA. Thus there occurs a post discharge increase in current density of over 300% compared to the continuous level. This post discharge increase in H^- current density has a rise time of roughly 90μs reaching a peak which then decays away exponentially with a decay rate of roughly t=100μs. The peak time appears to give an indication of the survival times of species in the post discharge, i.e. for production to continue up to 90μs then the electron density and the vibrationally excited states must survive, even allowing for an enhancement in production, approximately the same time. However while the vibrational density can be expected to have a long survival time in the post discharge, Lefebrue et al [6] give the characteristic loss time for $H_2(v^*)$ to be approximately 1ms, the same cannot be said for the electron density whose decay time has been given by

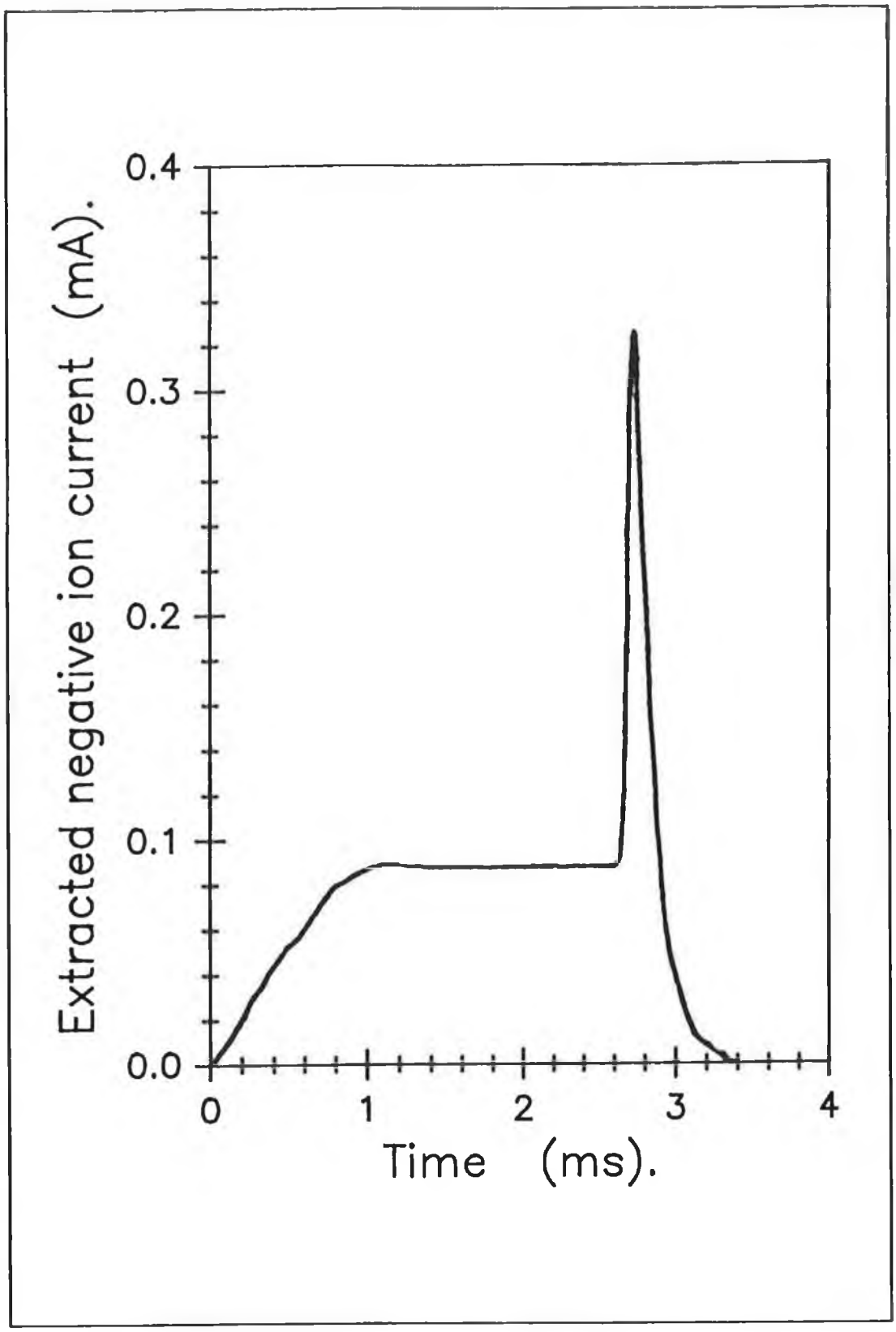

Figure 3.4. Time dependent extracted H^- current from a 15A, 2.4mTorr discharge. Repetition rate 87Hz and pulse length 2.7ms.

Hopkins et al [7] as t=30μs. Thus continued production in the post discharge at a rate greater than that during the discharge, even allowing for a much enhanced DA cross section, appears unlikely at times as long as 90μs after switch off. This long rise time must have another explanation and this will be discussed in chapter 5.

When considering the factors that lead to the post discharge enhancement it is important to note that this effect is dependent upon the conditions that the fast electron density is a major contributor to negative ion losses and/or the electron temperature during the discharge is relatively high resulting in enhancement in the DA cross section during the post discharge. In chapter 6 the dependence of the electron temperature with plasma parameters is discussed in detail. At lower source pressures, fast electron confinement time, τ_c, is much less than the mean time for inelastic collisions τ_i, thus most of the primary electrons are lost to the walls and there is little energy degradation [8]. At the lower pressures the electron temperature is high with a distinct fast electron tail. As the pressure is increased the mean time for inelastic collisions approaches that of τ_c and the fast electrons are degraded to thermal or bulk electrons. At higher pressures the electron temperature will have dropped and the fast tail will be less important. However here it is sufficient to note that at lower source pressures, 0.5-2.5mtorr, the electron temperature is high enough, >1.5eV, for processes such as dissociative attachment to be below its optimum value and also large numbers of fast electrons exist, thus for lower pressures an increase in the post-discharge is expected, figure 3.4. As the source pressure is increased the electron temperature falls and the density of fast electrons decreases due to a decrease in the mean free path for higher energy electrons and the energy degradation of these electrons to lower energy, bulk electrons, becomes more effective. This means that the optimisation of conditions for the two stage, E-V and DA, process for H^- production occurs during the discharge and therefore when the discharge is switched off there is no observed enhancement. Also large H^- losses due to collisional detachment may no longer occur as losses due to mutual recombination with ions and associative detachment become more important [9]

This effect can be seen in figure 3.5, where the extracted negative ion current densities are plotted against time for several source pressures. From figure 3.5 it can be that at the lower pressures, 0.5-2.5mtorr, a large increase in the post discharge

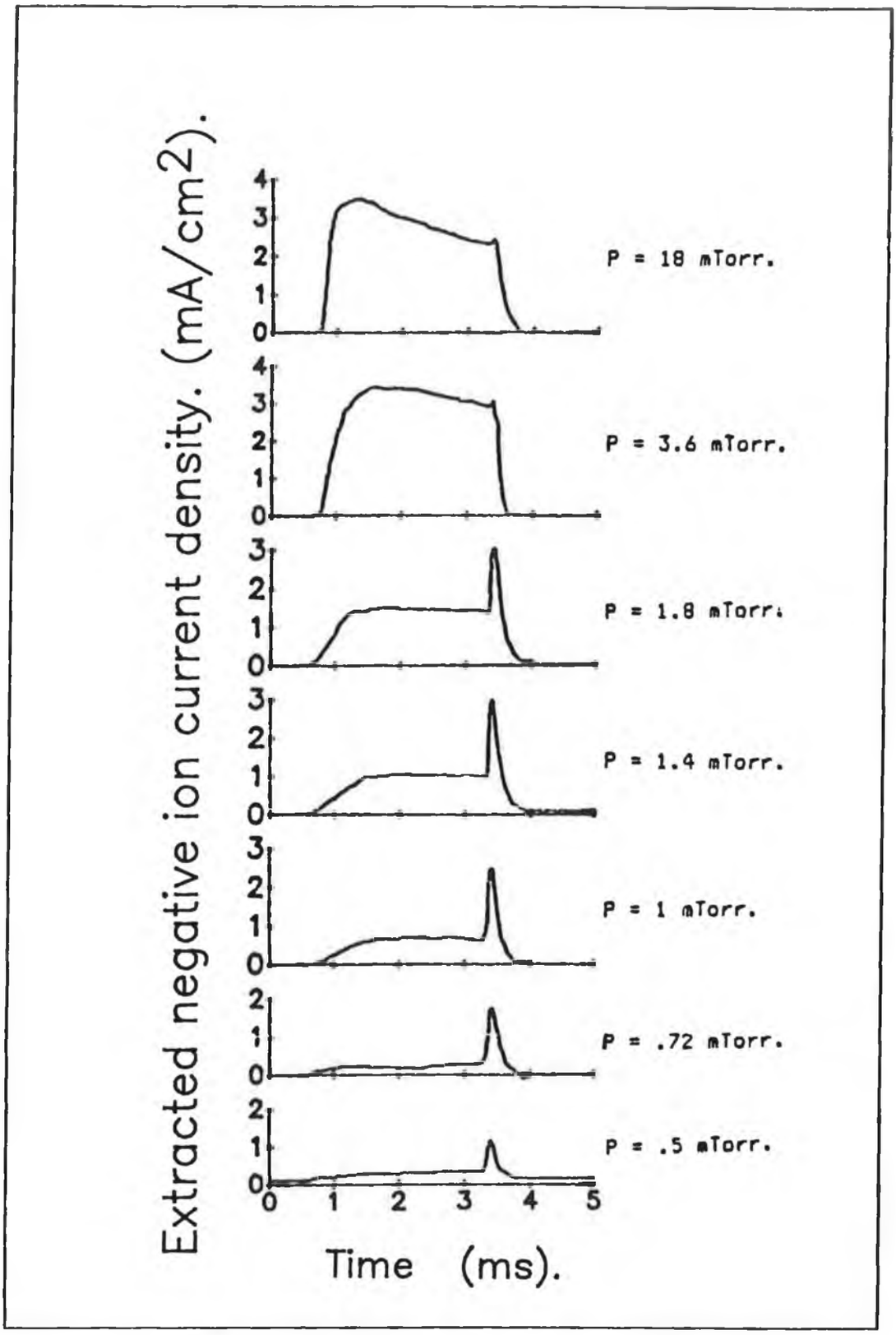

Figure 3.5. Extracted negative ion current density vs time for various source pressures.

negative ion current density occurs. At 0.5mtorr the steady state H^- current density is $0.3mA/cm^2$ and the peak value of the current density in the post discharge is $1.2mA/cm^2$, this gives a peak to continuous ratio of almost 400%. As the pressure is increased this ratio decreases as the steady state current density increases, at 1mtorr the continuous value is $0.7mA/cm^2$ and the peak/dc ratio is 300%, at 2mtorr the continuous current is approaching that of the post discharge peak, peak/dc is 200%, as the pressure is further increased through the pressure at which the maximum continuous current is extracted, 3-5mtorr, the ratio further decreases until at approximately 5mtorr there is no noticeable increase after switch off. This is due to the lower electron temperature with the maximisation of the DA production rate occurring during the discharge and collisional detachment losses being less dominant than other losses, i.e. mutual recombination and associative detachment. At higher pressures the H^- density increases at the start of the discharge and then decays as the discharge continues. This can be explained by the dissociation of the H_2 gas, resulting in the production of hydrogen atoms which can destroy the H^- through the reaction [10],

$$H^- + H \rightarrow H_2^-(\Sigma_g) + e^- \rightarrow H + H + e^- \qquad \text{Eqn. 3.1}$$

This production of atomic hydrogen evolves slower than the production of negative ions and thus we get a decreasing H^- as the atomic density builds up. Figure 3.6 gives the continuous and peak extracted current densities as a variation of the source pressure. Note that the continuous current density has a maximum in the pressure region 3-5mtorr but the post discharge peak current density at lower pressures can be greater than for a continuous discharge at higher pressures.

3.4. Extracted current density variation with discharge current.

Previous publications [11,12] have shown a marked dependence of the extracted current density with discharge current, they show that for low discharge currents the extracted current density increases almost linearly with discharge current, as the discharge current increases the extracted current starts to saturate. This is plotted in figure 3.7, where the time dependent extracted current densities are shown for several discharge currents, the source pressure is 1mtorr, discharge voltage 60V

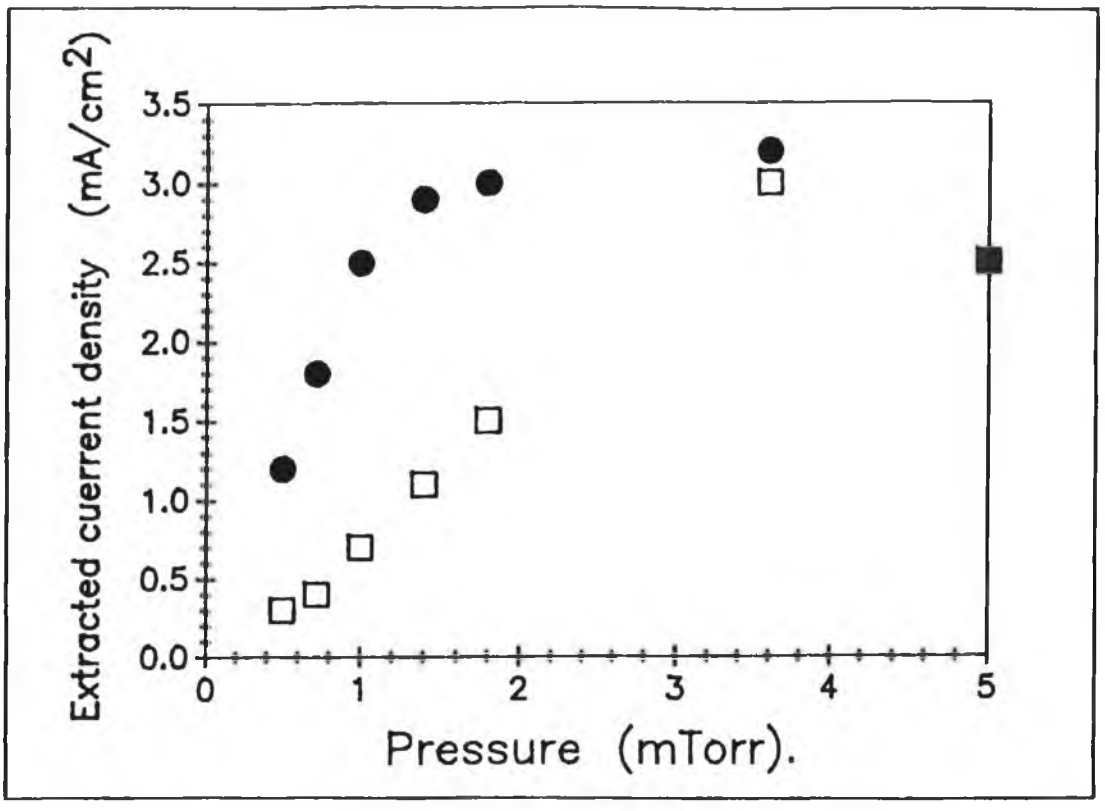

Figure 3.6. Peak/dc extracted H^- currents as a function of source pressure.

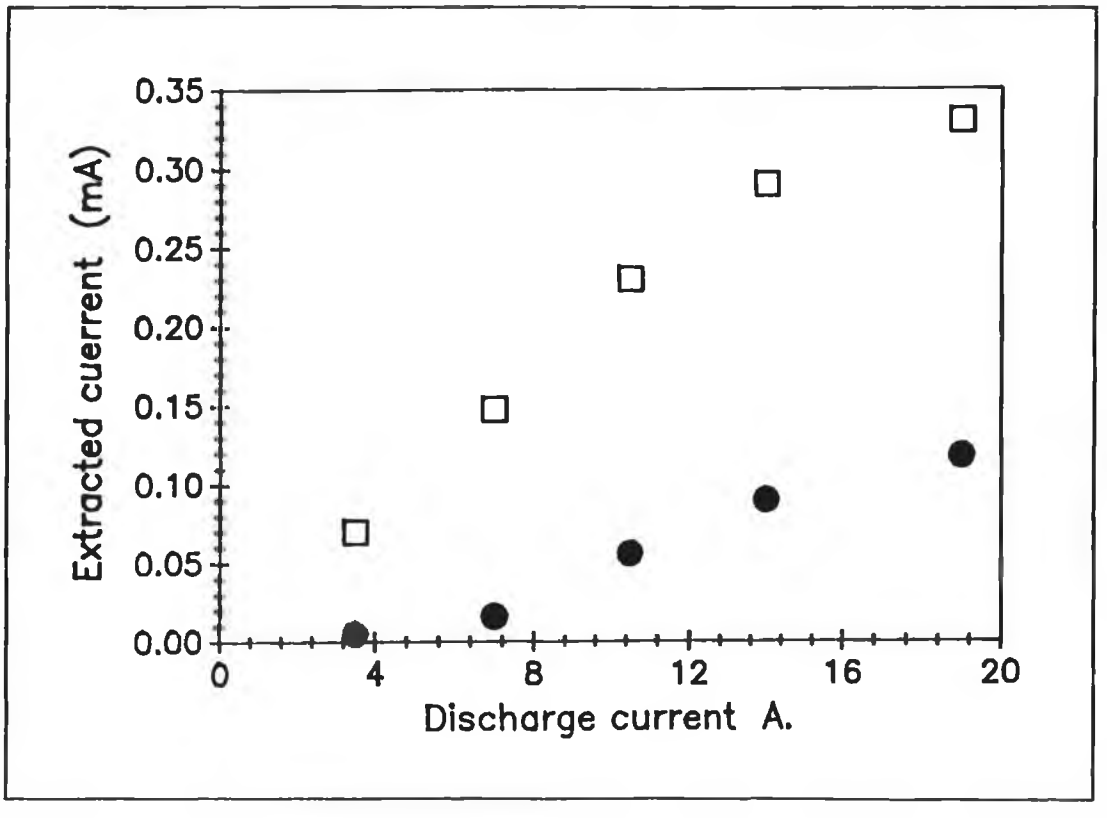

Figure 3.7. Peak/dc extracted currents as a function of discharge current.

and the pulse length 1ms.The important factor to be seen here is that as the steady state current increases from low currents the post discharge peak current density also increases but at a slower rate. In chapter 5 it will be shown that the negative ion density during the discharge in the centre of the source saturates at roughly 30A to 50A and the peak value continues to increase further at higher powers. The peak/dc ratio starts to increase again above the saturation current.

3.5. Extraction from a pulse modulated discharge.

The observed enhancement of the extracted H^- current density in the post discharge, as described in section 3.3, may possibly be used to improve the efficiency of the volume ion source for the extraction of negative ions, further large improvements may also be achieved from the reduction in the extracted electron current. However to achieve this improvement in the efficiency, the discharge current must be modulated on/off with a frequency and duty cycle determined by the characteristic production and loss times of the ion source in question. As given by Hopkins [13] the modulation frequency must be such that

$$\tau_{e^-} < t_{on} \quad , \quad \tau_{H^-} > t_{off} \qquad \text{Eqn. 3.2}$$

This modulation frequency must be low enough to allow the excitation of sufficient numbers of vibrational levels during the discharge and large electron densities, which are required for continued H^- production after the discharge is switched off, and the frequency must also be high enough to ensure that the increase in the post discharge leads to an overall increase in the time averaged extracted current, i.e the off time of the cycle should be of the order of the post discharge peak rise time. The pulse modulation of the discharge current is described in section 2.3.

Figure 3.8 shows the extracted current density in a deuterium discharge as a function of time for several different modulation frequencies. For low pulsing frequencies, f<1/t, 156Hz the extracted negative ion current density reaches a steady state value of 0.32mA/cm^2 in less than 1ms. After this time the discharge is switched off and the negative ion density increases to a peak value at approximately 100μs, it then decays away until the discharge is switched on again. In this case there is an increase in the effective time averaged extracted current density over the extracted

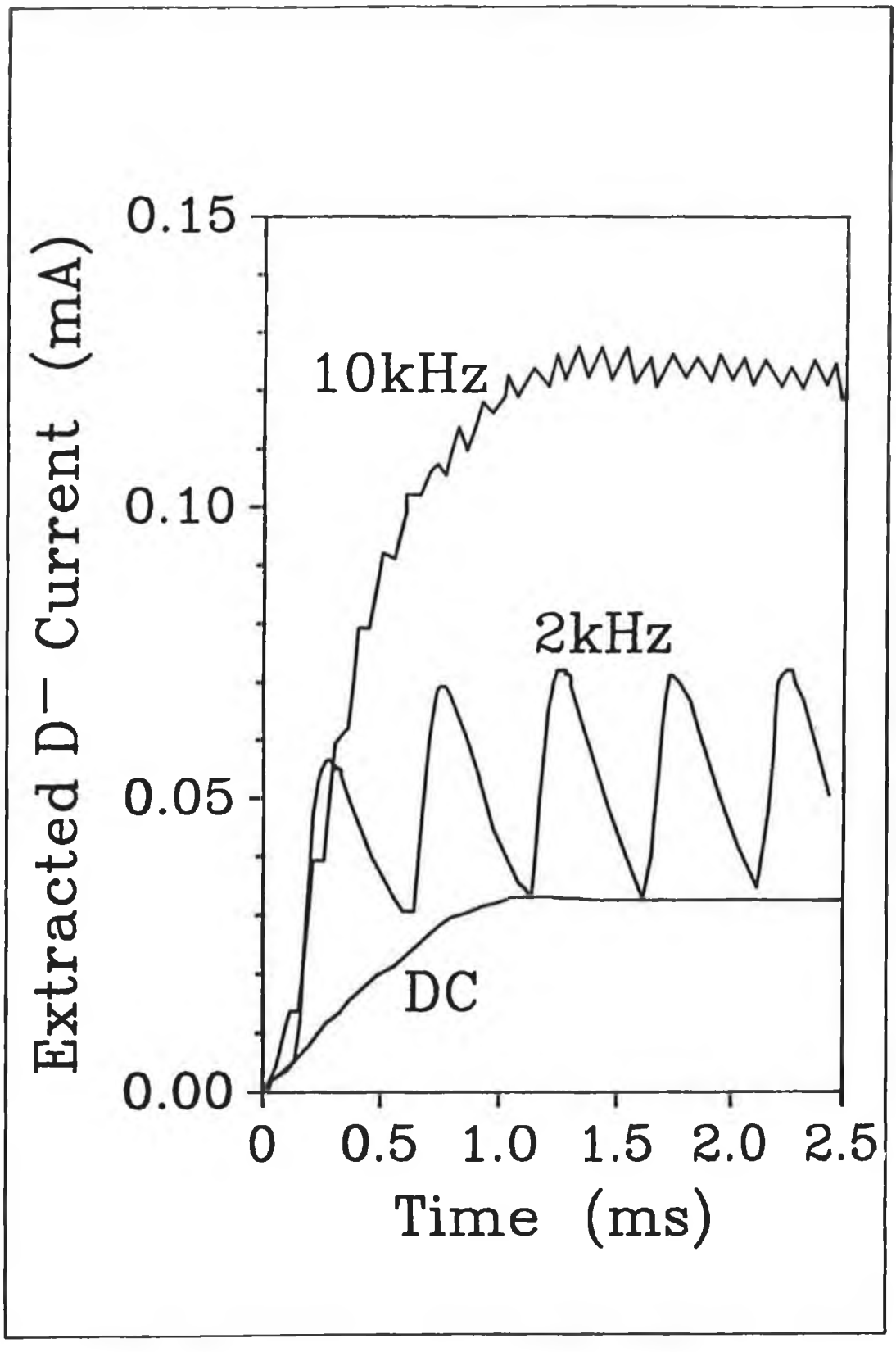

Figure 3.8. Extracted D^- current density as a function of time for different modulation frequencies. 10A, 2mTorr.

current density from a continuous discharge of the same time averaged discharge current, however this increase is highly modulated and does not show an increase over a continuous discharge of the same instantaneous current. As the modulating frequency is increased the redundant time in the post discharge, the time when the H^- density is less than the continuous level, is reduced, the signal becomes less modulated and the time averaged extracted current density is improved. In the case of this source, for modulation of the discharge current between 2-5kHz and a duty cycle of 50%, the time averaged extracted current approaches and eventually surpasses that of a discharge with the same instantaneous discharge current, however in the case of the modulated signal the time averaged discharge current is only half that of the instantaneous current. With a 2kHz modulation frequency the time averaged extracted current has reached a value of $0.54mA/cm^2$ but has a significant modulation of approximately 40%. At higher modulation frequencies where $f>1/t$, the time averaged extracted current has improved dramatically and the modulation has become small. This effect can be seen more clearly in figure 3.9, which shows the time averaged extracted negative ion and electron current densities as a function of modulation frequency for a deuterium discharge. The source pressure is 2.4mTorr, the discharge current 15A at 1kHz and 13A at 13kHz. The duty cycle is 50% and the discharge voltage is 60V. The change in the discharge current with frequency is due to the rise time of the current pulse which appears limited by the plasma and not the electronics. The electron current density is determined using a small Langmuir probe situated close to central axis of the source near the plasma electrode. The electron flux from the accelerator is not used as this may be affected by the magnetic fields of the electron trap. In figure 3.9 we see the current density is approximately $0.55mA/cm^2$ for modulation frequencies below 2kHz and the time averaged electron current density is $2.5mA/cm^2$. The ratio of extracted negative ion current to extracted electron current, J_H/J_{e^-}, is an important factor in the development of a high current source for use with modern accelerators [14] as the extracted electron current must be dumped before acceleration. In this instance, $f_{mod}<2kHz$ the ratio J_{H^-}/J_{e^-} is approximately $1/50^{th}$.

As the frequency is increased the time averaged negative ion current increases almost linearly for low modulation frequencies. At frequencies above 10kHz the extracted H^- current starts to saturate and it is expected that further increasing the

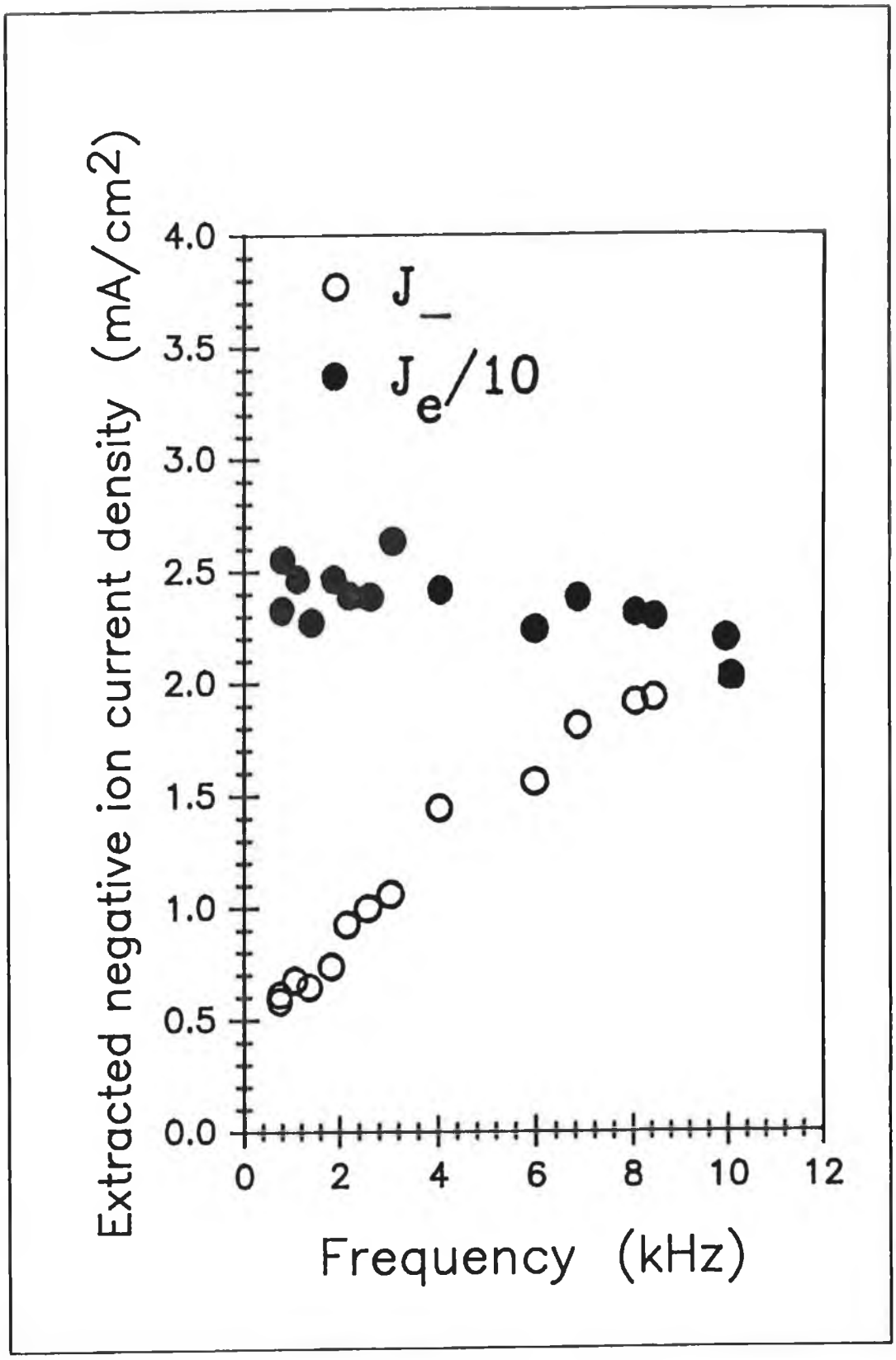

Figure 3.9. Time averaged extracted D^- current as a function of modulation frequency.

frequency will result in a decrease in this current as

$$\tau_{e}^{-} > t_{on} \qquad \text{Eqn. 3.3}$$

At a frequency of 10kHz the extracted negative ion current has increased to 2.2mA/cm^2, an increase of over four times that at lower frequencies. However the electron current, being proportional to Id, the discharge current, has dropped slightly and now the J_{H^-}/J_{e^-} ratio has risen to 1/10. The modulation of the H^- current is less than 2%, which is also important as modulation of the beam may affect the accelerator optics.

3.6. Dependence of extracted current density on duty cycle.

By varying the duty cycle at an optimum modulation frequency, 10kHz to 15kHz, further enhancements in the extracted negative ion current, and in the ratio of J_{H^-}/J_{e^-} can be achieved as the negative ion production is optimised. In this case the modulation frequency is 10kHz, the source pressure is 2.4mTorr and the discharge voltage is 60V. In figure 3.10 the extracted negative ion current densities against time are plotted for various duty cycles. For duty cycles of 88%, virtually a continuous discharge, the extracted current behaves similar to a dc pulse, figure 3.4. It shows a slow rise time to a steady state value of 1mA/cm^2 during the discharge, when the pulse is switched off there is a rapid increase in the extracted current to a peak of 1.6mA/cm^2. As the duty cycle is decreased the dc level approaches that of the post discharge peak value until at duty cycles of 40% to 60% the extracted current density is 2mA/cm^2. Given that the loss time for the thermal electrons in the discharge is approximately 30μs and the loss time in the post discharge for negative ions is greater than 100μs then this plateau in the extracted current, 40% to 60%, is the region which fulfils the condition for enhancement,

$$f_{mod} > \frac{1}{\tau_{e^-}} \qquad \text{Eqn. 3.4}$$

As the duty cycle is reduced below this value then the on time becomes less than the electron loss time and no build up in the densities can occur during the discharge. This can be seen more clearly in figure 3.11 where the time averaged

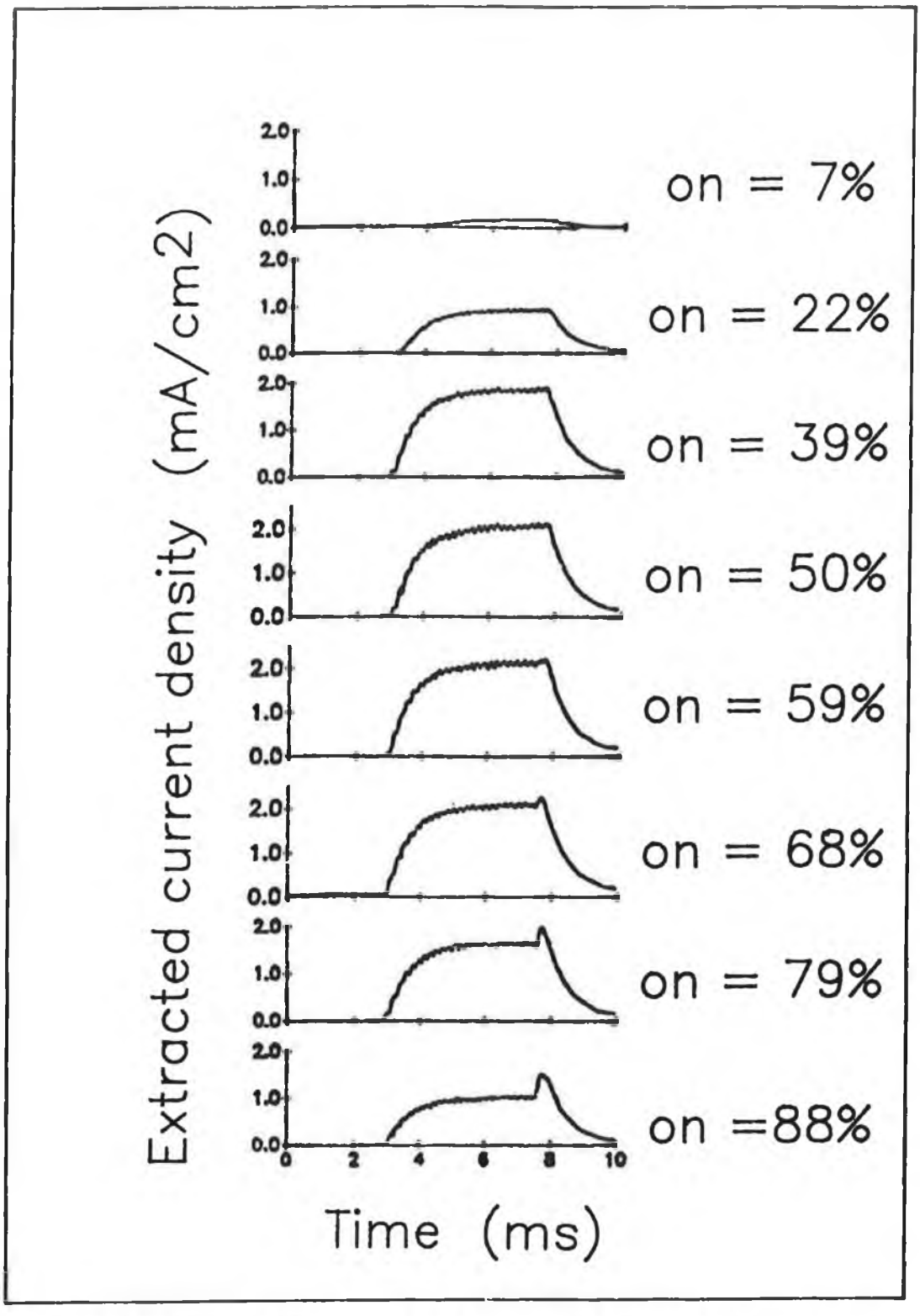

Figure 3.10. Extracted D^- current as a function of time for different duty cycles.

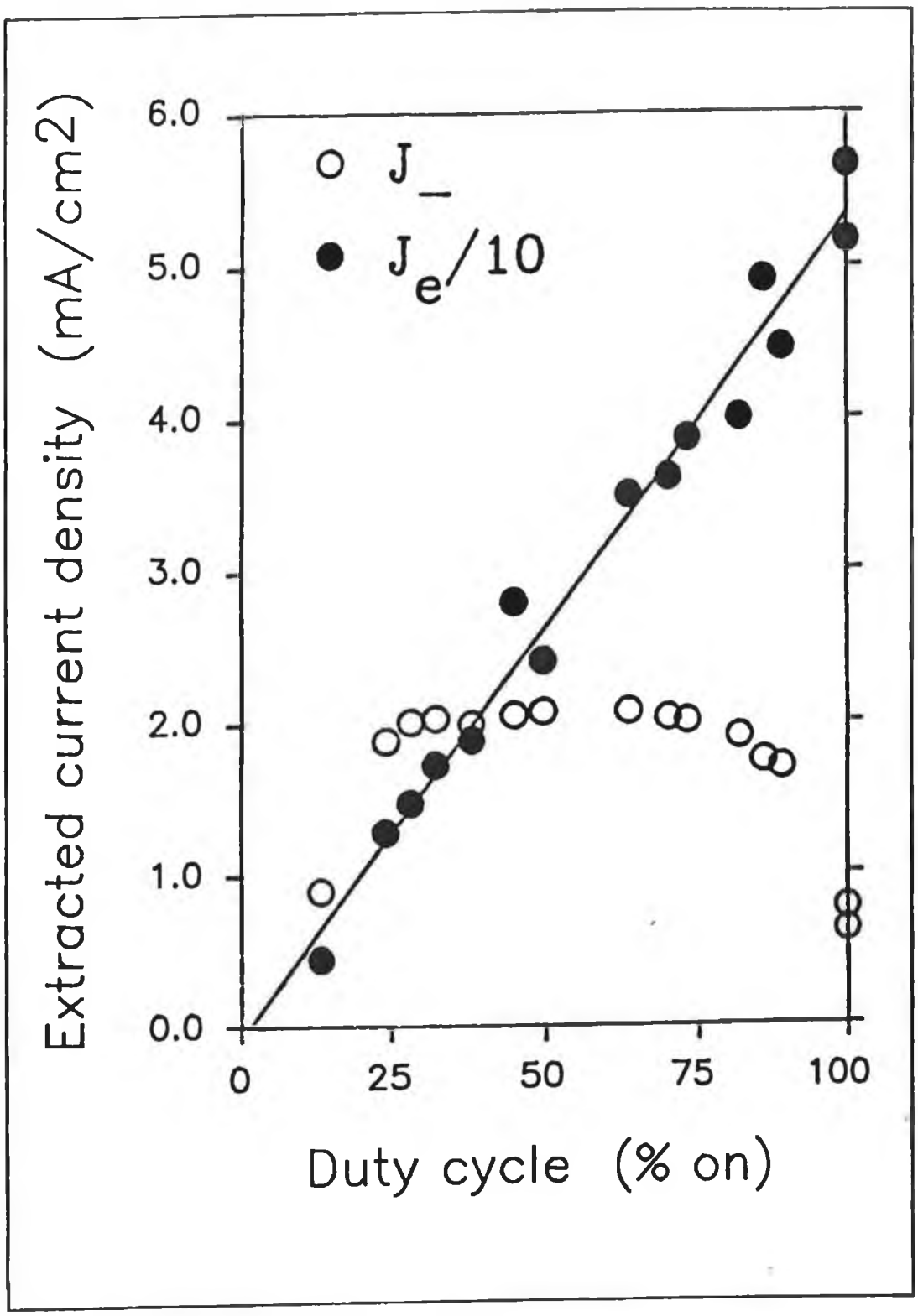

Figure 3.11. Time averaged extracted D^- current density as a function of duty cycle.

extracted H^- current is plotted as a function of duty cycle. At 100% duty cycle, a continuous discharge, and with discharge current of 15A, the negative ion extracted current density is 0.55mA/cm^2. As the duty cycle is decreased the extracted current increases to a plateau between 60% to 40%, here the extracted current density is 2mA/cm^2. Looking at the extracted current at 30% duty cycle it is seen that it has increased to almost four times the continuous level but the discharge current is only 30%, less than 5A, this shows a factor of 12 in overall improvement in the power efficiency, further the electron current to negative ion current ratio has improved from a factor of 100 to a factor of 8. Again the extracted beam is not modulated. This plateau region between 40% to 60% represents the optimum on/off conditions for two stage production of H^- for this source. For modulation duty cycles of 60%,

$$\tau_{H^-} \approx t_{off} \qquad \textbf{Eqn. 3.5}$$

below 30% on time the condition ,

$$\tau_{e^-} < t_{on} \qquad \textbf{Eqn. 3.6}$$

is not fulfilled as t_{on} <30μs, in this region the electron density does not have time to build up sufficiently during the discharge and the subsequent negative ion density starts to decrease. Due to their long lifetime the $H_2(v^*)$ levels may build up over several cycles to a higher, pumped, density but the rise time of the fast electrons after switch on may also limit the vibrational density by losses via ionisation by fast electrons.

3.7. Conclusion.

The increase in the extracted H^- current density after the discharge is switched off, as proposed in chapter 2, has been verified by extraction results, this increase appears to confirm the two stage H^- production process, EV and DA, as being a dominant mechanism in the volume source. This increase can be used, by appropriate modulation, to improve the time averaged extracted current density form the source. At a frequency of 10kHz and duty cycle 30% an extracted current density of four times that of a continuous discharge has been observed with less than 30% of the power. Further a parallel reduction in the electron current, with much improved J_H/J_{e^-}

ratio, can be achieved. The modulation of the beam was less than 2%. The frequency of modulation is shown to be dependent upon the characteristic loss times of the plasma species. Thus the pulsed discharge shows an improvement in the power efficiency of the source and also allows operation at much lower pressures.

References.

[1] Hopkins, M.B. and Mellon, K.N.
Physics Review Letters, 67 (4), p449, 1991.

[2] Hopkins, M.B, Bacal, M. and Graham, W.G.
Journal of Applied Physics, 70 (40), p2009, 1991.

[3] Heeren, R.M.A, et al.
Europhysics Letters, 17 (6), p503-508, 1992.

[4] Scanlan, J.V.
PhD Thesis, 1991.

[5] Janev, R.K, Langer, W.D, Evans, K. and Post, D.E.
"Elementary processes in Hydrogen-Helium Plasmas"
Springer-Verlag, Berlin, London, New York, 1987.

[6] Lefebure, M, et al.
"Proc. Production and Application of light negative ions"
Paris, 1986.

[7] Hopkins, M.B. and Graham, W.G.
Journal of Applied Physics, 69, p3461, 1991.

[8] Hopkins, M.B, Bacal, M. and Graham, W.G.
Journal of Physics D, Applied Physics, 24, p268-276, 1991.

[9] Bacal, M, et al.
Journal of Applied Physics, 55 (1), p15-24, 1984.

[10] Gorse, C. and Capitelli, M.
Private communication.

[11] Holmes, A.J.T, at al.
Review of Scientific Instruments, 58 (2), p223, 1987.

[12] Holmes, A.J.T, Dammertz, G. and Green, T.S.
Review of Scientific Instruments, 56 (9), p1697, 1985.

[13] Hopkins, M.B.
"4th European Workshop on the production and Application of light negative ions." 26-28 March, Belfast, 1991.

[14] Hemsworth, R.S.
"Plasma Physics and Nuclear Fusion Research."
Academic Press, London and New York, 1981.

Chapter 4. Modulation of the DENISE[1] source at FOM[2].

4.0. Introduction

A series of experiments were carried out on the volume negative ion source at FOM. These experiments were to investigate the effect of modulating the source at high frequencies, up to 20kHz, and to extract a negative ion beam from the modulated source [1]. While the FOM source differs from the D.C.U. source in several ways it is expected that the current density will show a similar behaviour after switch off. The FOM source and accelerator has been well characterised by Eenhuistra et al [2,3] for dc discharges. A simple model has been developed based on the FOM source and is used to confirm the extracted results. It is also expected that differences in the behaviour of the two sources will be an invaluable insight in to the processes leading to enhancements when pulsing discharges.

4.1. The DENISE volume ion source

The DENISE volume source is a medium sized multicusp ion source, figure 4.1. It is a magnetic multipole bucket source of dimensions 14cm * 14cm * 19cm. Three sets of two tungsten filaments are mounted on the front plate. The walls are watercooled and made from oxygen free copper and covered by a layer of tungsten evaporated from the filaments.

4.2. The extraction system

The plasma electrode is a 3mm thick plate with an aperature of 8mm diameter, figure 4.1. Mounted 3mm behind this plasma electrode is the extraction electrode, again with an aperature of 8mm diameter and can be biased 4kV positive with respect to the plasma electrode. This extraction electrode, which is 12mm thick, consists of two plates, small magnets are placed in these plates, in an octopole arrangement to prevent electrons reaching the detector. These magnets result in a magnetic field

---

[1] **DENISE:** *DEnse Negative Ion Source Experiment.*

[2] **FOM:** *Institute for Atomic and Molecular Physics*
Kruislaan 407, 1098 SJ, Amsterdam, The Netherlands.

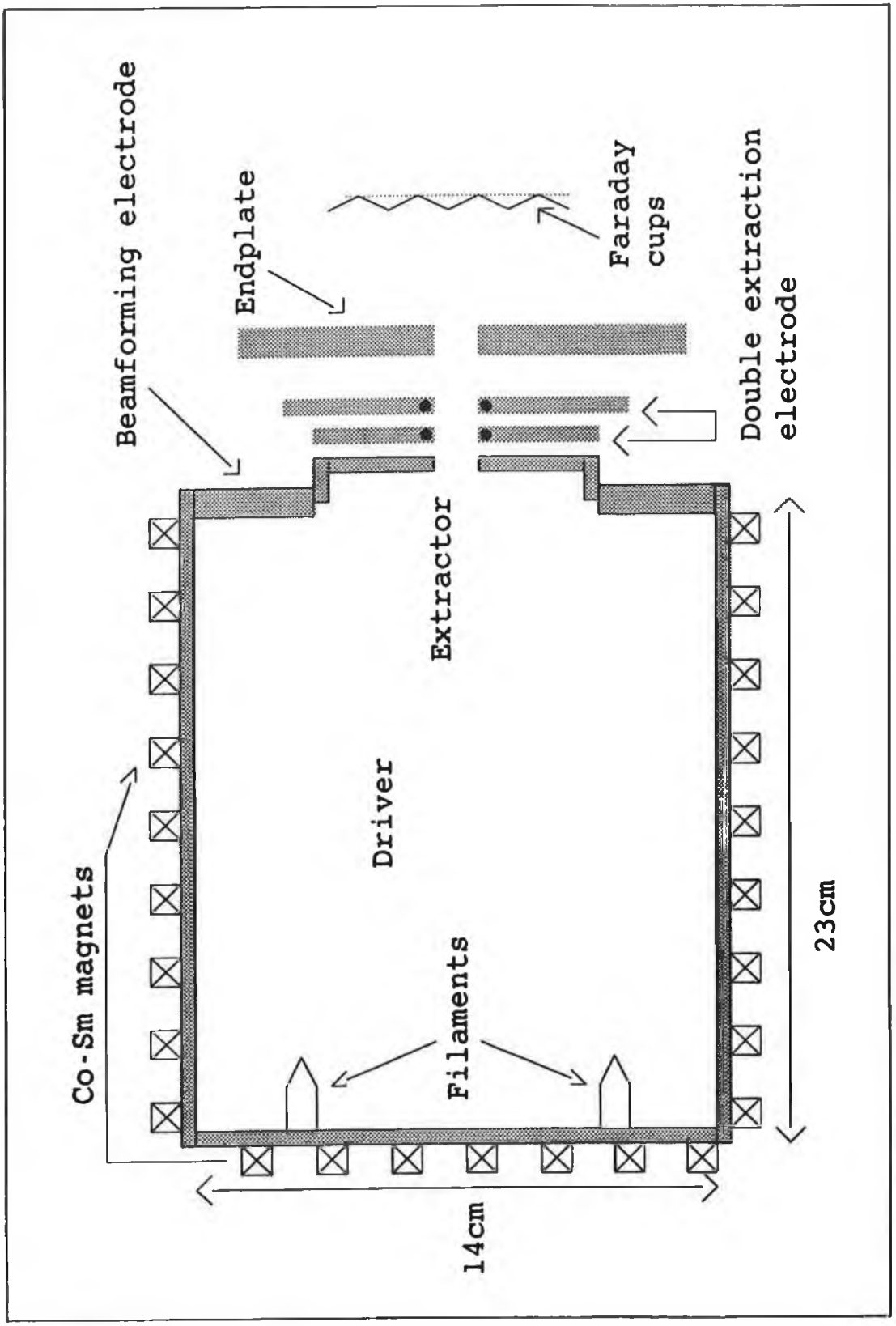

Figure 4.1. Schematic representation of the DENISE volume ion source at FOM in Amsterdam.

strength of B>1000G across the aperature. These two plates are connected by a 10kΩ resistor. If electrons arrive at the second plate it will become negative with respect to the first plate and this helps to suppress the electrons. Also secondary electrons emitted from the first plate are prevented from being accelerated to the detector [2]. Behind these plates an end plate is mounted and 30mm behind this are the faraday cups. The total acceleration voltage is 15kV. The source is run in this experiment without a magnetic filter and the front plate is on wall potential through a variable resistor.

4.3. Pulsing DENISE

A pulsing unit similar to the one described in chapter 3 was inserted in series with the arc power supply, this allowed the discharge current to be switched on and off at frequencies between 240Hz and 20kHz. The duty cycle was variable between 8% and 90%. For lower frequencies the rise time of the discharge pulse was negligible compared to the pulse width but at higher frequencies the rise time becomes comparable to the pulse width, f_{mod}>10kHz, while the fall time remains minimal. This effect is not due to the pulsing electronics but rather to the plasma itself. In this experiment the discharge is continuously modulated rather than pulse modulated, the accelerator is switched on some time after the discharge and the measurements were taken when the system had reached quasi-equilibrium. Also note that the filament current is on continuously and only the emission current is switched. This is not believed to be a major factor as the heater voltage is only 10V compared to 50V in the D.C.U. source and only low energy electrons can be emitted when the discharge current is off.

4.4. Extraction of negative ions from DENISE

The time resolved extracted current here shows a similar behaviour to that of the D.C.U. source. In figure 4.2 a plot of the extracted current as a function of time for a continuously pulsed discharge is shown. The modulation frequency is 240Hz, the discharge current is 4.7A, the extraction voltage is 2.99kV. The source pressure is 6.2mTorr and the plot shown is averaged over 1000 sweeps. The H^- current rises

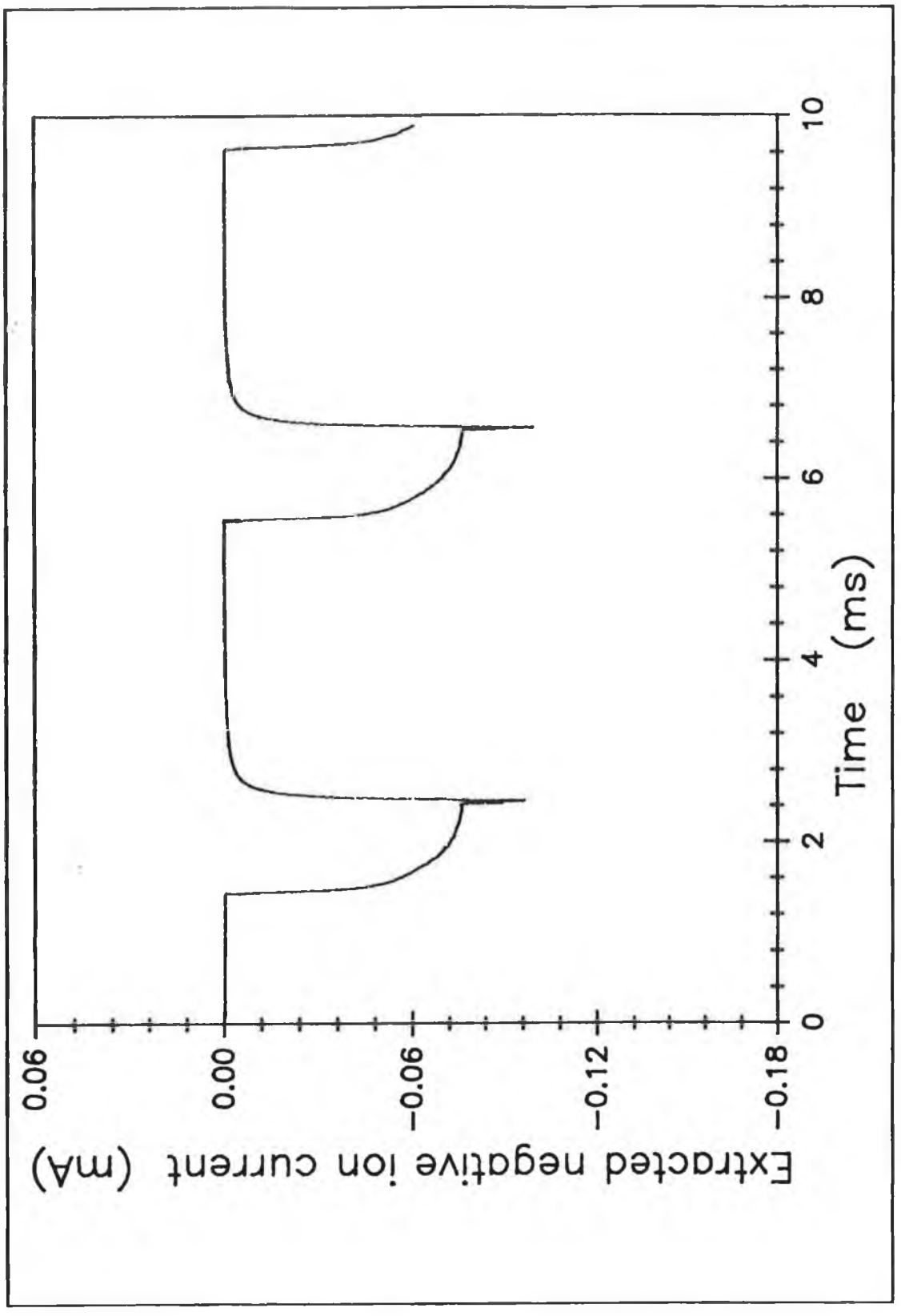

Figure 4.2. Extracted H^- current as a function of time from a continuously pulsed discharge. f_{mod}=240Hz, Id=4.7A, P=6.2mTorr.

slowly to a steady state level in approximately 0.6-0.7ms. The discharge is switched off after 1ms and as before, the extracted current shows a dramatic increase reaching a value 1.3 times that of the continuous, the dc value is 0.06mA, while the peak value is 0.081mA, the extracted current then decays away with a loss time of 90μs. This behaviour is as expected for a driver region however there are substantial differences than the results shown in chapter 3. The peak rise time is shorter, here it is only 40μs compared to 90μs and the source pressure is much higher, greater than 5mTorr. The rise time has been found to be a function of position in the chamber and is discussed in more detail in chapter 5. The higher pressure may be explained by the higher power densities in this source, 0.9W/m^2, than in the D.C.U. source 0.09W/m^2. The electron temperature will be higher and thus the cooling of the EEDF to a value optimised for DA will occur at higher pressures. As already discussed in chapter 3 the occurance of a peak in the post discharge is dependent upon a hot electron temperature >1eV and/or a high density of fast electrons. Eenhuistra et al [2] have shown that the maximum extracted H^- current from this source, operated in continuous fashion without a magnetic filter, occurs at 15mTorr. This is the pressure at which the two stage production process is most effective. In the D.C.U. source the maximum occurs at much lower pressures, 3-5mTorr, and subsequently the post discharge peak disappears at source pressures above 5mTorr. In the DENISE source the enhancements occur upto 15mTorr and above this no peak is observed. Eenhuistra has further shown the electron temperature for a 10A, 100v discharge to be 0.7eV at 15mtorr and to increase with lower pressures to 1.6eV at 2.5mtorr. This has been explained by the higher power densities in DENISE. Also the fast electron density has be given as approximately 1% the thermal electron density, thus the effect of CD losses in the post discharge will not be as dominant a factor as in the D.C.U. source and the enhancement in the post discharge, at high pressures 5-15mTorr, will be due to the high electron temperature during the discharge.

4.5. Model for negative ion production

A simple model based on the parameters for dc operation of the FOM source given by Eenhuistra [2,3], was used to predict the temporal behaviour of the pulsed discharge [1]. A similar but more rigorous model based on the D.C.U. source is

discussed in chapter 2 and results presented in chapter 6. Here the electron density, the atomic density and the ion density are given by Eenhuistra and are assumed to be constant in the discharge and the post discharge with the primary electron density being given for the discharge and set to zero for the post discharge.

The production and loss rates for $H_2(v^*)$ and H^- here are, as in chapter 2, combined in a set of differential equations. These equations are then used to model the behaviour of these densities in the pulsed discharge. During the on period of the discharge the evolution of the densities is given by equation 2.46 and 2.47,

$$\frac{dnv''}{dt}on = n_g n_p \langle \sigma_{EV} v_p \rangle - \frac{n''}{\tau''_{on}} \qquad \text{Eqn. 4.1}$$

$$\frac{dn^-}{dt}on = n'' n_e \langle \sigma_{DA} v_e \rangle - \frac{n^-}{\tau^-_{on}} \qquad \text{Eqn. 4.2}$$

The evolution of the densities in the post discharge is given by equations 2.52 and 2.53,

$$\frac{dnv''}{dt}off = -\frac{n''}{\tau''_{off}} \qquad \text{Eqn. 4.3}$$

$$\frac{dn^-}{dt}off = n'' n_e \langle \sigma_{DA} v_e \rangle - \frac{n^-}{\tau^-_{off}} \qquad \text{Eqn. 4.2}$$

Again the rate co-efficients are taken from Eenhuistra and are assumed to be constant. The assumption that the DA rate is constant in the post discharge excludes the enhancement of the negative ion density due to the cooling electron temperature and will lead to an underestimate of the density in the post discharge and it further excludes the reduction in the production rate upon switch on as the electron temperature rises. The second assumption here is that the loss time for the atoms is approximately 90μs. In the post discharge the density of atoms will decay away and the time averaged density will be substantially lower than in the discharge. For this reason only a fraction, F, of the atomic density during the discharge is used in the post discharge. The primary density is zero after switch off and thus the vibrational loss time in the post discharge is given by,

$$\tau''_{off} = \frac{1}{\left(\frac{V''}{b''L''}\right) + n_g\langle\sigma_g v_g\rangle + n_e\langle\sigma DA v_e\rangle + n_h\langle\sigma_{VT} v_h\rangle} \qquad \text{Eqn. 4.5}$$

and the loss time for H^- in the post discharge is,

$$\tau_{-off} = \frac{1}{\left(\frac{V^-}{L^-}\right) + n_h\langle\sigma_{AD} v_h\rangle + n_+\langle\sigma_{MN} v_+\rangle} \qquad \text{Eqn. 4.6}$$

Again for simplicity the mutual recombination and plasma density are kept constant in time in the post discharge giving an over estimation of the production rate but the loss rate due to mutual recombination is also over estimated. Using these assumptions the equations 4.1, 4.2, 4.3 and 4.4 can be solved yielding the time dependent vibrationally excited and negative ion densities. Figure 4.3 (a) shows the calculated H^- density as a function of time for a pulse frequency of 6.8kHz at various duty cycles for a 5.6mTorr, 20A pulse current and 100V discharge. The results shown are preceded by enough cycles to ensure that the system is in quasi-equilibrium. At t=0 when the discharge switches on, the H^- density starts to decrease. This because of the increased loss rates, as the primary density has a rise time of <1μs, and a decrease in production occurs as the DA cross section falls when the electron temperature increases. As the bulk electron density starts to increase, the production increases and the density rises. The moment the discharge is switched off the losses are reduced, the production increases and the density subsequently increases. After peaking the density decays away until the discharge is switched on again. The model predicts no time averaged increase in the extracted density, this is due to the loss of density at switch on. In order to determine the accuracy of the model figure 4.3 (b) shows typical oscilloscope traces of the extracted negative ion density from a pulsed source. The traces are the average of 1000 sweeps. Again these were taken sufficiently long after the start to ensure a quasi-equilibrium discharge. The discharge conditions are the same as the ones used in the modelled densities. The experimental data shows a similar behaviour to that of the calculations, there is no obvious enhancement in the extracted current in a pulsed discharge over a continuous discharge of similar power, although the data shows an enhancement in the post discharge this is countered by the

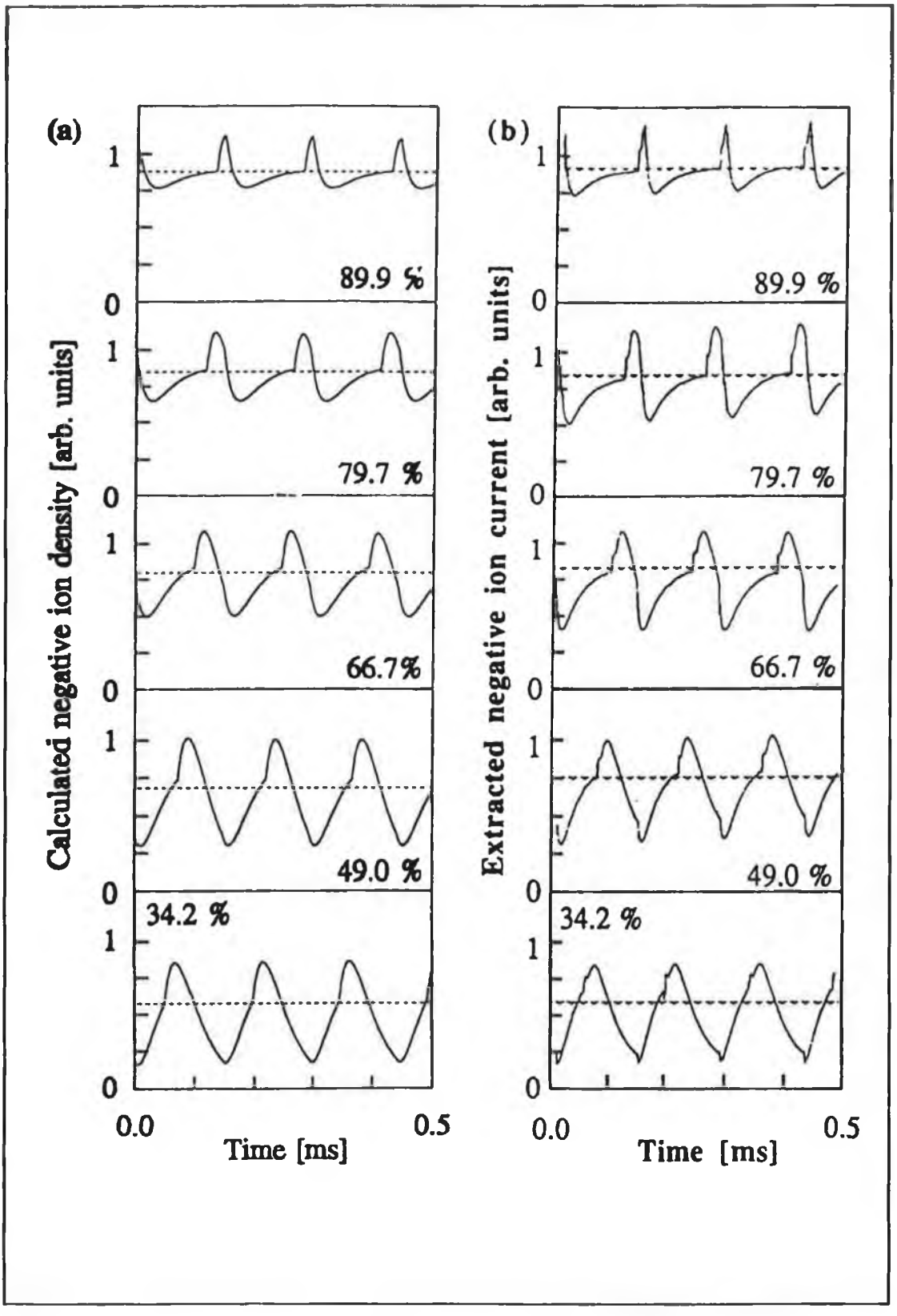

Figure 4.3. (a) Calculated H^- density and (b) extracted H^- current for several duty cycles in a 6.8kHz modulated discharge.

losses at the start of the pulse. This implies that the densities and other parameters used in the calculations, which were taken from the values given by Eenhuistra for a dc operated source appear to be accurate, also the calculations appear to indicate that the enhancement in post discharge is due to the effects of reduced CD losses and kT_e cooling. The model used here to predict the temporal behaviour of a modulated discharge gives a somewhat fortuitous agreement with the experimental data but nevertheless it is useful in giving an insight into the basic processes responsible for the temporal behaviour. It has several limitations which affect it's real usefulness in predicting accurately the post discharge and time averaged effects on the negative ion density. The most important of these is the use of a constant dissociative attachment rate in the model, this will change slightly from switch on to reaching a quasi steady state but more importantly the cooling of the electron temperature in the post discharge should result in a much different DA rate. While this is countered here by using a decreasing loss rate in the post discharge for AD by atomic hydrogen the effect is too important to be neglected. The requirement for a time varying DA rate can be verified by looking at the H^- density at switch on, the negative ion density is rapidly decreased at switch on, much more so than the model predicts. This depletion is due to the fast electron density rapidly building up, as shown in the model, and more importantly to the lowering of the DA rate as the electron temperature increases, the experimental traces show this much faster decrease. This depletion is a very important factor as it can be responsible for the depth of modulation of the extracted beam.

A second limitation of the model is that the electron density is not shown to be modulated but the vibrationally excited levels are assumed to be highly modulated. This modulation of the $H_2(v^*)$ density is explained as being due to their short lifetime, $\tau_{v^*}<50\mu s$. The model here assumes a high wall loss rate for $H_2(v^*)$, due to setting $b^{v^*}=1$, caused by the high power density of the source. Previous work has indicated that τ^{v^*} should be of the order of 1ms [4]. It is assumed here that the modulation of H^- is due to this $H_2(v^*)$ modulation when it appears more likely to be a result of the varying electron density.

4.6. High frequency modulation.

In the above figure no effective increase in the time averaged calculated density or the extracted current is observed. In this instance the pressure was 5.6mTorr, and the post discharge peak rise time was 20μs, assuming a loss time for the electron density of 30μs then the frequency of modulation needed for an enhancement is around 20kHz, under the conditions,

$$\tau_{e^-} < t_{on} \quad , \quad \tau_{-} > t_{off} \qquad \text{Eqn. 4.7}$$

In the D.C.U. source it was stated that at pressures above 5mTorr there was sufficient degradation of the primaries and cooling of the electron temperature during the discharge for no increase to occur. In this case an increase in the post discharge is seen but no enhancement occurs, this may due to the low modulation frequency and an insufficient enhancement of the DA rate. In figure 4.4, the time averaged extracted current for a pulsed discharge and the dc extracted currents are plotted against the average discharge current for two pressures. At the higher pressure of 5.6mTorr, the average extracted current from a 6.8kHz modulated discharge is similar to that from a dc discharge. However at a lower pressure, 2.8mTorr, the time averaged extracted current from a 10kHz discharge is approximately 35% higher than from a dc discharge of the same average power. It can also be seen that the average extracted current from a 10kHz pulsed discharge at 2.8mTorr is similar to the dc level at 5.6mTorr thus it is possible to reduce the operating pressure without decreasing the negative ion yield. Further in figure 4.5 the time averaged extracted current is plotted as a function of the average discharge current for two modulation frequencies at 50% duty cycle and 4.5mTorr. For a modulation frequency of 440Hz the time averaged current is similar to that from a dc operated discharge of similar power. However the discharge modulated at 5.8kHz shows an increase over the 440Hz discharge. At 5A an increase of 30% is observed, at 15A this is 38% and above this it increases to 44% at 23A. This improved enhancement at higher discharge currents is explained by an increasing electron temperature, in a 7.5mTorr discharge the electron temperature increases from 0.8eV at 5A to 1.4 at 30A [2], and increasing fast electron density. As will be shown in chapter 5, the post discharge enhancement increases dramatically at higher currents and an extrapolation of the extracted current densities would seem to indicate the

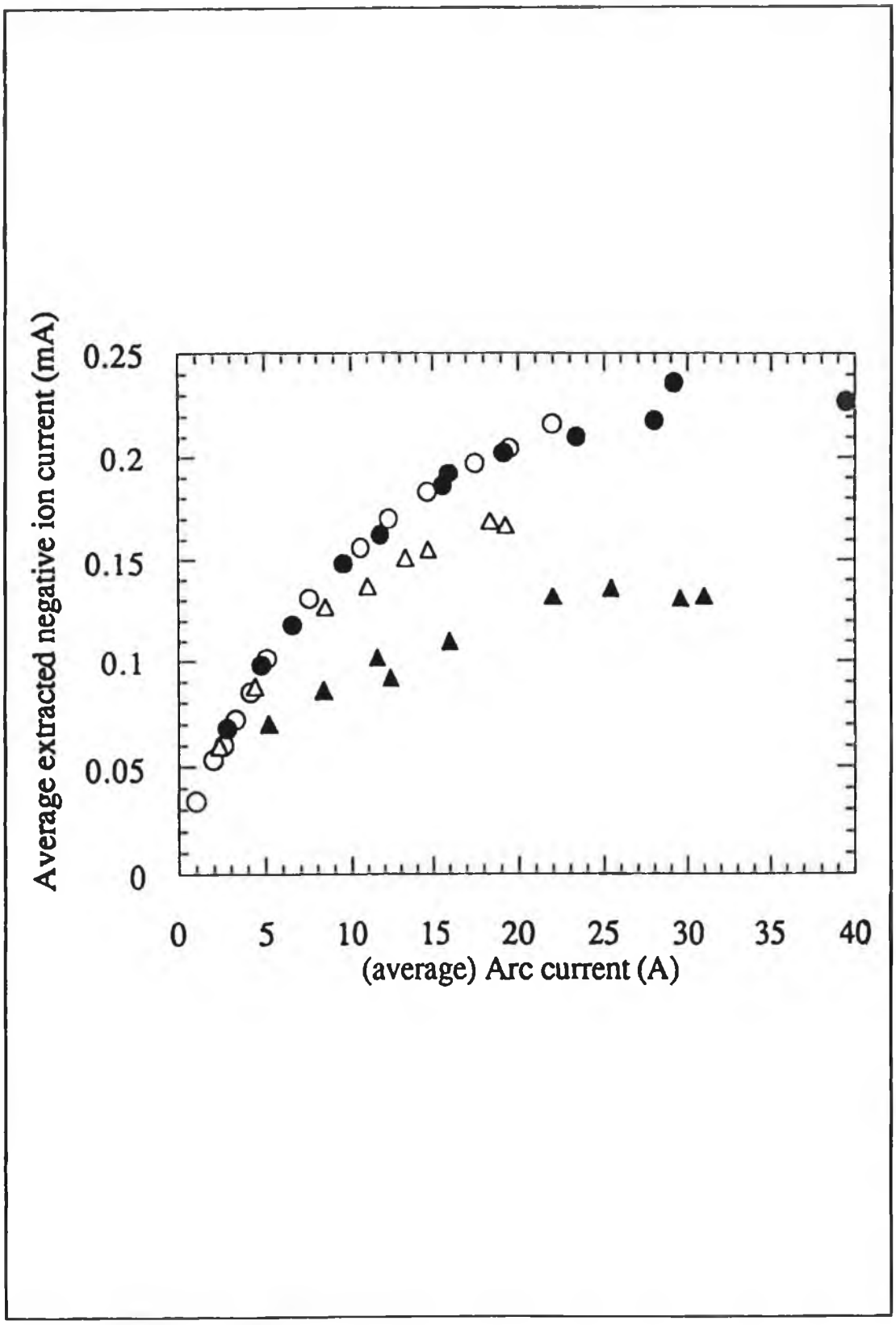

Figure 4.4. Extracted H^- current for a pulsed, (open symbols) and a dc, (closed symbols), discharge at 5.6mTorr and 2.7mTorr.

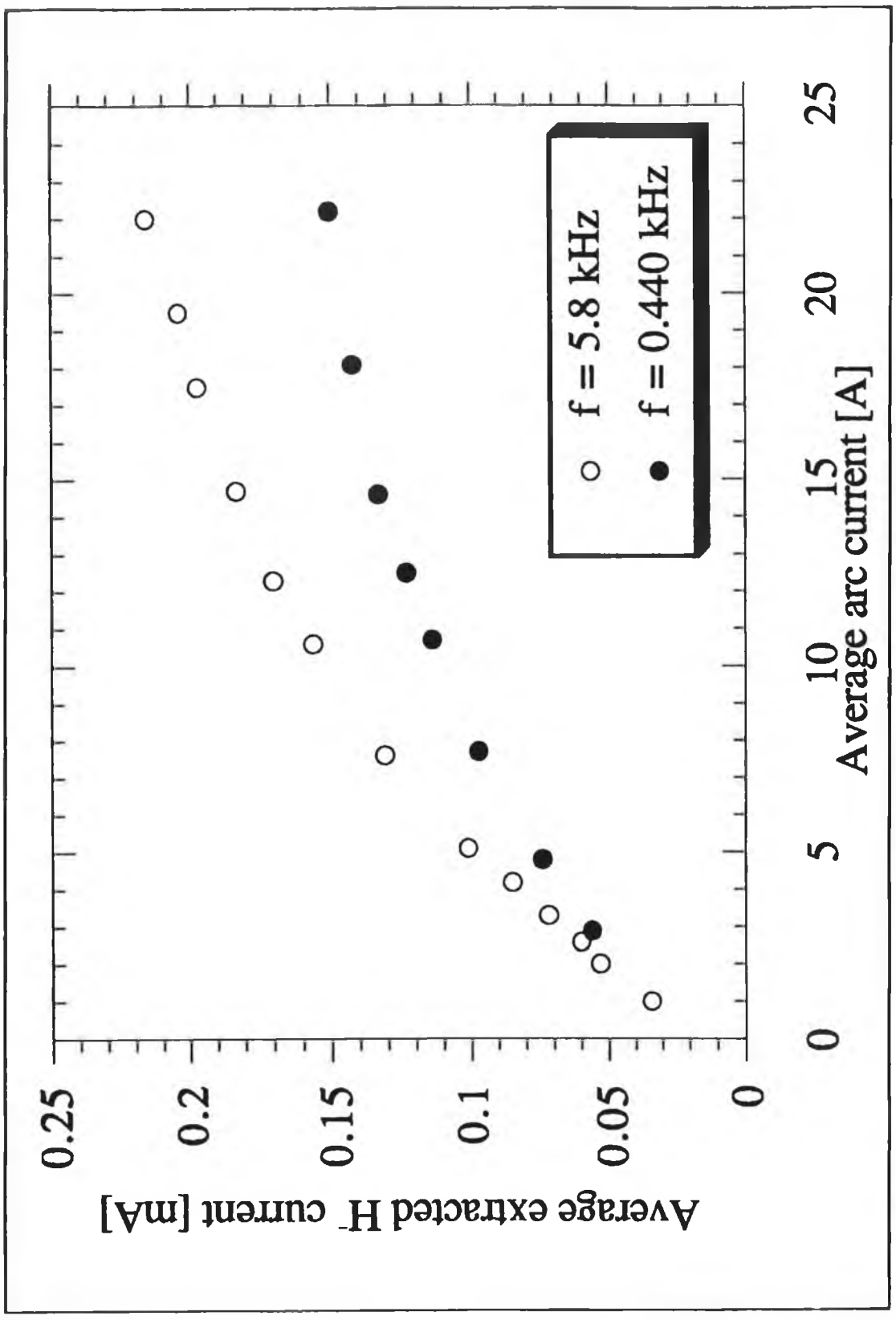

Figure 4.5. Time averaged extracted H^- current as a function of discharge current for 440Hz and 5.8kHz modulated discharges.

possibility of a much larger improvement by pulsing at higher powers, Id>100A. Also from figure 4.4 it can be seen that the enhancements in the time averaged extracted current are more significant at lower pressures, at 3.6mTorr a 35% increase is seen. Thus it can be speculated that a high power, greater than 100A, low pressure, less than 1mTorr, discharge pulsed at an optimum frequency and duty cycle would show a substantial increase over a dc discharge of similar power. However it is also predicted that the extracted beam in this case will be highly modulated.The dependence of the calculated densities upon discharge current agrees qualitatively with the experimental behaviour. At high pressures no enhancement is seen in the time averaged current. However the model also predicts that no enhancement in the average density occurs at lower pressures. This is because the model makes no allowances for the increase in the DA rate in the post discharge and it is this enhancement that results in the increase at lower pressures.

4.7. Peak rise times in the post discharge.

The time constants of the post discharge peaks can give invaluable insight into the processes responsible for production and destruction in the plasma. The loss rate in the post discharge is easily determined from the decay of the peak, and the loss times in the discharge may be determined from the rise time of the peak in the post discharge and it can be seen here to that this rise time is between 20μs and 40μs. The post discharge peak rise time can also give information on the process most responsible for the enhancement. If the peak is purely a result of decreasing loss rates then the rise time will be sharp. However it can be seen from figure 4.6, which shows the peak rise time as a function of pressure, that the peak rise time is dependent upon the source pressure. The discharge current is 13A, the pulse frequency 4.1kHz with 50% duty cycle. The peak can be seen to broaden exponentially with decreasing pressure from 15mTorr to 2.25mTorr. At the lowest pressures the peak rise time is approximately 40μs and at the highest it is 7μs. This effect cannot be explained purely in terms of decreasing loss rates but rather it is due to the electron temperature of the plasma. As already stated in chapter 3, the electron temperature has a strong dependence on source pressure, at lower pressures the plasma will be hot , with electron temperatures of 2eV to 3eV and as the pressure is increased the EEDF cools.

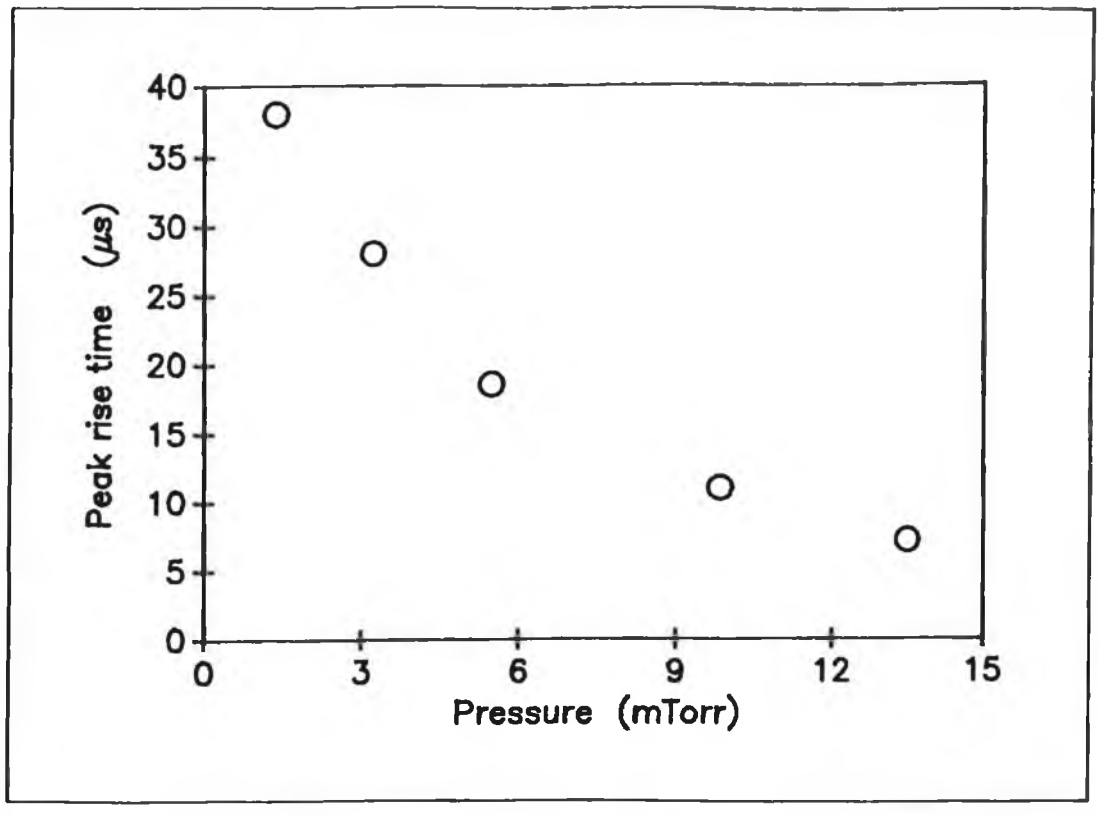

Figure 4.6. Post discharge peak rise time as a function of source pressure. f_{mod}=4.1kHz, Id=13A and duty cycle = 50%.

This change in the electron temperature with pressure [5] can explain the peak rise time dependence on pressure, if the enhancement in the DA cross section is seen as a major factor to the peak rise time then it will depend upon the cooling of the EEDF in the post discharge, at lower pressures the hotter electron temperature means that the production rate due to DA takes longer to reach an optimum value at electron temperatures below 1eV [6], as the pressure increases the EEDF cools sooner and the rise time and the amplitude of the peak decreases. The model used here predicts no change in the peak rise time and this indicates the significance of the enhancement of the DA rate in the post discharge as the model does allow for decreased CD losses. The pressure dependence of the rise time appears much stronger in DENISE than that observed at D.C.U. and again this is a result of the high power density. It will be shown that the peak rise time is dependent upon position in the source, this may also be the case here but it is possible that the high power and shorter distance to the plasma electrode will mean that the whole source operates as a production region.

4.8. Conclusion.

The time averaged extracted current has been shown to increase by almost 50% over a dc operated discharge by modulation at 5.8kHz in a 3.6mTorr, 22A discharge. It is proposed that at lower pressures, <1mTorr, and higher power, >100A, more substantial gains can be achieved by use of appropriate frequency and duty cycle. The source differs substantially from the D.C.U. source but these differences can be explained by the higher power density of the source. Enhancements of the H^- density in the post discharge have been seen at higher pressures than in the D.C.U. source, upto 20mTorr. A simple model based on the plasma parameters and time dependent densities given by Eenhuistra has been used to predict the temporal behaviour of the modulated source and the calculated densities show a reasonable agreement with the measured extracted currents. Again these results indicate that the enhancement is brought about by a coupling of an increased DA rate and decreased CD losses in the post discharge. The extracted results and simple model turn out to be a useful diagnostic tool for determining the processes involved in H^- production at DENISE.

References.

[1] Heeren, R.M.A, Mellon, K.N, Hopkins, M.B, Ciric, D. and Kleyn, A.W.
Europhysics Letters, 17 (6), p503, 1992.

[2] Eenhuistra, PJ, et al.
Journal of Applied Physics, 67 (1), p85, 1990.

[3] Eenhuistra, PJ, et al.
Physics Review A, 40, p3613, 1989.

[4] Lefebure, M, et al.
"Proc. Production and Application of Light Negative Ions."
Paris, 1986.

[5] Hopkins, M.B. and Graham, W.G.
Vacuum, 36 (11,12), p873,1986.

[6] Janev, R.K, Langer, W.D, Evans, K. and Post, D.E.
"Elementary Processes in Hydrogen-Helium Plasmas."
Springer-Verlag, Berlin, London, New York, 1987.

Chapter 5. Measurement of H^- density by Photodetachment.

5.0. Introduction.

The extraction measurements used to date in the preceding chapters have a limitation in that these measurements can only give an insight into the behaviour of the negative ions near the extraction aperture. To better understand the effect of modulating the discharge and to fully utilise the enhancements which may be possible it is necessary to gain information on the behaviour of the negative ion density as a function of position in the source as well as a function of time. Also the extraction results obtained to date do not dispel the possibility that the modulation effects may be purely an accelerator effect and that there is no real increase in the negative ion density in the source.

Several methods have been used to allow measurements of the H^- density to be carried out in the discharge, e.g langmuir probes [1,2] and mass spectrometry [3]. However one of the most successful methods to date is that of photodetachment of the H^- by a pulsed laser [4,5]. This technique is used to spatially resolve the H^- density throughout the discharge and give a better insight into the behaviour of the plasma. Here we present the results of such temporal and spatial measurements in a pulse modulated discharge.

5.1. Measurement of negative ion densities by photodetachment.

Non-laser phtotdetachment measurements were carried out in the 1950's, Branscomb [6]. These experiments used a well collimated beam of light from a carbon arc lamp to detach the electrons from the negative ions in the beam path. However the use of laser beams has made this technique simpler and more versatile.
The photodetachment reaction,

$$H^- + h\upsilon \rightarrow H + e^- \qquad \text{Eqn. 5.1}$$

where $h\upsilon$ has sufficient energy to detach the electron, (electron affinity = 0.75ev), results in a localised increase in the electron density n_e. If the laser

is aligned along a langmuir probe then the probe can be used to detect this increase in n_e. Since the increase in electron density due to photodetachment occurs in the order of 3-5μs temporal resolutions of less than 10μs are possible, this is an important factor as the time scales of processes in the discharge are the order of 10's of microseconds.

A light pulse from a ND-YAG laser can be used for this purpose as the photon energy, 1.1ev, is sufficient to detach the e^- from the negative ion, but is still low enough not to result in other processes such as photoionization, $H \rightarrow H^-$, etc.

The fraction of negative ions in the beam path detached by the laser pulse, $\Delta n^-/n^-$, can be determined from the equation [4] 5.2,

$$\frac{\Delta n^-}{n^-} = 1 - \exp\left[-\frac{energy}{area} * \frac{\sigma^{ph}}{h * \upsilon}\right] \qquad \text{Eqn. 5.2}$$

where σ^{ph} is the cross-section for photodetachment at the photon energy being used, in this case $3.6*10^{-17}$ cm^2 [7,22]. However the cross-section is not necessary if the laser energy is large enough to saturate the photodetachment signal [8]. Once the signal is saturated then the density of negative ions is proportional to the amplitude of the photodetachment signal, ΔI_{e^-}. To calculate the absolute values of H^-, both n_e, the electron density, and I_{e^-}, the plasma and primary electron current to the probe must be known. Then the negative ion density is given by equation 5.3, [4],

$$n_- = n_e * \frac{\Delta I_{e^-}}{I_{e^-}} \qquad \text{Eqn. 5.3}$$

To ensure that the photodetachment signal is free of probe voltage effects and that the signal has saturated, the measurements were made with 45 volts on the probe.

5.2. Apparatus for Photodetachment

The photodetachment configuration is shown in figure 5.1. The langmuir probe used is constructed from tungsten wire, diameter 0.5mm and length 1.5cm, immersed in the plasma. The probe is supported by a glass tube with a ceramic sleeve at the end, the probe holder is inserted in the chamber using a Wilson seal allowing movement of the probe through the plasma. The ceramic sleeve is placed around the

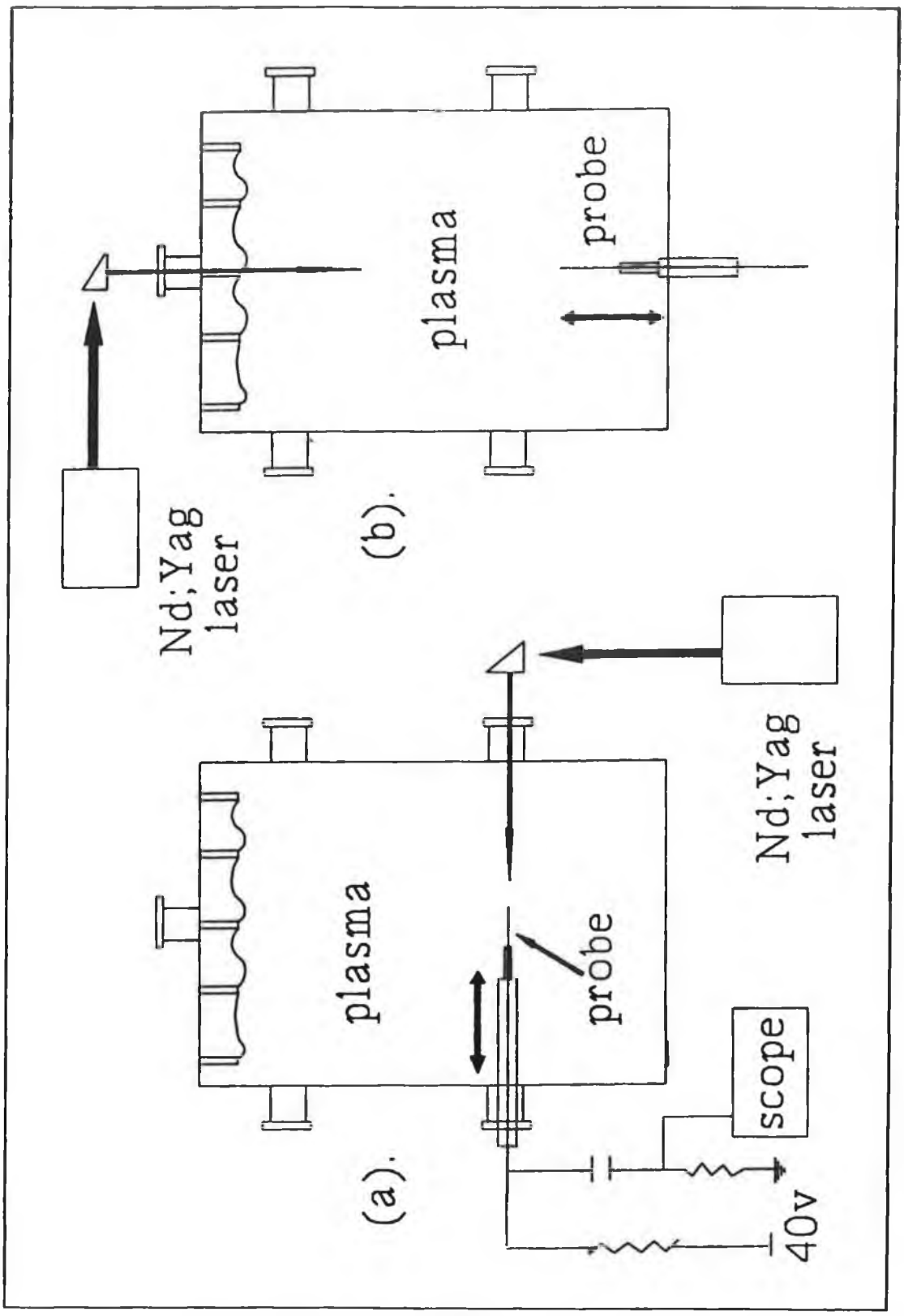

Figure 5.1. **Schematic representation of the photodetachment apparatus showing the configurations for radial (a) and axial (b) measurements.**

tungsten wire, but not touching it, this is to ensure that the probe area is not changed by deposition of carbon or other contaminants on the surrounding probe supports. In the first experiment the probe is inserted through the side of the chamber and the laser enters via the porthole opposite, figure 5.1.(a), this allows radial photodetachment measurements to be made at this position.

The second set of measurements were made with the probe inserted though the end flange, where the accelerator is normally situated, with the laser beam entering though a porthole in the front of the chamber, figure 5.1.(b). This configuration allows spatial measurements to be made in an axial direction through the centre of the chamber.

The laser used is a ND-YAG laser, capable of delivering pulses of 300mJ for 7ns, aligned along the length of the probe. The laser power is measured from the 4% reflected light from the glass port. The electron current signal from the probe is fed into a high pass filter which allows through the fast signal increase due to the photodetachment but filters out the dc level due to the electron current, however the electron current is also recorded. The signal is then captured on a fast storage oscilloscope and can be transferred to a personal computer.

The laser is triggered by a signal which can be moved along the discharge cycle allowing time dependent measurements to be carried out in the discharge and post-discharge periods, figure 3.2.

5.3. Photodetachment Measurements.

Figure 5.2 shows a typical photodetachment signal collected by the probe, configuration 5.1.(a), situated in the centre of the discharge and 15cm from the front wall. The signal was taken in a 2mtorr, 20A discharge with discharge voltage of 60V. The probe voltage is 45V. The rise time is 0.1μs and the decay time 1.1μs. For the purposes of determining the densities of H^- in the discharge we are only concerned with the amplitude of the current increase and not the time scales. However it has been shown that the signal rise and decay times can give information about negative ion transport properties in the discharge [5],[8].

To ensure that the measured signal is in fact the photodetachment of H^-, and not some other photon effect, several precautions are necessary. The photon energy

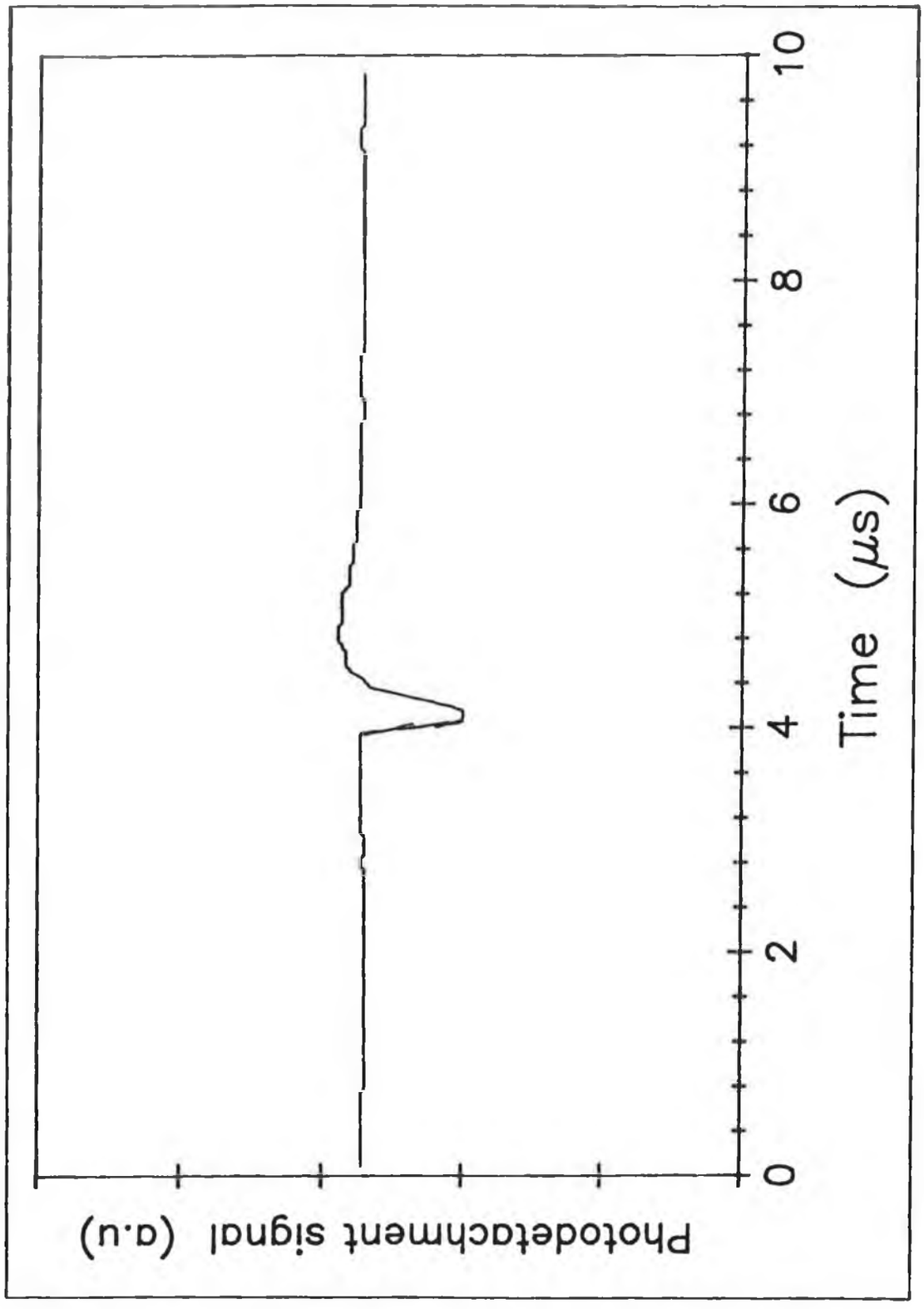

Figure 5.2. Typical photodetachment signal for a 20A, 2mTorr discharge.

must be such that it is high enough to overcome the electron affinity for H^-, (0.7ev), but still low enough to be below the threshold of other photon interactions such as photoionization, photoemission or photodetachment of other species. Species such as OH^-, O^- and O_2^- may be detached at the energy being used, but the cross-sections for these are one or two orders less than for H^- [6].

The fraction of negative ions detached for a given energy is given by equation 5.2,

$$\frac{\Delta n^-}{n^-} = 1 - \exp\left[-\frac{energy}{area} * \frac{\sigma^{ph}}{h*\upsilon}\right] \qquad \text{Eqn. 5.2}$$

This theoretical value can be compared with an experimental plot of laser energy against the percentage of H^- in path of laser beam detached, a correlation between these two ensures that the signal is a negative ion effect.

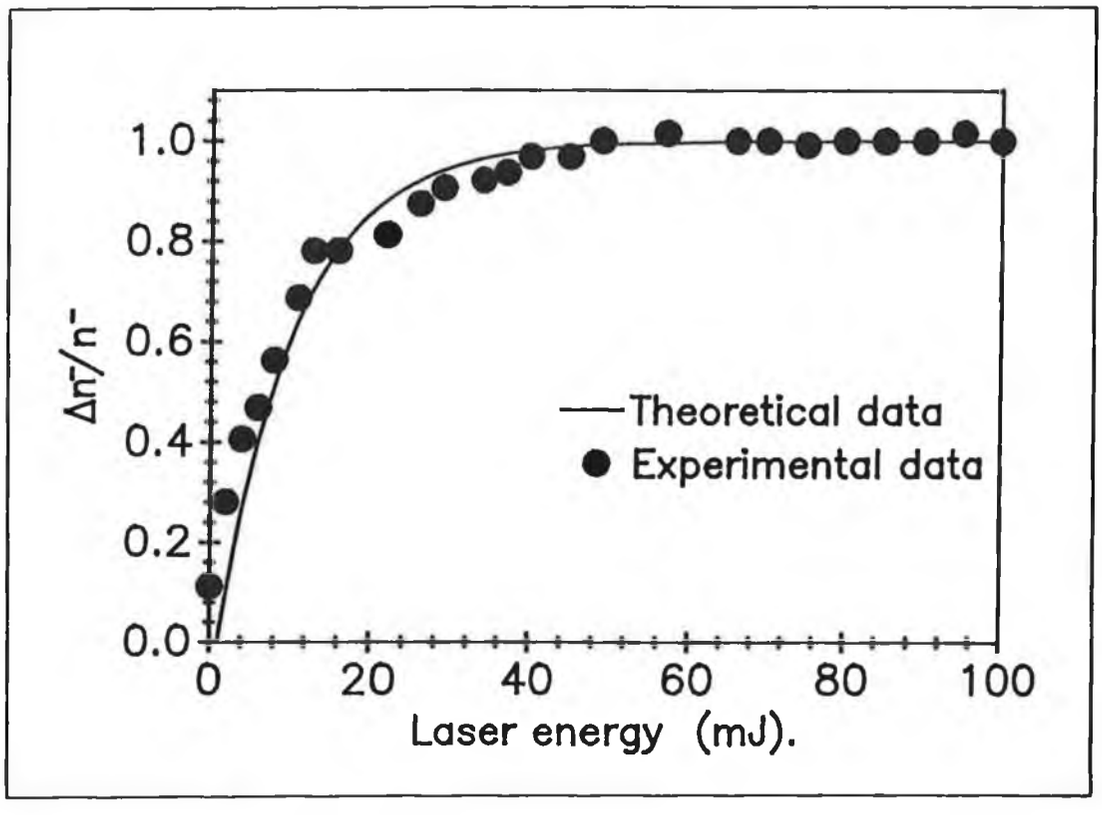

Figure 5.3. Theoretical and experimental dependence of $\Delta n/n$ on laser energy. Id=10A, P=1mTorr.

Figure 5.3 shows both the theoretical and experimental saturation curves, the

experimental signal saturates at energy levels above 50mJ giving good agreement with the theoretical curve.

The dependence of the photodetachment signal with probe voltage is plotted

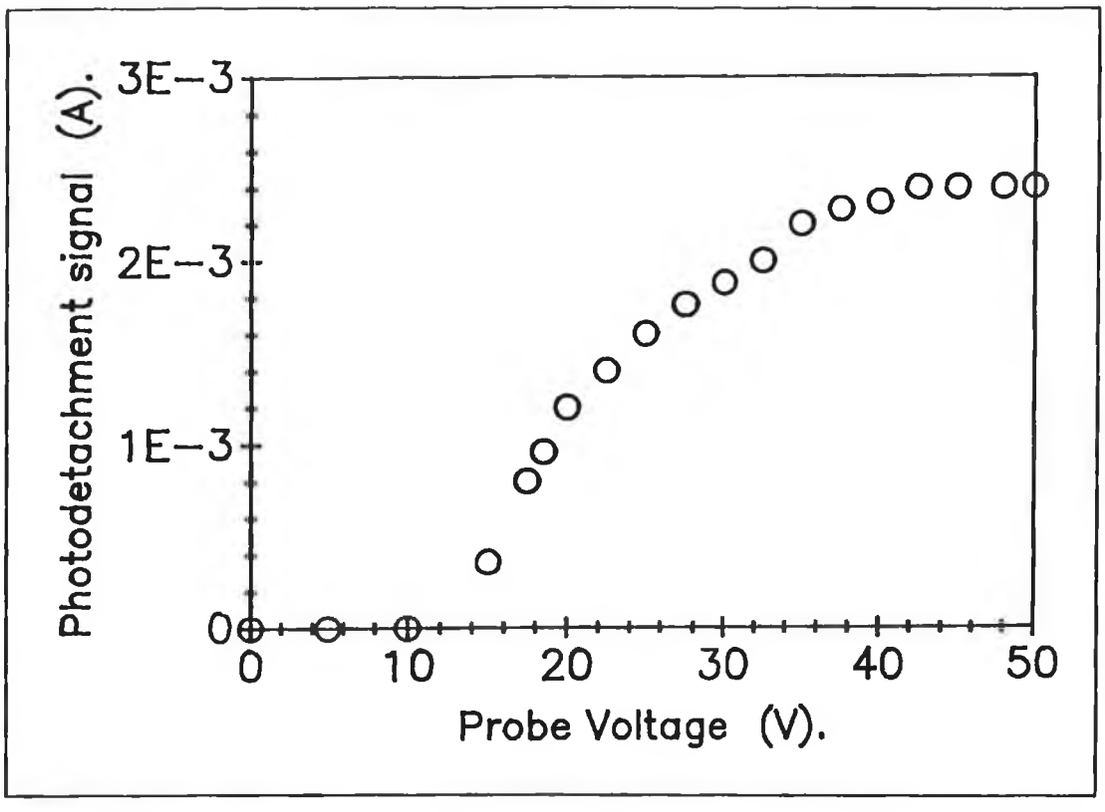

Figure 5.4. Photodetachment signal dependence on probe voltage. Id=10A, P=1mTorr.

in figure 5.4. Again to avoid the possibility of probe voltage effects all photodetachment measurements are taken in the saturation region of the curve at 45V. Other tests taken are to run the plasma with the laser off and ensure that no signal is present and to prevent the possibility of effects due to laser interactions with the probe or surroundings, the laser is fired with no plasma present. Finally the laser is fired at the probe in an inert gas discharge, argon or helium, to check if the effect is due to positive ions or electrons. Before measurements are taken the probe must be cleaned, the laser beam re-aligned and the signal must be checked for saturation with laser energy.

5.4 Current and Pressure dependence of the Photodetachment signal.

The dependence of the negative ion density with pressure and current was measured with the configuration as in 5.1.(b). The probe was in the centre of the chamber 19.5cm from the plasma electrode. The discharge voltage was 60v and the probe voltage was 45V. Figure 5.5 shows the pressure dependence of the photodetachment signal for discharge currents of 10A and 50A. Previous publications [9,10], and the extraction results presented in chapters 2 and 3, have already shown the negative ion density in the source to be a strong function of pressure.

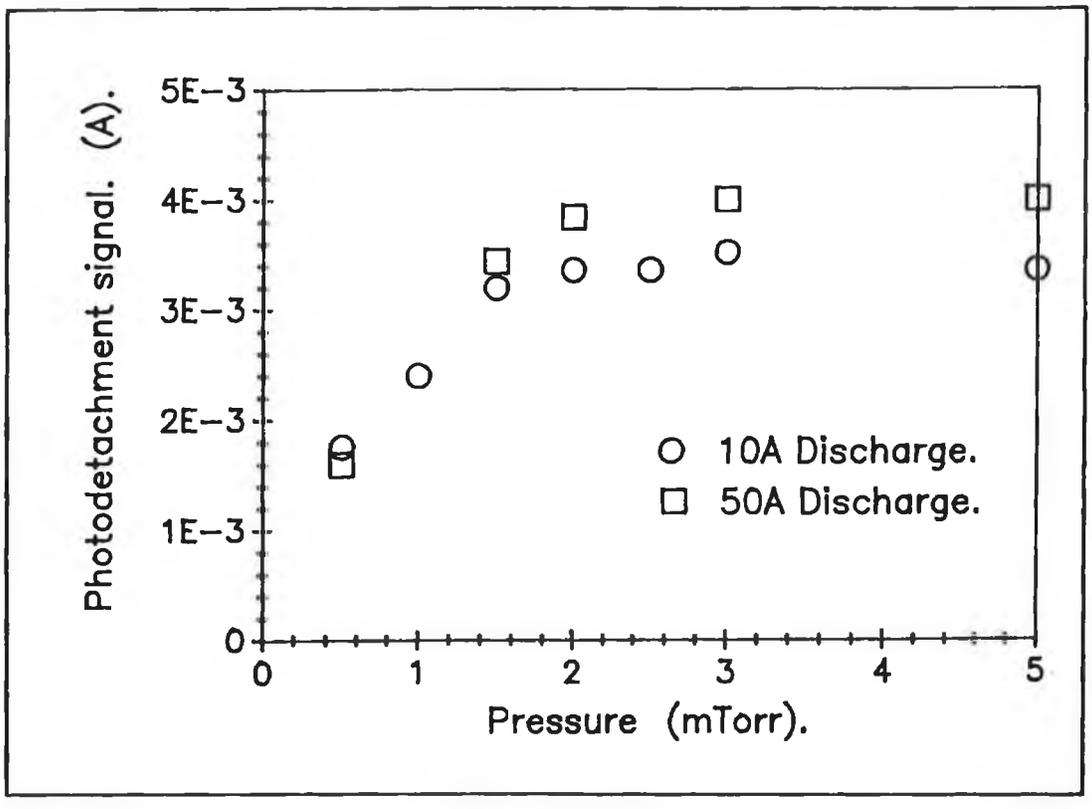

Figure 5.5. Photodetachment signal as a function of pressure. The discharge current is 10A (a) and 50A (b).

This effect is again observed in the photodetachment measurements taken in the source B. In the 10A case upon increasing the pressure from low pressures, 0.5mtorr, the signal increases rapidly from 1.8mA to reach a plateau of 3.6mA before decreasing as the pressure is further increased. This pressure plateau represents the optimum conditions for H^- production taking into consideration the two stage process, assumed as the major production mechanism [11], of excitation of vibrational levels,

E-V process, and the subsequent dissociative attachment by thermal electrons to form H^-. This effect has been discussed in greater detail in chapter 2.

The pressure plateau is observed in the pressure region 2.5-5 mtorr depending on other plasma parameters. The plot shows the optimum conditions at 3mtorr for a 10A discharge, but for the 50A discharge the signal appears to be saturating at 5mtorr. This change in the pressure plateau can be explained by the differences in the electron temperature of the 10A and 50A regimes. The temperature in the 50A case will be higher than in the 10A and therefore a higher pressure is required for optimisation of the production of H^-.It is this high pressure maximum plateau that can limit the use of volume sources for neutral beam heating, as modern accelerators will require lower operating conditions [12].

Note that the increase in the optimum pressure with increasing current is similar in effect to the pressure at which the post-discharge peak disappears in a pulsed discharge. In the pulsed discharge it has been found that the peak rise time goes to zero at greater source pressures for higher discharge currents. In fact this effect appears to be a function of the power density rather than discharge current. This is further borne out by the extraction results from the DENISE source at FOM, here Eenhuistra et al give the maximum extracted negative ion current density, for a source without a filter, at 13mTorr [8], and extraction results, chapter 3, from a pulsed discharge shows the peak rise time to go to zero at 13mTorr to 15mTorr [13]. These two effects are clearly related as the post discharge peak occurs because of a maximisation of the DA cross section as the electron temperature in the post discharge cools to below 1eV [14], the decrease in the losses due to CD cannot be as effective if the production rate drops at switch off. Thus the region of maximum continuous H^- density is expected to be slightly lower than the pressure at which the post discharge peak will disappear. Moreover this indicates that the pulsing of the discharge will only result in enhanced H^- density if the operating pressure is well below this plateau pressure.This effect is then due to the electron temperature in the source and this is dependent upon the power density, in the case of the D.C.U source the power density is $0.09W/m^2$ and in the DENISE source the power density is $0.9W/m^2$.This is further discussed in section 5.9. Also the pressure plateau may also depend upon the position at which the measurements are made, as the electron temperature and electron density

are spatially dependent.

Figure 5.6 (a) and (b) show the measured photodetachment signal against

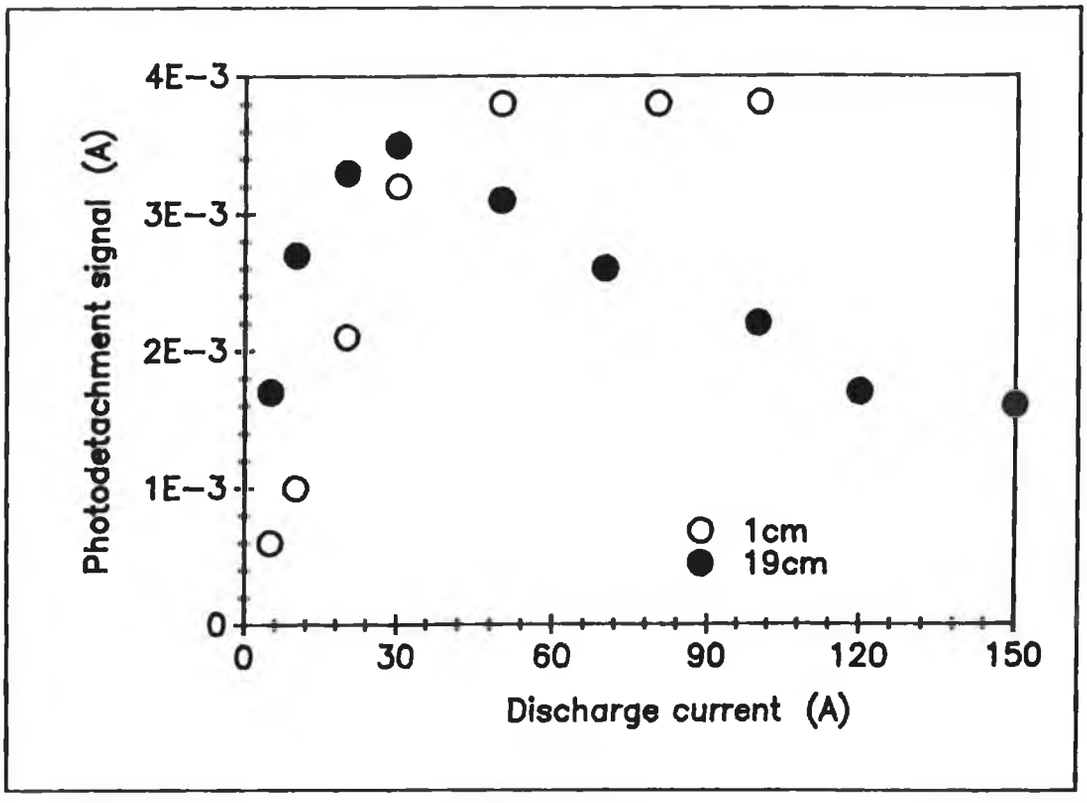

Figure 5.6. Photodetachment signal dependence on discharge current. Taken at 19cm and 1cm from the plasma electrode. P=1mTorr.

discharge current in a 1mTorr discharge. The measurements were taken as in figure 5.5, but at 19cm (a) and 1cm (b) from the plasma electrode. Holmes et al [15] have shown the extracted H^- current density to increase with increasing discharge current at low power and to saturate as the discharge current increases at high power. They speculate that I_{H^-} may start to decrease as the power is still further increased. This effect is observed here for the measurements taken at 19cm from the plasma electrode. The signal increases with increasing current up to 30A, where ΔI^- is 3.5mA, above this value it decreases, at 100A ΔI^- is 2.1mA. In the measurements taken at 1cm this is not observed as the photodetachment signal continues to increase up to 100A. This is discussed in more detail in section 5.7.

5.5. Time resolved Photodetachment measurements.

Previous results have shown the extracted negative ion current density in a low pressure, high power, volume ion source to increase after the discharge has been switched off [12,16,17], however this has yet to be verified by photodetachment measurements in the discharge. Here we present the results of such measurements. Figure 5.7.(a) shows a plot of the photodetachment signal variation with time in the discharge and post-discharge periods. The pressure is 1mtorr and the discharge current is 10A, the pulse duration is 2ms and repetition rate 10hz. This plot was taken by probe configuration 5.1.a, with the probe in the centre of the discharge, 15cm from the extraction aperture.

The signal evolves with a slow rise time [17] 0.5 to 0.8ms, (not shown), to reach the steady state during the discharge, the steady state signal is 2.3mA. When the discharge is switched off, 0μs, the signal shows a dramatic increase to a peak of 5mA This increase occurs with a rise time of approximately 14-20μs. The signal exhibits similar behaviour to the extracted results presented in chapters 3 and 4, and by Hopkins and Mellon [18] and Heeren et al [12], with the post discharge density reaching a value of 2 to 3 times the steady state value. The photodetachment signal increase in this case is seen to be roughly twice the dc level, however the actual H^- density, figure 5.7.(b), is given by 5.3,

$$n_- = n_{e^-} * \frac{\Delta j_{e^-}}{j_{e^-}} \qquad \text{Eqn. 5.3}$$

The electron current collected by a probe, assuming the bias voltage is greater than the plasma potential is given by 5.4 [19],

$$I_o = \frac{(n_e e V_e A)}{4} \qquad \text{Eqn. 5.4}$$

where the average electron velocity is given by 5.5,

$$V_e = \left[\frac{8kT_e}{\pi m_e}\right]^{\frac{1}{2}} \qquad \text{Eqn. 5.5}$$

thus,

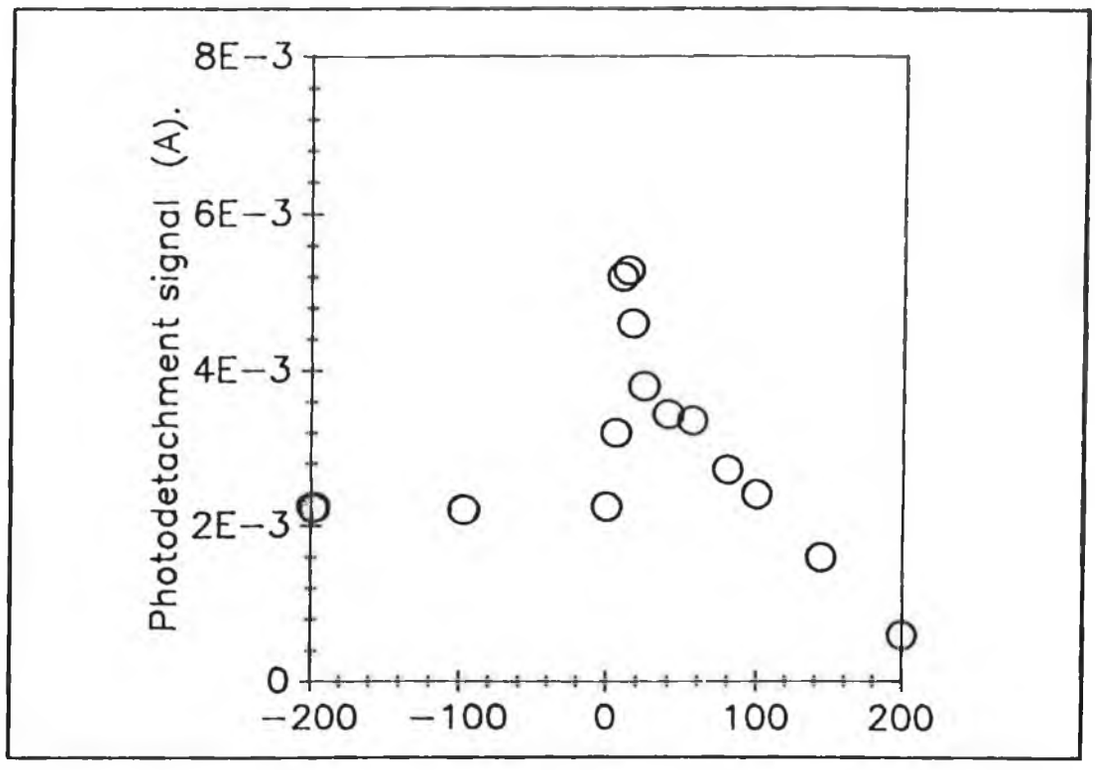

Figure 5.7.(a). Time resolved photodetachment signal in the discharge and post discharge periods. Id = 10A,P = 1mTorr.

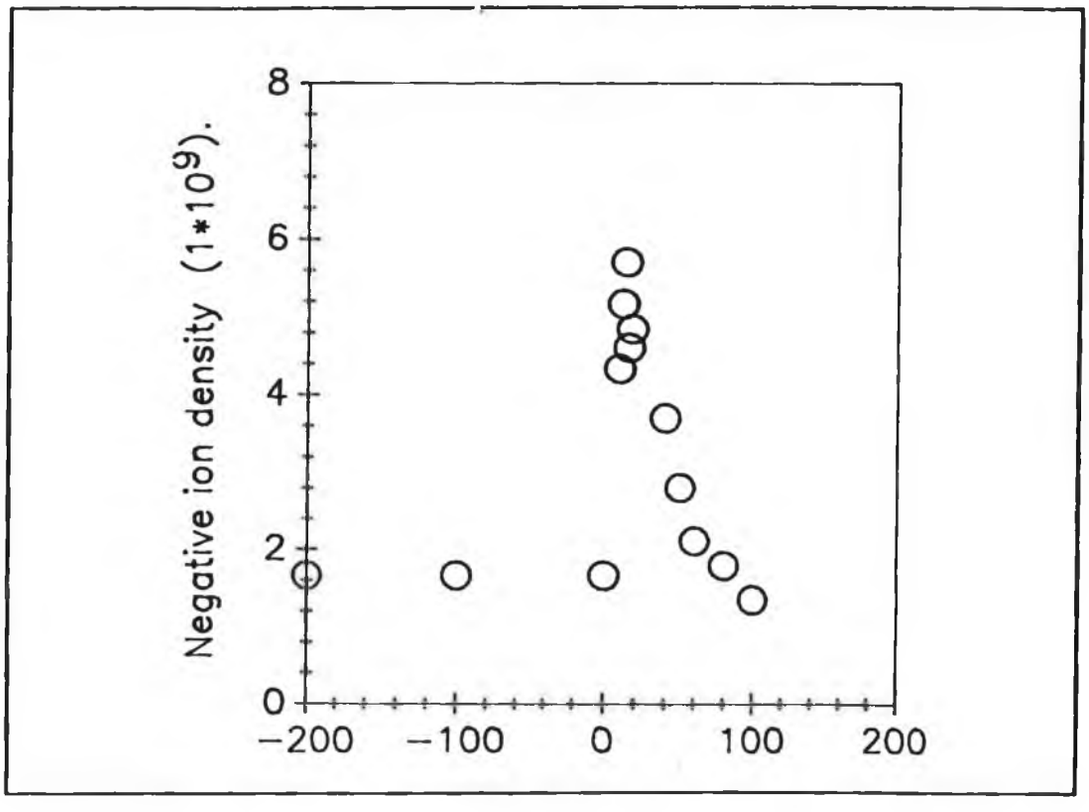

Figure 5.7.(b). Time resolved negative ion density in the discharge and post discharge periods. Id = 10A,P = 1mTorr.

$$n_- \propto \frac{1}{(kT_e)^{\frac{1}{2}}} \qquad \text{Eqn. 5.6}$$

Thus while the excess electron flux increases in the post-discharge by a factor of 2, as the electron temperature cools in the post-discharge this increase in flux represents a more dramatic increase in negative ion density, approximately 3 or 4 times the density during the discharge, figure 5.7.(b). However the photodetachment result in this case shows the rise time to be much sharper than previously observed, 10-20μs, while extraction results from other sources show rise times of 90μs, D.C.U. [15], and 40μs, FOM [12]. The rise-time of the peak in the post discharge is an important factor as it gives information about the loss times of the discharge and subsequently it is important for determining the frequency of modulation at which an enhancement can occur. Also the rise times can be used to determine the mechanisms involved in production, loss and transport of negative ions in the source. Further results show that this rise-time is both spatially dependent and dependent upon other plasma parameters, i.e the electron temperature, positive ion and electron densities, and the fast electron density. This is further discussed in section 5.9. Figures 5.7 (a) and (b) are important in that they verify that the increases reported for extraction from pulsed discharges are due to a real increase in the H^- density in the source and are not due to some effect of the extraction system.

5.6. Pressure dependence of the time resolved photodetachment signal.

As already discussed in chapters 3 and 4, it is expected that with increasing source pressure the ratio of the post discharge density to the steady state density will decrease until there appears no increase in the post -discharge. Figure 5.8 shows the measured time dependent photodetachment signal as a function of pressure in a 20A, 60V discharge. The probe is as in figure 5.1.b, in the centre of the chamber 1cm from the plasma electrode. As expected at the lower pressures the post-discharge peak is substantially larger than the steady state level, at 0.5mtorr an increase of 2.8 occurs in the post-discharge, as the pressure increases, the ratio of $\Delta I^{-peak}/\Delta I^{-dc}$ decreases, at 2mTorr being only a factor of 2, at 4mTorr it has fallen to only 1.6 and at pressures

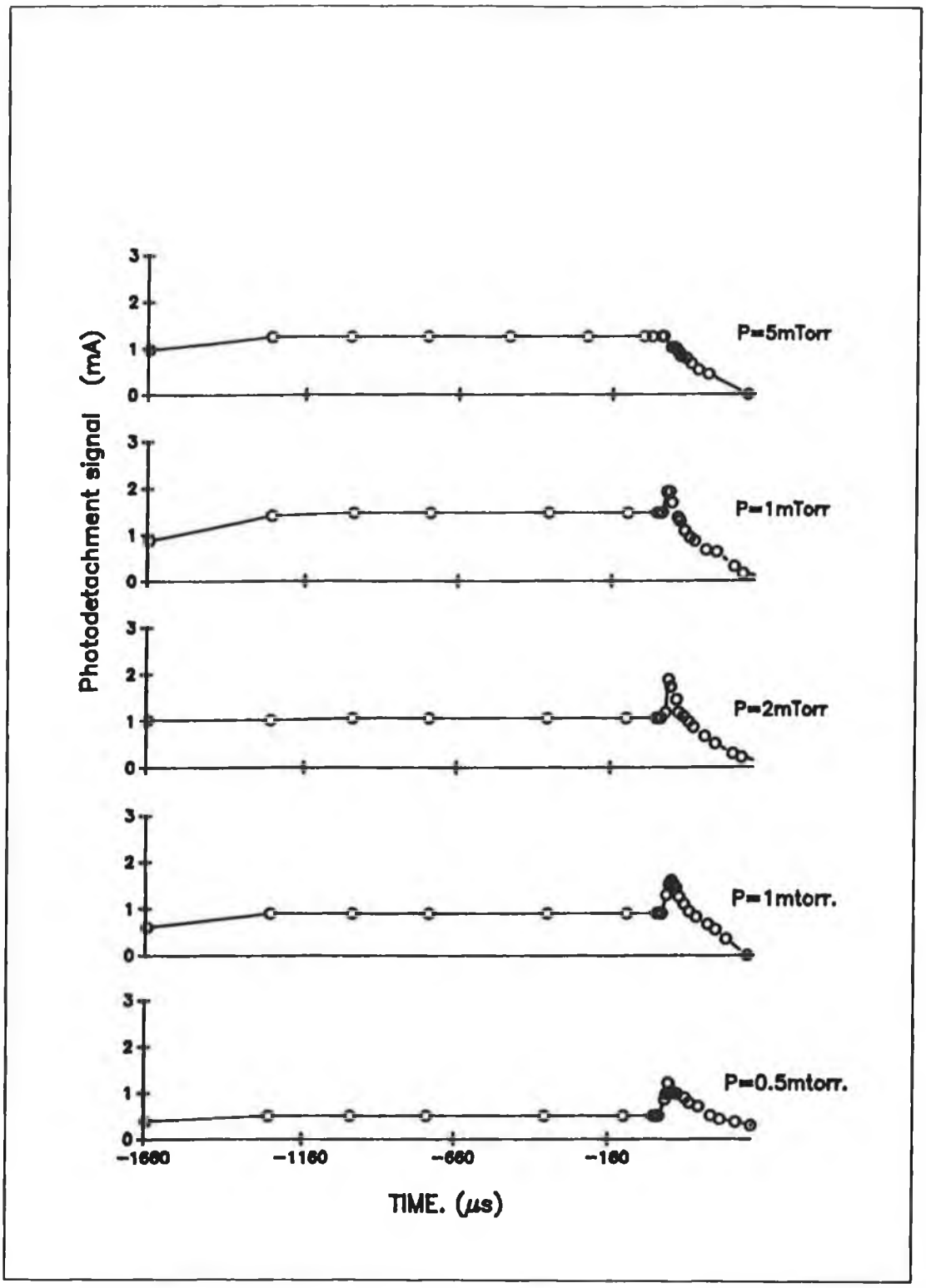

Figure 5.8. **Time resolved photodetachment signals for different source pressures. Id=10A. Taken at 1cm from the PE.**

greater than 5mTorr $\Delta I^{-peak}/\Delta I^{-dc}$ goes to unity indicating no enhancement for higher pressures. This corroborates the effect seen in the extraction results in chapter 3, which show the peak disappearing above 5mTorr. Here again the peak value at 0.5mTorr is of the same magnitude as the dc level at higher pressures, indicating an optimisation of conditions for production in the immediate post-discharge. As discussed in section 5.5, the post discharge peak to continuous ratio variation with pressure is dependent upon the discharge current regime. Figure 5.9 shows the peak/dc ratios, 15cm from the PE, against pressure for a 10A and 50A discharge. It can be seen that in the 10A case the peak/dc ratio goes to zero at 5mTorr but in the 50A case the ratio is small at 5mTorr but extends to higher pressures before going to zero.

5.7. Current dependence of Photodetachment signal.

In section 5.3 we saw that as the current was increased the photodetachment signal increased for lower currents but at higher currents appeared to saturate and above this decreased again. Here we show the peak and dc signals for various currents, figure 5.10. The probe was in configuration 5.1.(b), 19cm from the plasma electrode. The source pressure is 1mtorr and discharge voltage 60V. Again we see the photodetachment signal increase with discharge current at lower discharge currents, at 5A ΔI^- is 1.7mA, at 30A this has become 3.5mA, above this current the signal amplitude falls off, at 50A ΔI^- is 3mA and at 100A ΔI^-=2mA. This decrease in the photodetachment signal can be explained by an increase in kT_e and the density of fast electrons as the current is increased. At low currents this increase leads to an increase in H^-, via singlet state excitation of $H_2(v^*)$, however the increasing fast electron density results in both increasing losses for H^- and $H_2(v^*)$. Thus for continued increases in the discharge current the H^- density can fall. Also as the electron temperature increases with current the cross-section for DA decreases and the cross-section for CD increases.

However the post-discharge peak value continues to increase, At 5A it is 3.1mA, with $\Delta I^{-peak}/\Delta I^{-dc}$ = 1.8, at 50A the peak has increased to 8.0mA and the ratio is 2.63, at 100A the ratio has increased to a factor of 5. This is consistent with an increasing electron temperature and increasing losses due to fast electrons as both of these effects are controlled by switching the plasma off.

In the above case the measurements were made in the centre of the chamber

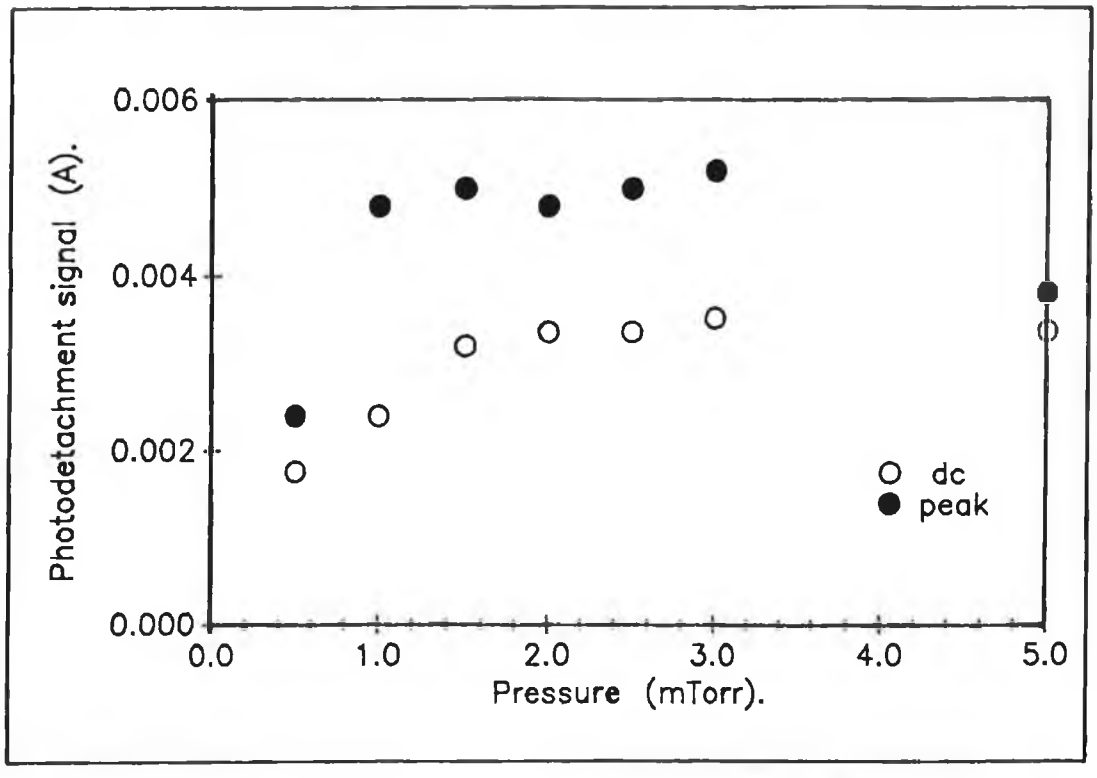

Figure 5.9.(a). Peak and dc photodetachment signals as a function of pressure in a 10A discharge. Taken 15cm from the PE.

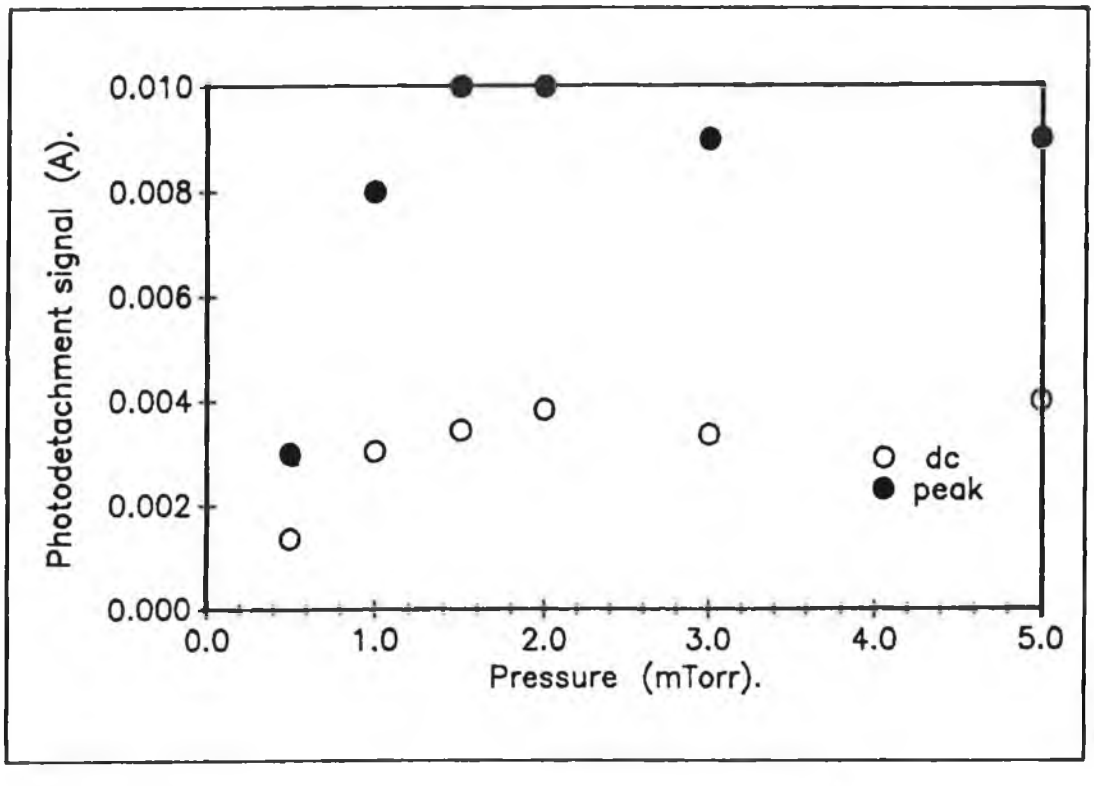

Figure 5.9.(b). Peak and dc photodetachment signals as a function of pressure in a 50A discharge. Taken 15cm from the PE.

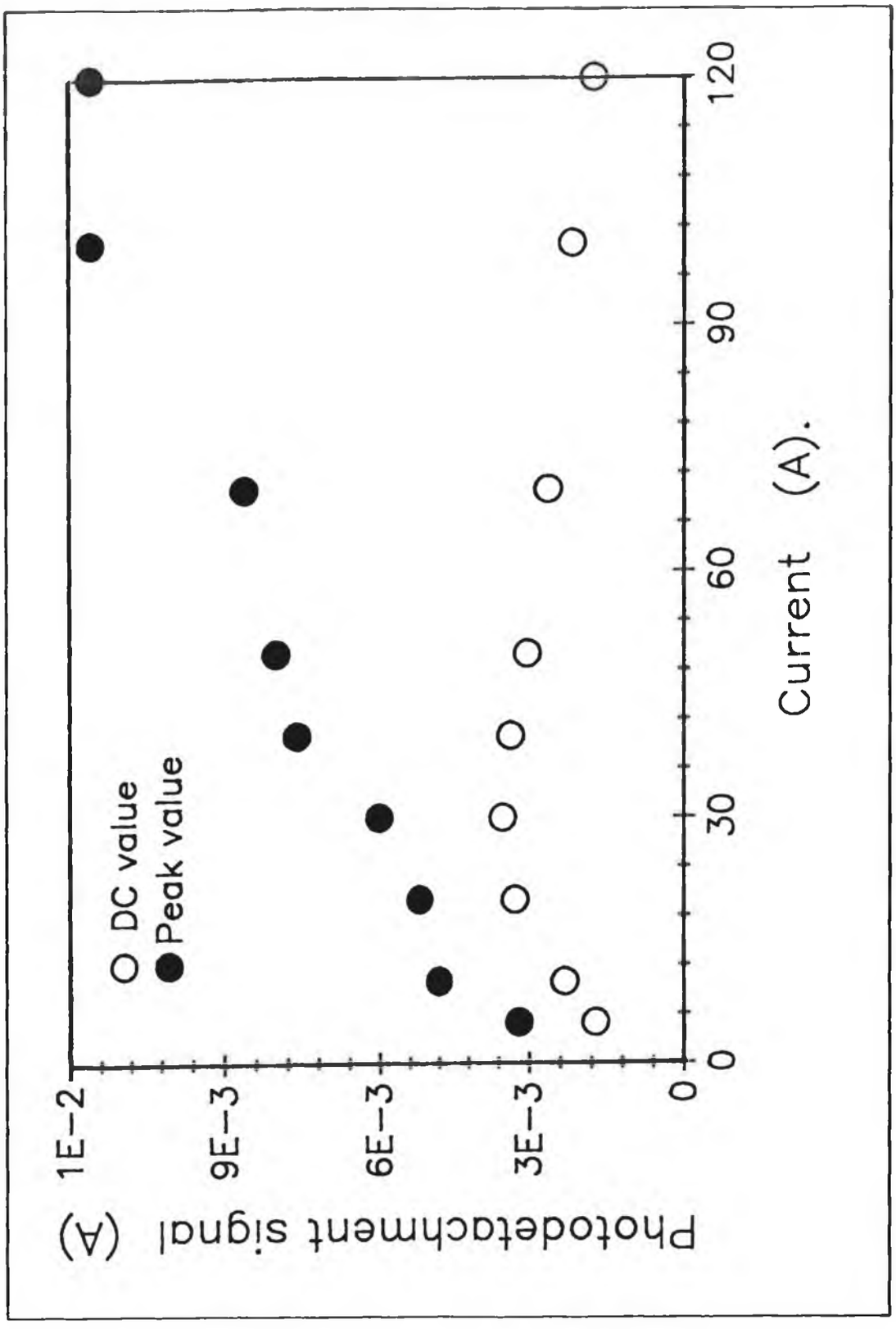

Figure 5.10. Peak and continuous photodetachment signals as a function of discharge current. Taken at 19cm from the plasma electrode. P=1mtorr.

near the filaments. Probe measurements , chapter 6, have shown high densities of fast electrons in this region. In figure 5.6 photodetachment values are plotted against current for measurements taken near, 1cm, the plasma electrode. In this region the signal increases with current even up to 100A, while the peak also increases with current. Probe measurements have indicated lower fast electron densities in this region, approximately 4% and the electron temperature is lower than in the central region of the source. However this in itself cannot explain the continued increase. As the current is increased, in the central region losses of $H_2(v^*)$ occur by ionisation with fast electrons,

$$e_f^- + H_2(v'') \rightarrow e^- + H_2^+ + e^- \qquad \text{Eqn. 5.7}$$

The vibrationally excited states are expected to have a long lifetime, ≈1ms and therefore can drift towards the plasma electrode where there are less losses, thus increasing the production of H^-. It is not expected that this is due to the movement of negative ions as these have a relatively short lifetime, t<20μs, during the discharge, which means that their mean free path is short. It should be noted that for extraction measurements on this source no decrease in the current density was observed, however the maximum discharge currents used in the extraction measurements was small.

5.8. Peak Rise-Time dependence upon Pressure.

Previous work has shown that the post-discharge peak rise time is dependent upon the source pressure [12], again this effect is observed here. In figure 5.11 the risetime to the post-discharge peak is plotted against source pressure. These measurements were taken at 1cm from the plasma electrode, in a 20A, 60v discharge.

At higher pressures, 5mtorr no peak occurs, as the discharge conditions are optimised for H^- production by dissociative attachment from vibrationally excited levels. As the pressure is lowered, 4mtorr, the peak rise time is short, 6μs and the peak continues to broaden until at lower pressures, 0.5 mtorr, the risetime is approximately 50μs. As the electron temp in the post discharge cools leading to an increase in H^- production due to DA, an increase in the negative ion density occurs, the time for this increase to reach its peak depends upon the time for the EEDF to

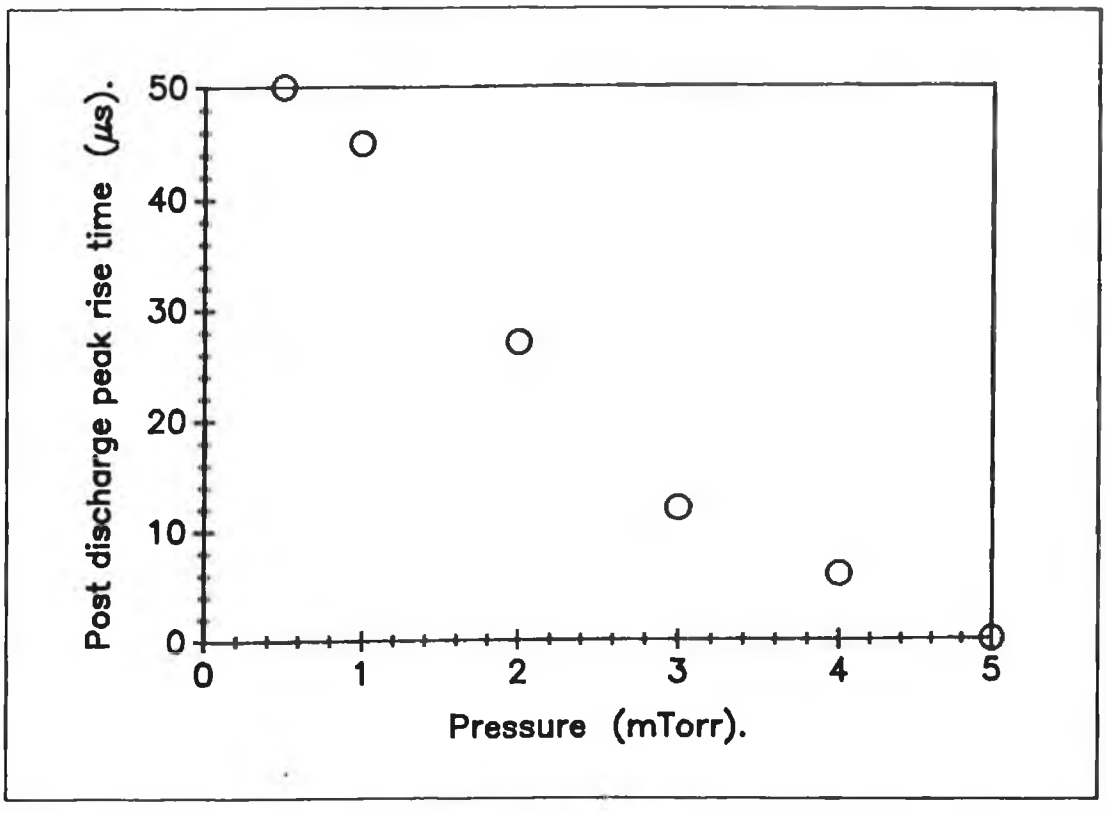

Figure 5.11. Post discharge peak rise times as a function of pressure. Id=20A.

cool to an optimum value for DA, 1ev. The plot shows an exponential decrease in the peak risetime as the pressure is increased, this corresponds to a similar exponential decrease in the time for the electron temperature to cool below 1eV, chapter 6. This cooling may also lead to reduced H^- losses. H^- losses due to electron detachment, while possibly being influential in the post-discharge increase, do not appear to be fully responsible for the effect as the fast electron decay is expected to occur within less than 1μs. In the extracted currents from Denise at FOM the peak rise time shows a much stronger pressure dependence than that observed here. Also the peak is sustained to much higher pressures than in the D.C.U. source. This has been explained by the higher power density of the FOM source, 0.9 Watts/cm^3 compared to the 0.09 Watts/cm^3 of the D.C.U. source. However this rise time dependence upon pressure is observed in both sources.

5.9 Spatially and temporally resolved photo detachment signals.

Previous publications, [20], have reported that many ion source plasma

parameters have a large spatial dependence ie. electron temperature, electron density. Knowledge of the spatial behaviour of the pulse discharge is important as further insights into the processes occurring with switching can be gained as well as information on the best location of the accelerator, filaments, etc. The spatial and temporal dependence of the negative ion densities in a volume ion source will be discussed here.

5.10. Radial dependence.

The radial measurements were made with the configuration as in 5.1.(a). The probe is moveable across the radius of the chamber, 15cm from the front plate. From figure 5.12 the radial dependence of both the peak and continuous photodetachment signals at this position can be seen, the measurements were made in a 1mtorr, 10A, 60V discharge. In the centre of the discharge, 0cm, the signal current is 2.3mA, as the probe is moved towards the wall the signal increases slowly until about 6cm from the wall the signal is 3.5mA, after this the ion density increases dramatically to a level of about 6mA at 4cm from the wall, the wall is 10cm from the centre, nearer to the wall the signal starts to fall off. The peak value follows a similar trend, increasing slowly from 4.8mA in the centre to 7mA at 6cm from the wall, moving nearer to the wall the peak value increases further and then falls off. It is important to note that the peak/dc ratio is almost 2 in the centre, but while the peak and dc values both increase initially going towards the wall the ratio falls off, with a slight increase at around 6cm from the wall, to 0.5 at 4cm to unity at 2cm from the wall. Moreover if we look at figure 5.13, which shows the peak rise time versus distance from the wall, we note that the rise time slowly increases until again at about 5cm from the wall the rise time shows a sharp decrease and continues to decrease until at 2cm from the wall no post-discharge peak is observed.

An explanation for this may be given by considering the multipole magnetic field on the anode wall, this field extends into the chamber to approximately 3-4cm. This field will, as discussed in chapter 3, prevent the primary electrons in the central region moving towards the wall, the principal of primary confinement. Also note in figure 5.14, the electron temperature kT_e and electron density n_e, variation with radial distance from the centre of the source.

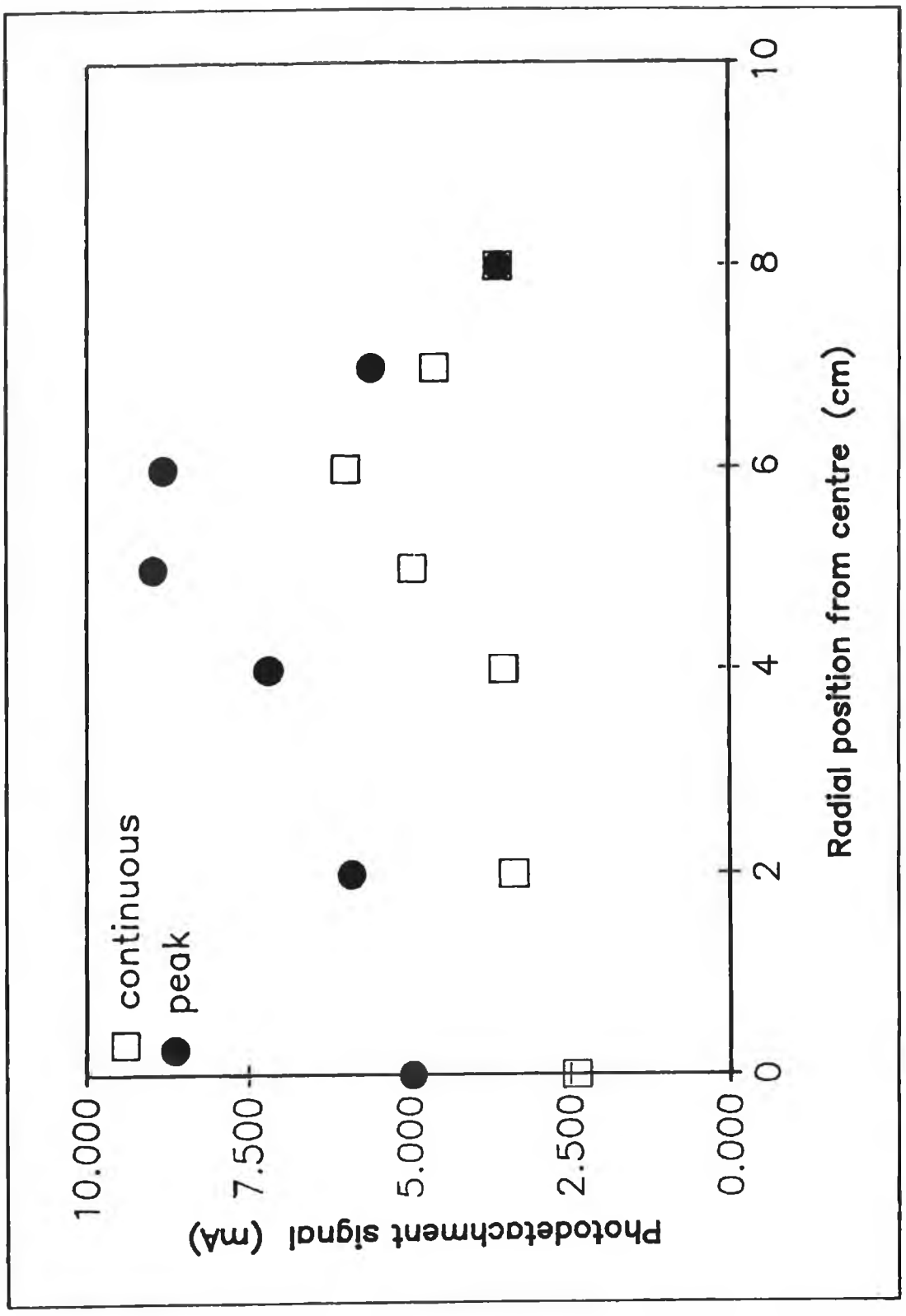

Figure 5.12. Peak and continuous photodetachment signals as a function of radial position in the chamber for a 10A, 1mTorr discharge.

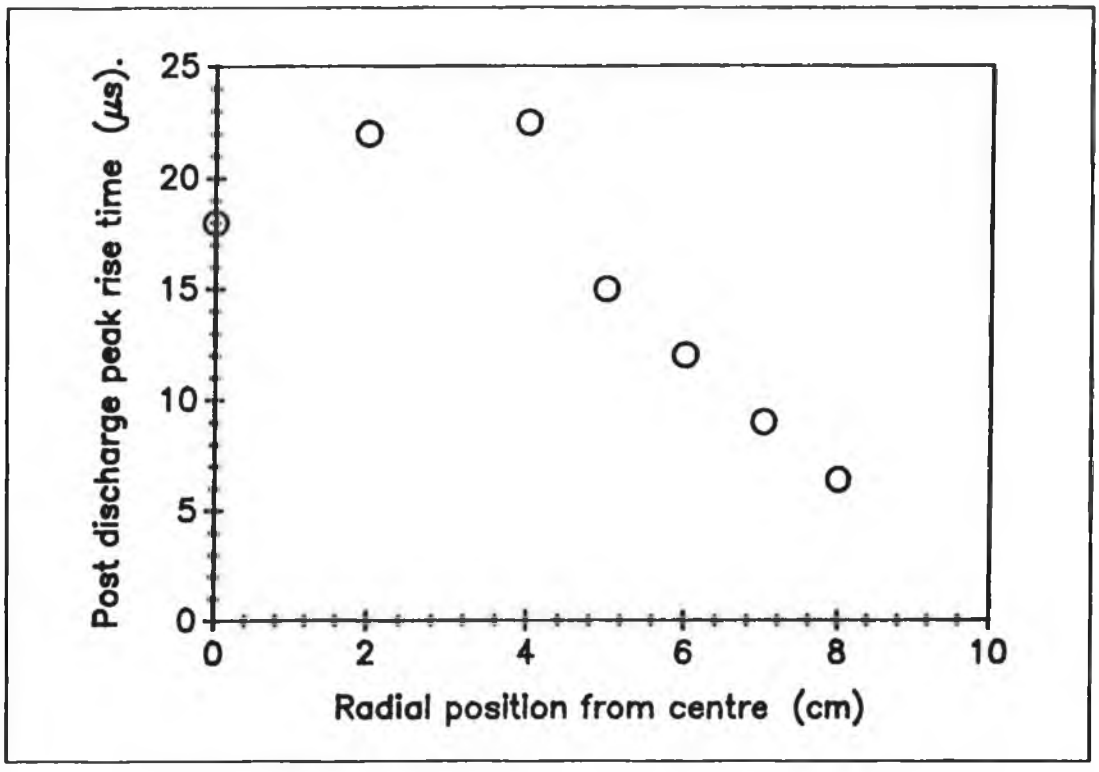

Figure 5.13. Post discharge peak rise time as a function of radial position. Id=10A, P=1mTorr.

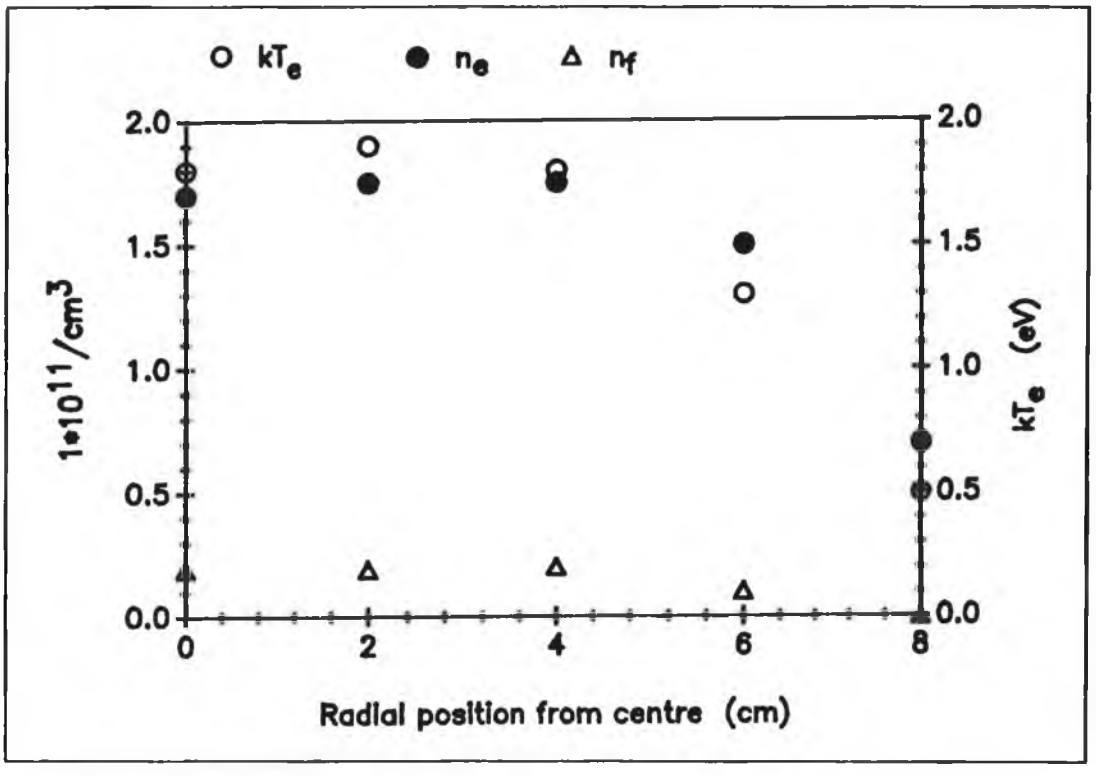

Figure 5.14. Electron temperature and electron density variation with radial position in the chamber. Id=10A, P=1mTorr.

The temperature in the centre of the chamber is hot, >2eV, and moving towards the wall this temperature increases slightly, however when we enter the magnetic field the plasma becomes much cooler, as with the filter field in a tandem source, this may indicate that the centre of the plasma is a hot production region while the field region allows the vibrational states to drift through into a much cooler region leading to a higher negative ion density approaching the wall. The peak/dc ratio indicates that this is precisely what is happening. The production of H^- during the discharge in the cooler regions approaching the wall increases as the lowering electron temperature leads to improved DA rates. The fast electron losses now become diminished. The peak value increases approaching the wall, possibly pointing to an increase in the vibrational density, the electron density also increases slightly as the fast electrons become more degraded. The decreasing peak/dc ratio points to a reduction in the dominance of CD losses and a cooler kT_e during the discharge results in a less dramatic post discharge increase in negative ion density. The electron temperature near the wall, <2cm, is low, 0.6eV and no fast electrons appear to be present and subsequently no peak occurs. The fall in the H^- density close to the wall is due to the very low electron density, $0.8*10^{11}/cm^3$. These measurements were taken in the centre of the magnetic field where it extends furthest into the chamber. It is expected that in the cusp regions the H^- dependence on position will be different. The slight increase in both the DC signal and peak values maybe due to the position of the filaments, the filaments are placed approximately 3cm from the centre of the chamber. This is borne out by the variation of kT_e, n_e and n_f, as both the electron temperature and electron density increase slightly at about 3-4cm from the centre. This indicates that the position of the filaments has a major effect on the localised H^- density. This field region near the wall, with low kT_e and few fast electrons and an increase in the H^- density, may be considered as similar to the extraction region in a tandem source.

The above concept may also account for the peak rise time variation with radial position. In the hot centre region, 0-4cm, the electron temperature is high and there exist large numbers of fast electrons, thus upon switching off the discharge the decrease in fast electrons and the slow cooling of the EEDF lead to a slow rise time away from the centre, approximately 2-4cm, the rise time increases slightly again due to the higher kT_e and fast electron density. Moving towards the wall the EEDF is

cooler, fewer fast electrons exist and a shorter rise time is observed, as we further approach the wall the fast electrons are removed and the EEDF cools sufficiently for no optimisation to occur after switch-off and thus no peak to be observed.

5.11. Axial dependency of the photodetachment signal.

Again these measurements are made in the centre of the chamber along an axial direction, figure 5.1.b. The probe can be moved between 1cm to 29cm from the plasma electrode. Note that the filaments are located 22cm from the plasma electrode. The variation of negative ion density with axial position, for a 10A and 1mtorr discharge, is shown in figure 5.15. The negative ion density has a strong dependence upon the axial position. At 29cm from the PE, 1cm from the front wall, the photodetachment signal is 5.6mA as the probe is moved away from the front wall the signal falls rapidly until at about 20cm to 15cm from the PE, the signal levels out, with densities in this region of 2.3mA. Moving nearer to the PE the density falls off again and continues to do so until at 1cm the density is only 0.7mA. The large increase in density near the front wall is explained, as in the case of the axial dependency, by a cooling of the EEDF in the field region of the front wall magnets, this is borne out by the plot of ion density vs position with no front magnetic field present, figure 5.15. An explanation for the fall off approaching the PE may be given as follows, in the centre region 15-25cm, there exists a hot dense, largely non-maxwellian plasma, in this region, as in the driver region of a tandem source, the main excitation of the vibrational levels occurs, along with high H^- production rates. However in this hot region there are large collisional detachment, CD, losses of H^-. In this region the electron temperature near the filaments is 2.7eV and the electron density $2.5e^{11}/cm^3$, with fast electron densities of 10%. The electron temperature and electron density variations with axial position are plotted in figure 5.16. Close to the filaments the fast electron losses during the discharge are substantial and after switch off the decay of CD losses leads to a rapid post-discharge increase in the negative ion density. As we move towards the plasma electrode, the plasma becomes less intense, 1.5-2eV, and the fast electron density falls off, leaving the EEDF more maxwellian. In this region, towards the plasma electrode, the negative ion density falls off. However the electron temperature remains reasonably constant 1.5-1.7eV, but the

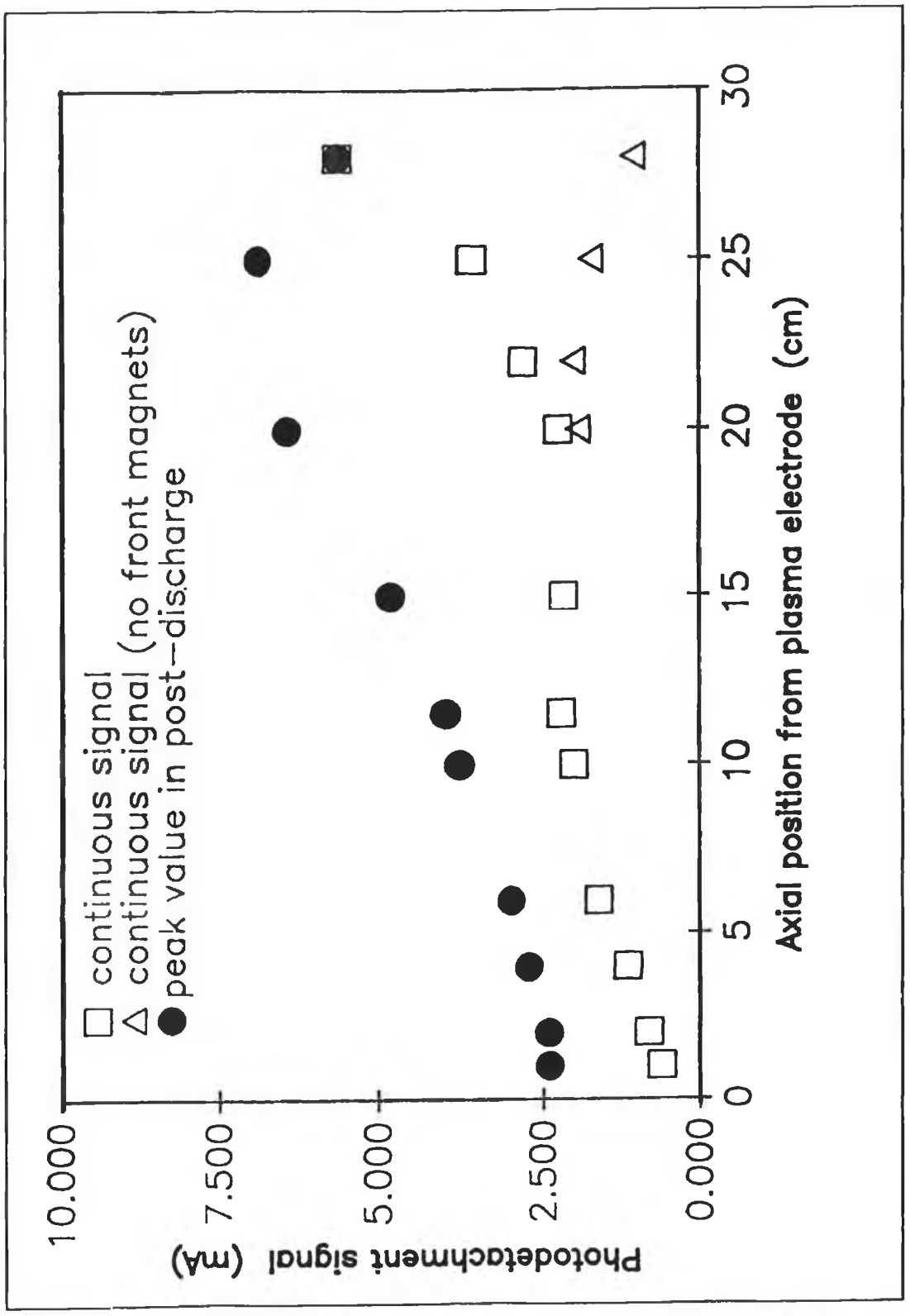

Figure 5.15. Peak and continuous photodetachment signals as a function of axial position in the chamber for a 10A, 1mTorr discharge.

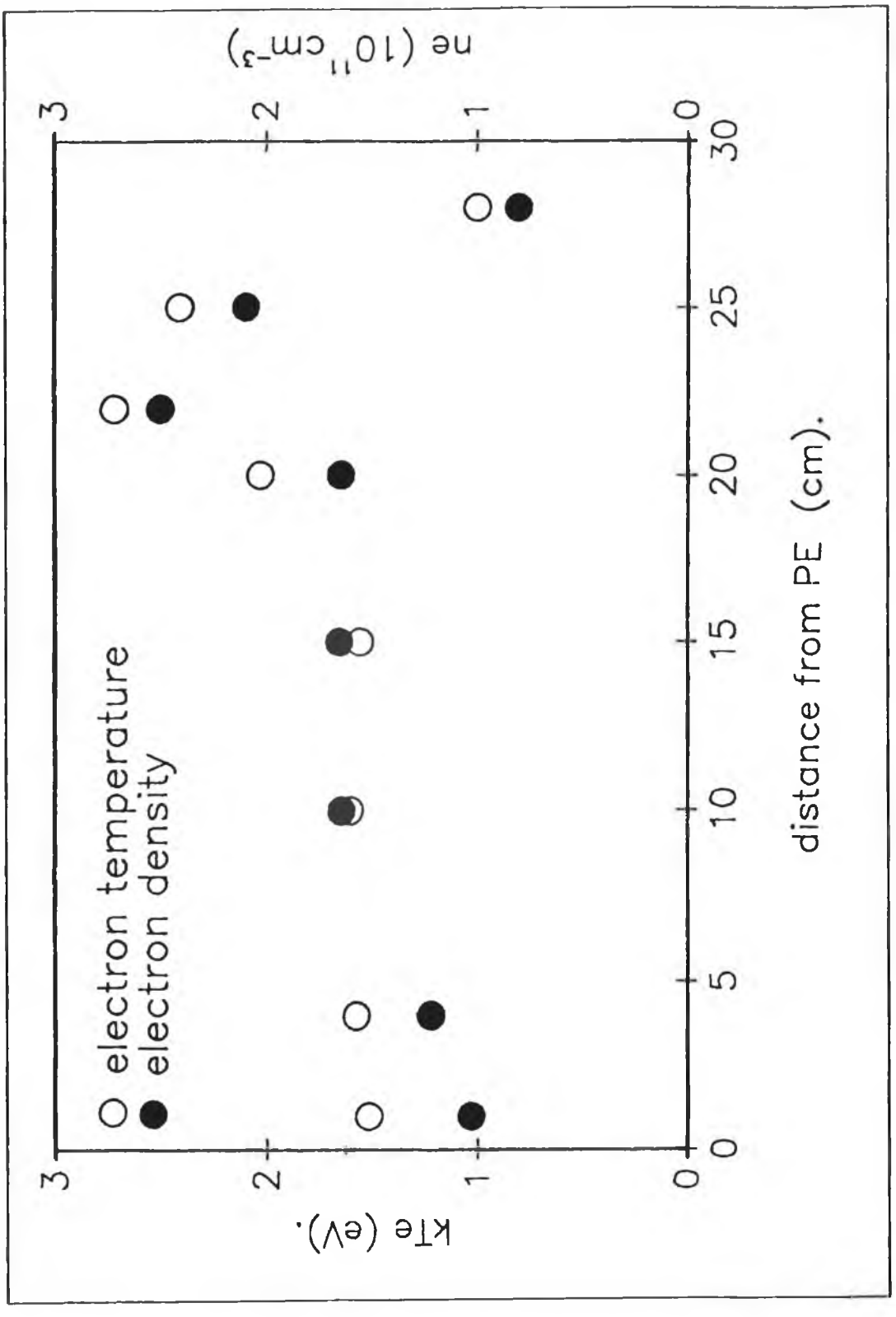

Figure 5.16. Electron temperature and electron density variation with axial position in the chamber for a 10A, 1mTorr discharge.

electron density falls off to roughly $1*10^{11}/cm^3$. This fall off in n_e results in the dc H^- density diminishing near the plasma electrode. However the constant kT_e results in a slightly enhanced $\Delta I^-_{peak}/\Delta I^-_{DC}$ ratio just approaching the plasma electrode.

In figure 5.17, the peak rise time vs distance from the PE is plotted. The rise time in the central region, 15-25cm, is roughly 10-14μs, as we move towards the front plate this time decreases rapidly until at 29cm no peak is present.

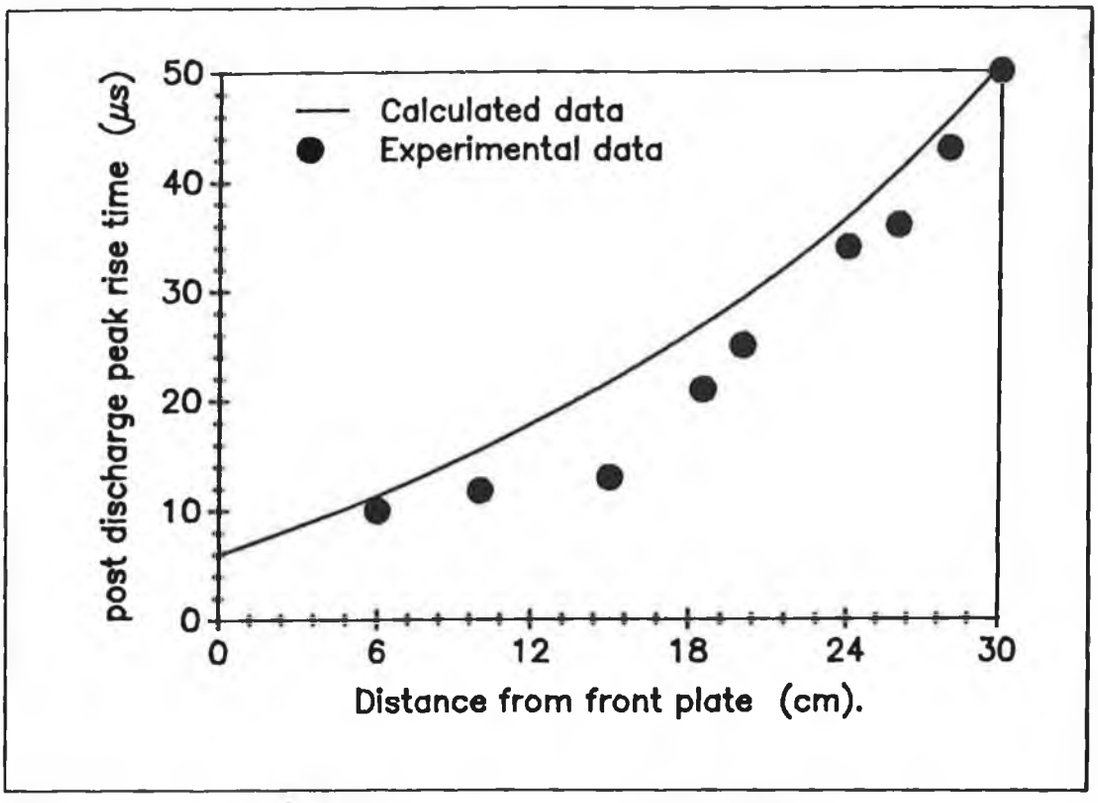

Figure 5.17. Post discharge peak rise time as a function of axial position in the chamber for a 20A, 1mTorr discharge.

Looking at the electron temperature variation, figure 5.16, with position along axis, the temperature falls off towards the wall, also the electron density falls off. There are few fast electrons in this region due to the magnetic fields and thus collisional detachment losses are small. As in the radial case the magnetic field cools the temperature and restricts the movement of primary electrons towards the front wall. Thus the continuous H^- density is optimised and no peak occurs.

Moving away from the central region towards the PE, the negative ion density falls off and the peak rise time increases almost exponentially. Also in this region the fast electron density falls off. The peak rise time broadening going to the plasma

electrode cannot be explained by the scenario given for broadening with decreasing pressure. In this case the electron temperature falls and the fast electron density is less than in the central region, this should indicate that the rise time becomes shorter approaching the plasma electrode. In the case of the electron density, assuming a loss time of t_e<30μs, at 50μs after switch off near the plasma electrode the density will have fallen from just over $1x10^{11}/cm^3$ to less than $1.9x10^{10}/cm^3$, thus the enhancement of H^- over the DC at such late times would appear impossible even allowing for a dramatic increase in the reaction rate for DA with electron temperature cooling, at this time in the post discharge the electron temperature will most likely have cooled through the maximum cross section for DA and thus the production will be decreasing. However these time scales have been seen for the extraction results from both the D.C.U. and FOM sources. In the centre of the source the post discharge rise time is less than 20μs. The survival of $H_2(v^*)$ will be possible on these time scales but to little benefit due to the low electron density and DA rate.

An explanation for this can be given by assuming that, as proposed by Eenhuistra et al [8], the H^- ions can drift from the central production region towards the plasma electrode. In the post discharge the loss time of negative ions is 50μs or higher, thus the ions produced in the central region have a larger mean free path than in the discharge and can drift a substantial distance throughout the source. It is further shown that H^+ ions enter the sheath of the extraction region with an ion acoustic velocity, the Bohm sheath criterion, where

$$V_a = \left[\frac{(kT_e + 3kT_i)}{m_i} \right]^{\frac{1}{2}} \qquad \text{Eqn. 5.8}$$

Eenhuistra claims that if the H^- ions participate in this drift, then the velocity can be approximated to V_a and has shown that the H^- drift and ion acoustic velocity agree reasonably well over a large parameter range. If this is true we can expect a scaling of H^- velocity with $\sqrt{kT_e}$.

Assuming a linear variation of kT_e with distance in the chamber, then the temporal and spatial dependence of kT_e can be expressed by eqn. 5.9.

$$kT_e(x,t) = \left[(m*d) + kT_e(0,0) \right] \exp^{-\frac{t}{\tau_{kT}}} \qquad \text{Eqn. 5.9}$$

Where d is distance in the chamber, m is the slope of the linear variation of kT_e, t is time in the post discharge and t_{kT} is the characteristic decay time of kT_e in the post discharge. Assuming t_{kT} is 30μs and using eqn. 5.8 to determine the velocity then the time for a negative ion to travel from the production region to the plasma electrode can be given as

$$T_{total} = \int_{o}^{length} \frac{\delta d}{V_e} \qquad \text{Eqn. 5.10}$$

The calculated peak rise times are plotted in figure 5.17 along with the experimental data points. The central region of the calculated trace does not show the same flattening as the experimental data, this is due to the assumption that the electron temperature variation is linear with distance which is not the case. However the calculated data does show a reasonable agreement with the experimental results. This would seem to indicate that the drift of H^- ions plays an important role in the post discharge rise time away from the central production region.

Note that the FOM results appear more dependant upon pressure than those of the D.C.U. source and may therefore be due more to the effects of temperature cooling and decreased losses in the post discharge than the drift of H^-. The FOM source is shorter, with the plasma electrode closer to the production region than in the D.C.U. source and it is expected that the high power densities gives the longer life times seen in DENISE.

It should further be noted that while this dependence of H^- drift velocity on $\sqrt{kT_e}$ appears to give a plausible explanation and this scaling of the negative ion drift velocity with $\sqrt{kT_e}$ has also been reported by Devynck et al [5], Bacal *et al* [21], found no scaling of H^- velocity with electron temperature in their hybrid source.

5.12. Photodetachment measurements in a pulse modulated discharge.

In chapter 3 it was shown that extracted current density was enhanced above the DC level by modulating the discharge under the conditions

$$\tau_{e^-} < t_{on} \quad , \quad \tau_{H^-} > t_{off} \qquad \text{Eqn. 5.11}$$

However in that case the condition was fulfilled in the frequency region 12kHz to

15kHz as the peak discharge rise time was 90μs. The extracted beam from the D.C.U source shows very little modulation but in the DENISE source the extracted beam was highly modulated. In both of the sources the post discharge peak rise time was substantially longer than the photodetachment results in the centre of the source show. It is this interaction of the production of H^- in the post discharge and the drift of negative ions from the central region to the plasma electrode when modulating the discharge that is of importance to establish the relationship between the enhancement of the density in the source and the extraction of an improved unmodulated ion beam.

In figure 5.18.(a) and 5.18.(b) the time resolved photodetachement measurements in a modulated discharge at frequencies of 2 kHz and 15kHz are plotted. These were taken in a 20A discharge, with duty cycle 50% and pressure 1mTorr, in configuration 5.1.(b), 20cm from the plasma electrode. In the 2kHz case when the discharge is switched off, 0μs, the photodetachement signal increases from 2.1mA to 5mA in less than 20μs. The signal then decays with a loss time of 100μs for approximately 100μs and then at a slower decay rate of 200μs. This change in the

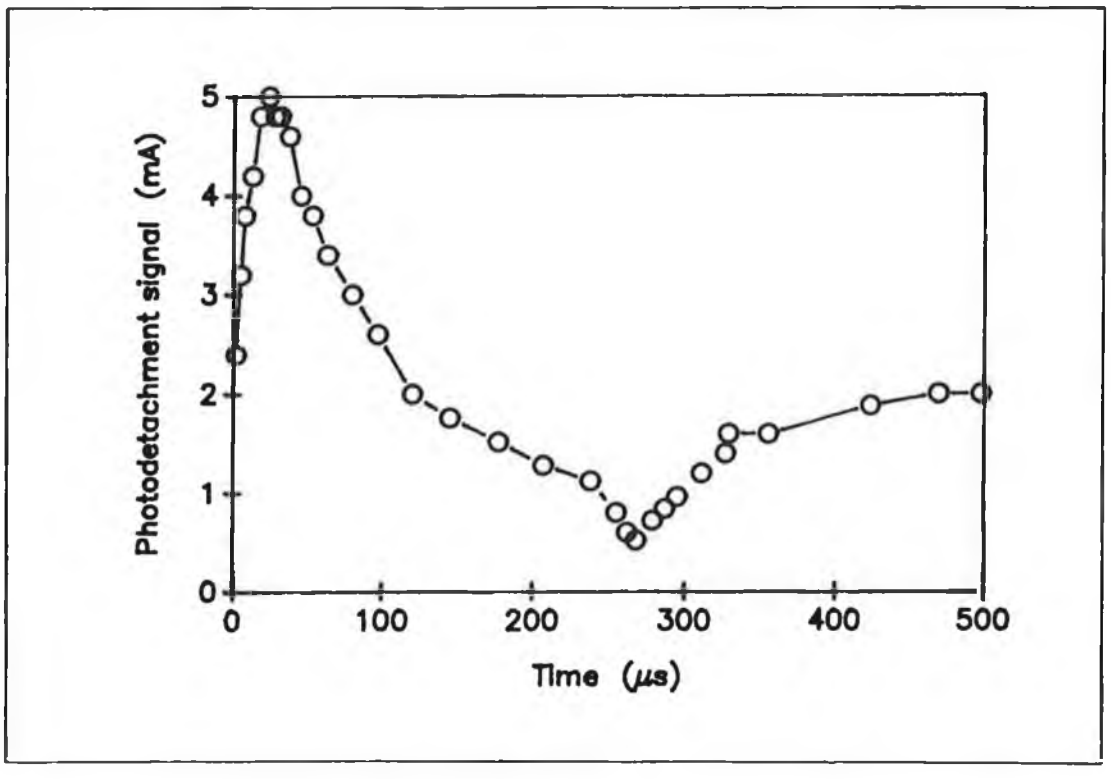

Figure 5.18.(a). Time resolved photodetachment signal in a 2kHz modulated discharge. Taken at 20cm from the PE. Id=10A, P=1mTorr.

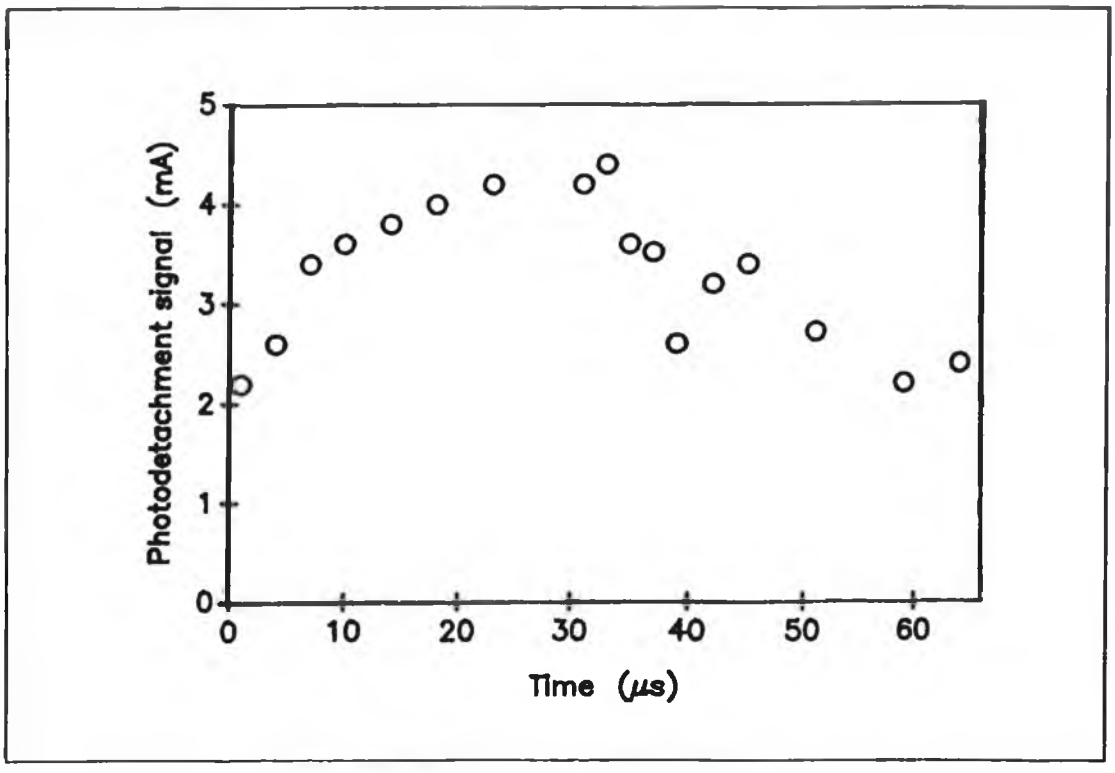

Figure 5.18.(b). Time resolved photodetachment signal in a 15kHz modulated discharge. Taken at 20cm from the PE. Id=10A, P=1mTorr.

decay rate at 100μs can be due to the decay of destructive species for H-, i.e. associative detachment by atomic hydrogen which has a decay time of 90μs [12] and mutual recombination by H_+ which has a decay rate similar to that of bulk electrons, approximately 30 μs, and wall losses becoming the more dominant H- loss mechanism. At 250μs the discharge is switched on again, at this stage the loss rate increases rapidly for approximately 15μs to 20μs and after this the H- density recovers reaching a quasi-steady state value of 1.99mA which is similar to the dc level. This cycle shows an increase in the time averaged density over a continuous discharge of similar power. This increase is more pronounced than figure 5.18.(a) shows due to the cooling of the EEDF in the post discharge. The post discharge peak value may be expected to be a factor of four over the discharge "on" level thus the time averaged level will be larger than the continuous level. However the important factor to note is the rapid decrease in the H^- density upon switch on of the discharge, the density falls below the density for a continuous discharge and must then start to build up again. Effectively this means that the gains in the post discharge due to decreasing CD

loss rates are lost upon the discharge being switched on. Again in figure 5.18.(b) the photodetachment signal for a 15kHz modulated discharge is shown.

At switch off, 0μs, the photodetachment signal increases from 2.1mA to 4.4mA in the post discharge. Upon switch on, 33μs, the signal starts to decrease, it decreases below the dc level and then starts to increase again. This rapid depletion of H^- density at switch on can be explained by the large increase in collisional detachment losses of the H^- by fast electrons. As the discharge is switched on the fast electron density increases rapidly, ≈1μs, this means that the CD losses become the dominant loss, however the plasma electrons have a rise time of around 30μs. Even if the vibrationally excited density remains unmodulated, although the large increase in fast electrons may reduce $H_2(v^*)$, the production of H^- can only evolve slowly implying that the CD losses at the start of the pulse far outstrip the production rates and this results in the decay of the H^- density. Thus at 15kHz there is a time averaged increase of up to three times the level for a dc discharge, the negative ion density is still highly modulated. This time averaged increase is due more to the enhancement of production after switch than to the decay of fast electrons. The reduction in CD losses in the post discharge is countered by the increased losses upon switch on. Note that the depletion of the H^- density at switch on is similar to that seen in the extracted results from FOM source, where the extracted current remained modulated even at high frequencies. The extracted results from the D.C.U. source show a very different and significant behaviour.

In figures 5.19.(a) and 5.19.(b) the photodetachment signal in a 2kHz and 15kHz discharge are plotted for the same conditions as in figure 5.18, here the measurements were taken 1cm from the plasma electrode. At 2kHz the ΔI^- rises from 1.2mA at switch off to roughly 2.7mA, 50μs after switch off and then decays with a loss time of 100μs. At 250μs the discharge is switch on again, the ΔI^- signal falls below the dc level but then starts to recover to reach a steady state of 1.2mA. Similar to the measurement at 20cm the H^- density falls off upon switch on, however here the effect is not so pronounced. At 15kHz the ΔI^- increases upon switch off from 1.2mA to 3mA and then decays after switch on and finally starts to increase again. In both these cases the ΔI^- signal for a 10A continuous discharge is 0.7mA. Thus we see an improvement in the H^- density of over 300% over the dc level. This is as effective an

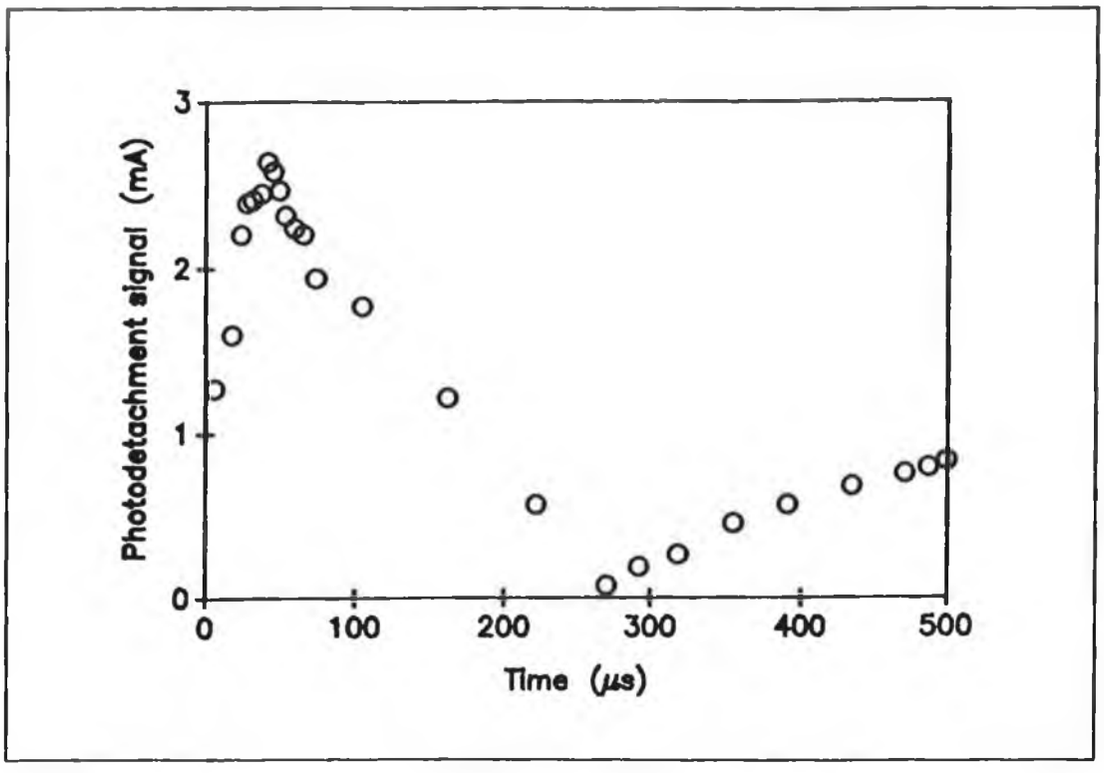

Figure 5.19.(a) **Photodetachment signals in a 2kHz modulated discharge. Taken at 1cm from PE. Id = 10A(avg). P = 1mTorr.**

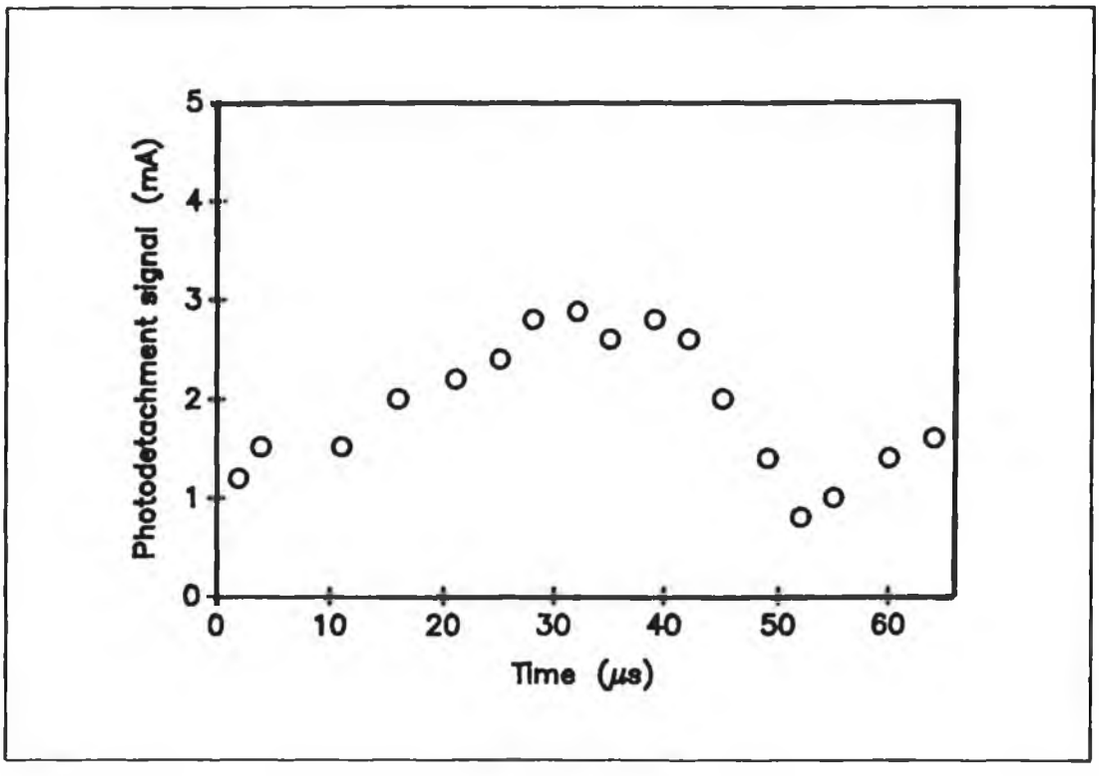

Figure 5.19.(b) **Photodetachment signals in a 15kHz modulated discharge. Taken 1cm from PE. Id = 10A(avg). P = 1mTorr.**

improvement as that for the extracted results in chapter 3, except that the density in the source is highly modulated.

5.13. Conclusion

In this chapter the photodetachment technique was used to investigate the negative ion density in a pulse modulated discharge. These results verify the enhancement of the H^- density in the post discharge as previously reported for extraction results. In the centre of the source increases in the negative ion density of three to four times the continuous value have been measured. This is congruent with the increases reported for extraction measurements. The results also indicate a very strong dependence of the negative ion density and post discharge effects of spatial position in the source. The peak rise time is also shown to be spatially dependent, with rise times in the centre of the source of 15μs to 20μs and this peak broadens approaching the plasma electrode to around 50μs. Further these spatially resolved results show a strong increase in the continuous H^- density in regions with magnetic fields, and a corresponding decrease in the peak/dc ratio is observed. This shows the effectiveness of the magnetic filter in the tandem source. Pulse modulation results show that the time averaged negative ion density can be improved by a factor of 3-4 in the regions near the extraction aperture, however this density is still highly modulated.

References.

[1] Katsch, H.M. and Quandt, E.
"4th European Workshop on the Production and Application of Light Negative Ions.", Belfast, 1991.

[2] Ameniya, H.
Journal of Physics D: Applied Physics, 23, p999, 1990.

[3] Nicolopoulou, E, Bacal, M. and Doucet, H.J.
Journal de Physique, 38, p1399, 1977.

[4] Bacal, M. and Hamilton, G.W.
Physical Review Letters, 42, p1538, 1979.

[5] Devynck, P, et al.
Review of Scientific Instruments, 60 (9), p2873, 1989.

[6] Branscomb, L. M.
"Atomic and Molecular Processes", Academic Press 1962.

[7] Smith, S.J. and Burch, D.S.
Physics Review, 116, p1125, 1959.

[8] Eenhuistra, P.J, et al.
Journal of Applied Physics, 67 910, p85, 1990.

[9] Holmes, A.J.T, et al.
Review of Scientific Instruments, 58 (2),p223, 1987.

[10] Ehlers, K.W, et al.
"4th International Symposium on the Production and Neutralisation of Negative Ions and Beams", Brookhaven, 1986.

[11] Bardsley, J.N.
"2nd International Symposium on the Production and Neutralisation of Negative Ions and Beams", Brookhaven, 1980.

[12] Heeran, R.M.A, et al.
Europhysics Letters, 17 (6), p503-508, 1992.

[13] Janev, R.K, Langer, W.D, Evans, K. and Post, D.E.
"Elementary processes in Hydrogen-Helium Plasmas"
Springer-Verlag, Berlin, London and New York, 1987.

[14] Holmes, A.J.T, Dammertz, G. and Green, T.S.
Review of Scientific Instruments, 56 (9), p1697, 1985.

[15] Mellon, K.N. and Hopkins, M.B.
"4th European Workshop on the Production and Application of Light Negative Ions.", Belfast, 1991.

[16] Katsch, H.M. and Quandt, E.
Journal of Physics D: Applied Physics, 25, p430, 1992.

[17] Coonan, B.P, Mellon, K.N> and Hopkins, M.B.
"6th International Symposium on the Production and Neutralisation of Negative Ions and Beams", Brookhaven, 1992.

[18] Hopkins, M.B. and Mellon, K.N.
Physical Review Letters, 67 (4), p449, 1991.

[19] Scanlan, J.V.
PhD Thesis, Dublin City University, 1991

[20] Mullan, A.A. and Graham, W.G.
Review of Scientific Instruments, 61 (1), p451, 1990.

[21] Bacal, M, at al.
"2_{nd} European Workshop on the Production and Application of Light Negative Ions.", Amersfoort, 1986.

[22] Bates, D.R.
"Atomic and Molecular processes"
Academic press, New York and London, 1962.

Chapter 6. Probe measurements and calculated negative ion densities.

6.0. Introduction.

The previous chapters have dealt with the measurement of negative ion densities and extracted H^- currents in a pulse modulated discharge. These measurements have shown a consistent behaviour which has been explained by the decrease in the H^- losses and the cooling of the EEDF in the post discharge. In this chapter probe measurements are presented showing the effect of pulsing the discharge current on the time averaged electron temperature, confirming that control of the EEDF can be achieved by variation of the duty cycle. The I-V characteristic measurements support the proposed mechanism of enhancement as being due to the dual effects of improved production from the cooling electron temperature and reduction of losses in the post discharge.These probe measurements are then used to model the negative ion density using a model based on the time dependent differential equations for production and losses given in chapter 2. The calculated H^- densities also show the measured densities to be consistent with the processes believed to be responsible for H^- production in volume sources [1], [2].

6.1. Using Langmuir probes

Langmuir probes are one of the most versatile diagnostic tools available for use on plasmas and are a simple means of determining internal discharge parameters such as the electron temperature, electron density, primary electron density and the ion density as well as the plasma potential, the floating potential and the electron energy distribution function. The probe method consists of measuring the current drawn on a small metal insert in the plasma, usually a thin tungsten wire although spherical and plane probes can also be used, as a function of the applied voltage. The resultant plot is called the I-V characteristic of the plasma. The understanding of probe theory and application is a well developed technology [3], [4], [5], however here only a brief analysis of the probe characteristics is presented.

6.2. Probe theory.

The discussion of langmuir probe theory can be divided into two categories which are distinguished by the conditions in which they are used [3]. Here we only deal with the low pressure, small probe situation. A typical I-V trace is shown in figure 6.1,

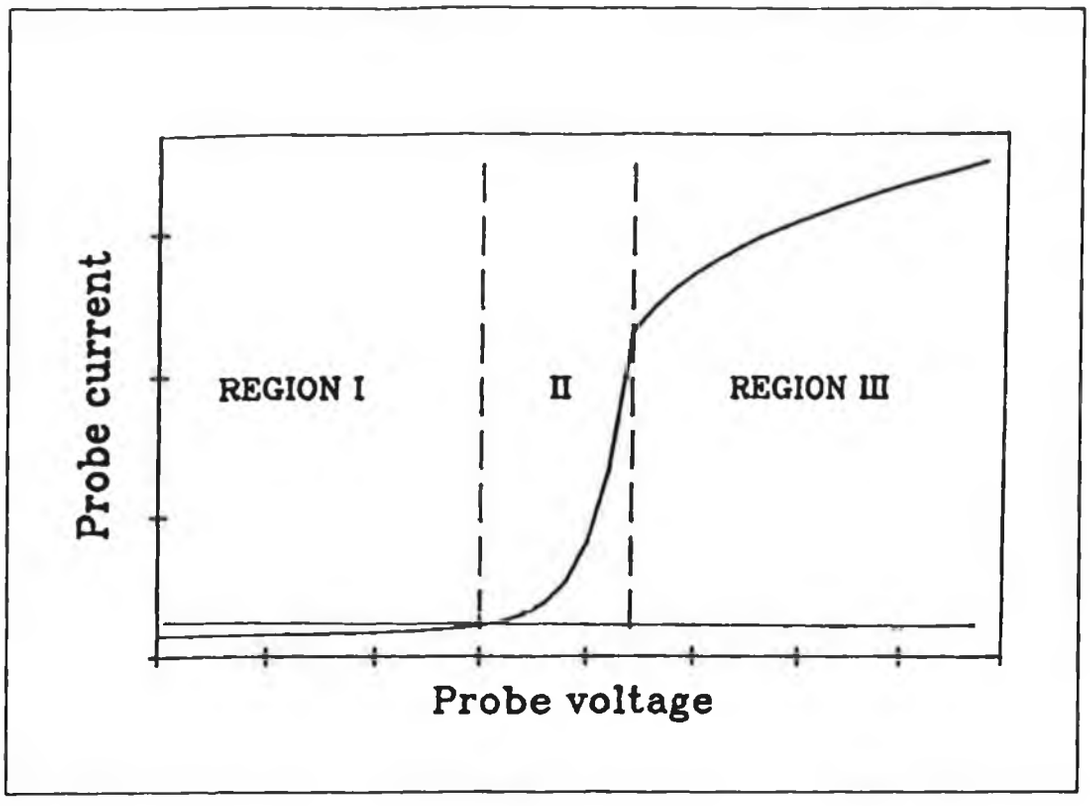

6.1. Typical probe I-V characteristic.

When the probe is biased strongly negative with respect to the plasma, then the plasma electrons are repelled and only positive ions are collected, region 1. The current collected is called the ion saturation current and is given by,

$$I_+ = \left[\frac{n_+ e V_+ A}{4}\right] \qquad \text{Eqn. 6.1}$$

where V_+ is the average or ion acoustic velocity, A is the probe sheath area. When the probe bias is made less negative then e^- start to be collected. This is region 2, the electron retardation region. At an applied potential equal to the floating potential, V_p, the ion and electron currents are the same and no net current is collected. In region

2 the electron current collected is,

$$I_e = I_o \exp\left[\frac{e(V-V_p)}{kT_e}\right] \qquad \text{Eqn. 6.2}$$

From this we get,

$$\ln I_e - \ln I_o = \frac{eV}{kT_e} - \frac{eV_p}{kT_e} \qquad \text{Eqn. 6.3}$$

Thus

$$\frac{d}{dv}(\ln I_e) = \frac{e}{kT_e} \qquad \text{Eqn. 6.4}$$

Therefore a plot of $\ln I_e$ against probe voltage will yield a slope of e/kT_e, and from this the electron temperature can be determined. The semi-log plot should be a straight line and departures from linearity are indicative of non maxwellian electron distributions [4].

For probe potentials greater than V_p, the plasma potential, the electron saturation current is collected and,

$$I_o = \left[\frac{n_e e V_e A}{4}\right] \qquad \text{Eqn. 6.5}$$

Where the average electron velocity V_e is

$$V_e = \left[\frac{8kT_e}{\pi m_e}\right]^{\frac{1}{2}} \qquad \text{Eqn. 6.6}$$

This electron saturation current is shown in region 3, and from this the electron density can be determined.

6.3. Experimental apparatus

The probe configuration is shown in figure 6.2. It consists of a small tungsten wire, 0.5mm diameter and 15mm in length, supported by a glass tube. It is similar to

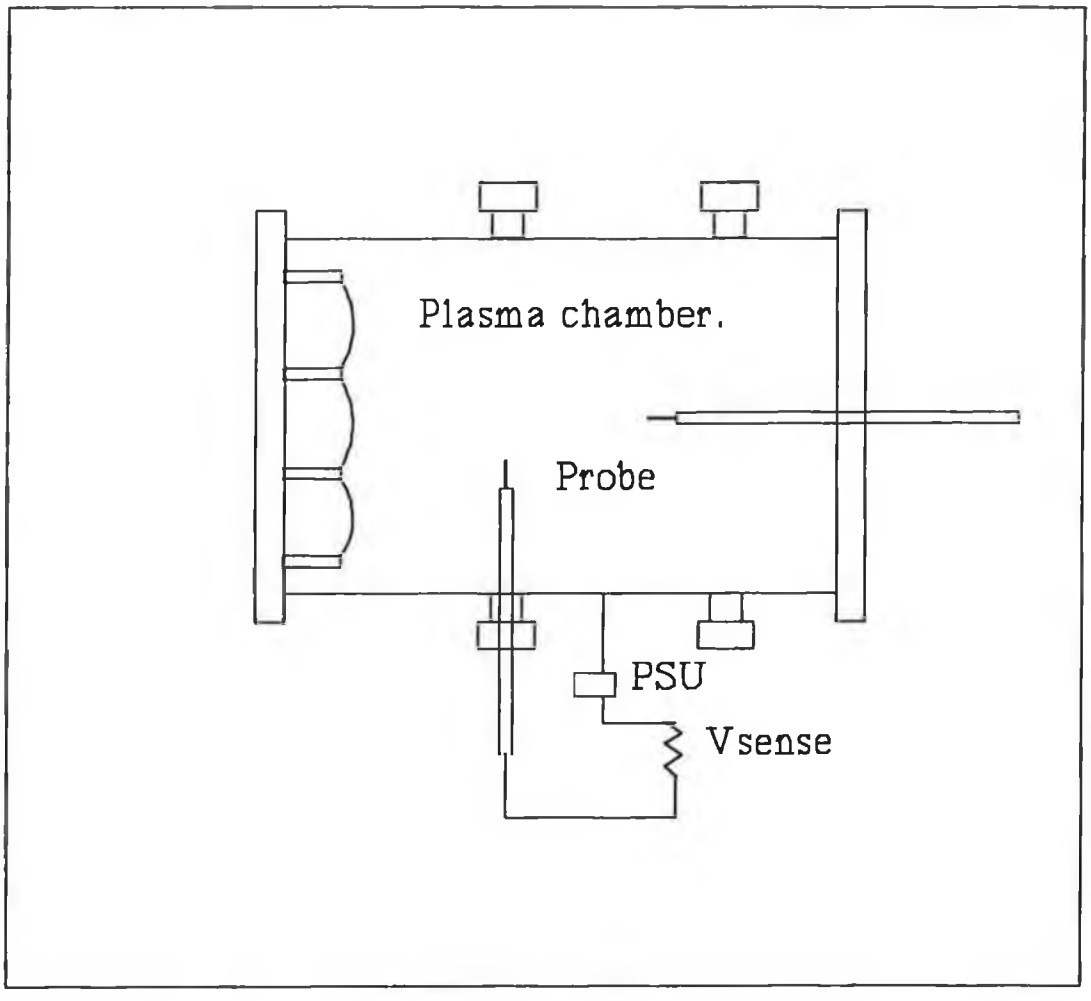

Figure 6.2. Schematic diagram of the Langmuir probe configuration used to obtain I-V characteristics.

the probes used in the photodetachment experiments described in figure 5.1.It can be moved either radially or axially in the chamber. A variable voltage is applied to the probe, -50V to 50V, and the current drawn is measured as a voltage across a 50Ω sensing resistor. This voltage is then displayed on a fast storage oscilloscope, from which it is time resolved using a diagnostic trigger as in figure 3.2.

The resultant current and voltage points are plotted giving the I-V characteristic, the characteristics can be spatially and temporally resolved throughout the discharge. These characteristics are then analysed manually to determine the plasma parameters. This individual analysis suffers from being subjective in the visual determination of changing slopes, saturation currents and plasma potentials. A computerised technique for probe analysis, similar to that described by Hopkins et al

[7], is under construction which will allow more detailed probe measurements to be carried out. Nonetheless simple analysis can still give valuable insight in to the discharge parameters and the effects of rapid modulation of the discharge current on the electron temperature, electron density and fast electron density.

6.4. I-V characteristics.

A typical characteristic is shown in figure 6.3.(a), it was taken in a 10A, 1mTorr discharge, 20cm from the plasma electrode using probe configuration 5.1.b, the discharge voltage is 60V.

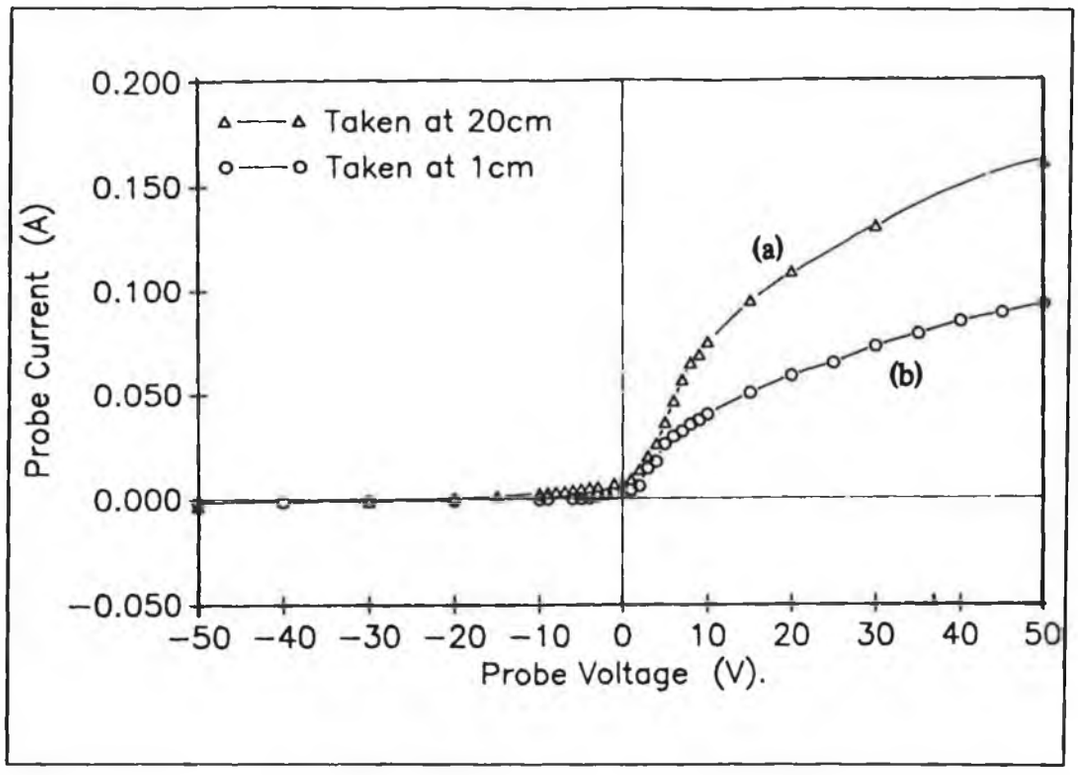

Figure 6.3. I-V characteristics taken in a 10A, 1mTorr discharge at 20cm (a) and 1cm (b) from the plasma electrode.

Firstly it is noted that there is a significant electron current between the applied voltages -10v to 0V, this second slope indicates a non maxwellian electron distribution [6], this is due to the presence of large numbers of fast electrons.

In this case the electron temperature is found to be 2.1eV, the electron density $2*10^{11}/cm^3$ and the fast electron component to be roughly 10%.

The characteristic in 6.3.(b) was taken under the same conditions as 6.3.(a)

except at 1cm from the plasma electrode. In this case the electron temperature has dropped to 1.5eV, the electron density is $1.2*10^{11}/cm^3$ but more importantly the fast electron density is only 4%. This fall in both the electron temperature and the fast electron density is expected when moving away from the filaments, and also can explain the drop in the H^- density approaching the plasma electrode.

In figure 6.4 I-V characteristics are shown for the same conditions as in figure 6.3, in this case the probe measurements were taken radially, in the centre of the source (a) and 2cm from the chamber walls (b).

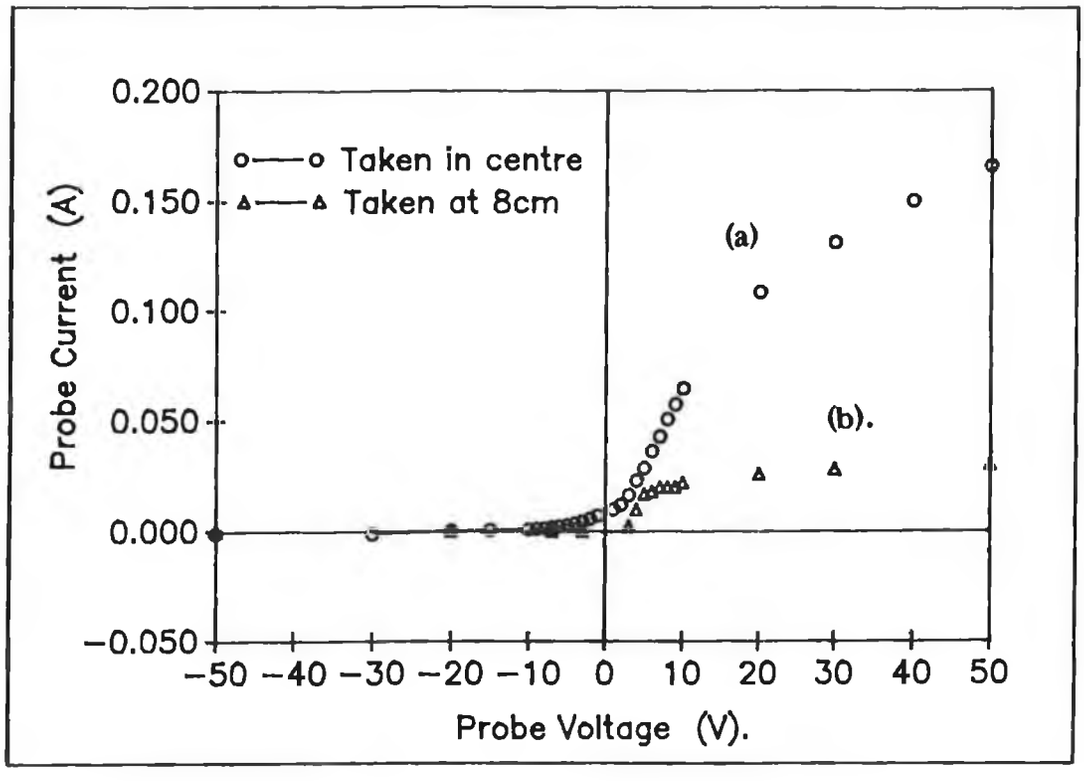

Figure 6.4. I-V characteristics taken radially in a 10A, 1mTorr discharge at the centre (a) and 8cm from the centre (b) of the chamber.

In the centre the parameters are similar to 6.3.(a) with a high kT_e and large n_f component, nearer to the wall the plasma has cooled dramatically, the slope of lnI_e is linear implying a maxwellian distribution with a low electron temperature and no fast electron component, this is consistent with the magnetic filtering near the walls as discussed in chapter 5.

6.5. Current and pressure I-V characteristics.

In previous chapters the dependence of the post discharge peak was explained by the cooling of the electron temperature and a reduction in the fast electron density. These conditions exist in the I-V's shown above. The decay of the peak/dc ratio at higher pressures was explained as being due to a cooling of the kT_e and reduction of n_f during the discharge as the source pressure is increased. Characteristics are shown in figure 6.5 for various source pressures in a 10A discharge.

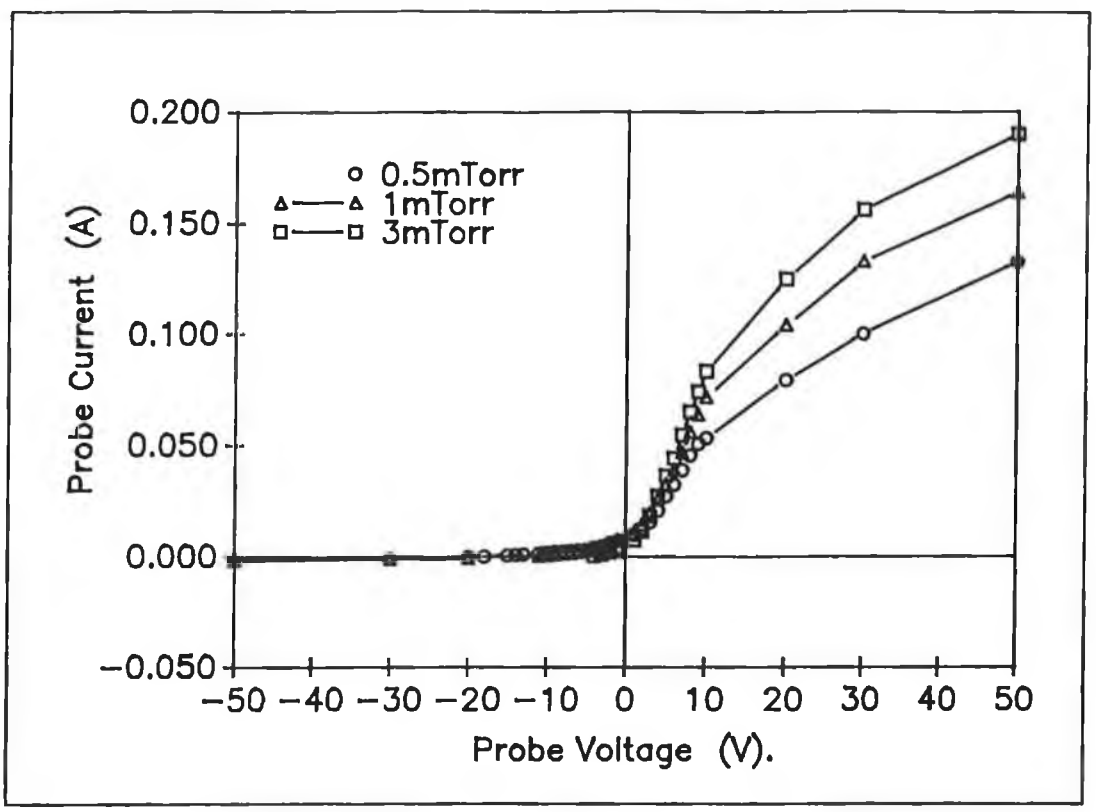

Figure 6.5. I-V characteristics taken in a 10A discharge for different source pressures.

At 0.5mTorr the presence of large numbers of fast electrons is obvious, and the electron temperature is 2.7eV, with $n_e=1.7*10^{11}/cm^3$. As the pressure is increased we see the electron temperature fall as the mean free path for collisions decreases and the fast electron density decay as energy degradation of the primaries becomes effective, this increase in the primary confinement time results in more ionisation of the background gas and a subsequent increase in n_e occurs. Moving through 1mTorr, the electron temperature has fallen to 2eV, with a slightly lower fast electron component.

The electron density has increased to $1.8*10^{11}/cm^3$. At 3mTorr the increase in the electron density is even more obvious and the electron temperature has fallen to 1.5eV. Interestingly here the collected electron current in the -10V to 0V has virtually disappeared, indicating a fall off in the energetic electron density.

Figure 6.6 shows I-V's for 10A, 50A, and 75A discharges at 1mTorr taken 15cm from the plasma electrode.

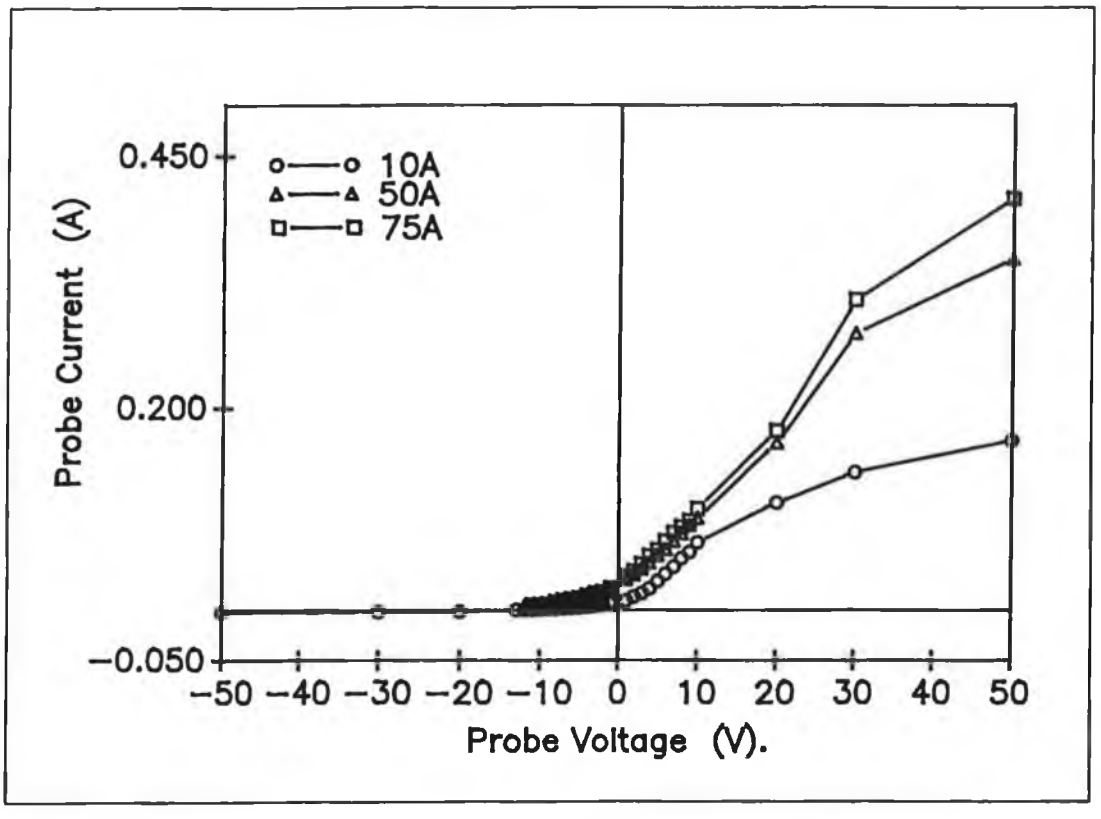

Figure 6.6. I-V characteristics taken in a 1mTorr discharge for different discharge currents.

As the discharge current increases the kT_e can be seen to increase from 2.2eV at 10A to 2.75eV at 75A, also there is an increase in the fast electron density at higher currents. This increase in kT_e and n_f is the reason for the decay in the dc photodetachment signal above saturation as described in chapter 5.

6.6. Time dependent variation of the electron temperature and electron density in a pulsed discharge.

In figure 6.7 the I-V characteristics in a 10A, 1mTorr discharge during the

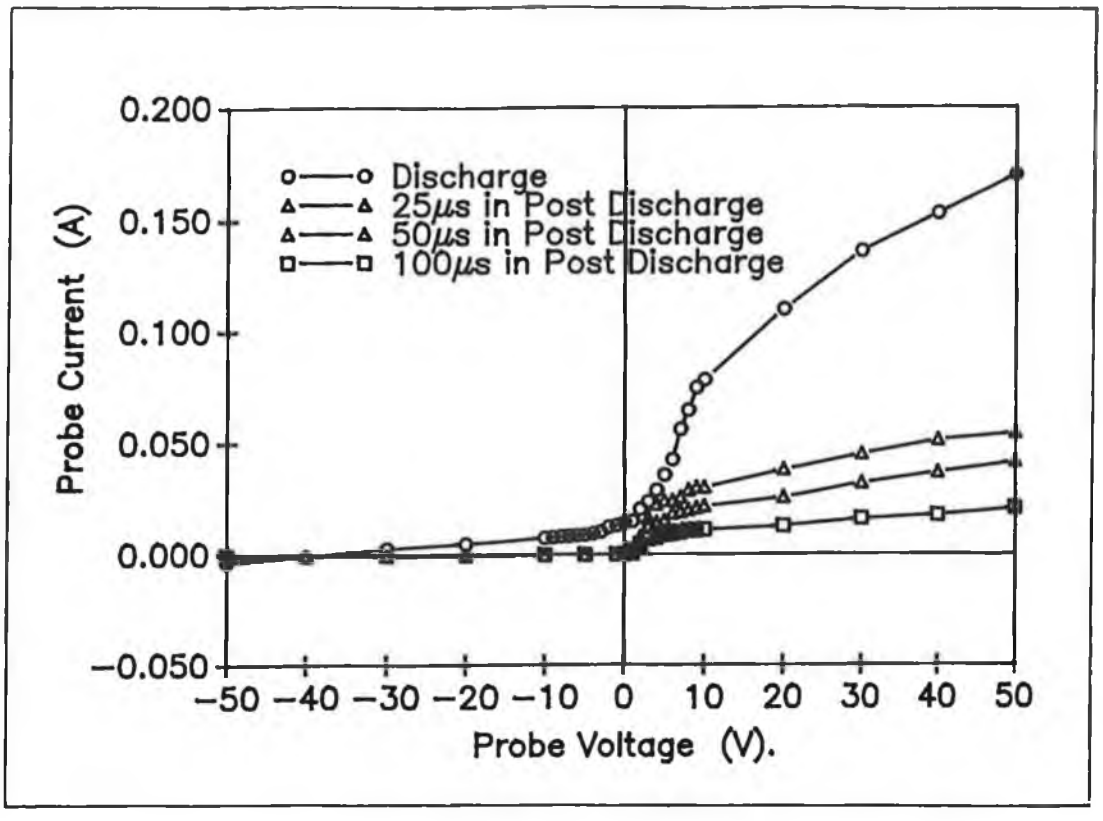

Figure 6.7. I-V characteristics taken in the discharge (a) and post discharge, 25μs (b), 50μs (c) and 100μs, periods of a 10A, 1mTorr plasma.

discharge (a) and post discharge, 25μs (b), 50μs (c) and 100μs (d), periods are plotted. The most notable aspect of this is the absence of electron current in the -10V to 0V region of the curve in the post discharge implying no fast electrons are present. In the discharge the kT_e is 2.1eV, $n_e = 1.7*10^{11}/cm^3$ with n_f of 10%. In the early post discharge the primary density has disappeared and the kT_e has dropped to 1.1eV, with n_e of $1.2*10^{11}/cm^3$. At this point the plasma has reached conditions comparable to the extraction region of a tandem source [8]. Further into the post discharge the electron temperature and density decrease exponentially, with $t_e \approx 30\mu s$. It is this decay in the electron temperature and disappearance of n_f that are needed for an enhancement in H^-. The loss rate by collisional detachment can be seen to decay, figure 6.11, while the dissociative attachment rate increases by a factor of almost 3 in the post discharge. The DA rate increases from $0.9*10^{-8}cm^3s^{-1}$ during the discharge to over $2.7*10^{-8}cm^3s^{-1}$ as the EEDF cools. The CD rate falls by up to two orders of magnitude in the first 50μs of the post discharge.

6.7. Electron temperature and density variation in a modulated discharge.

Figures 6.8.(a) and (b) show electron temperature ,electron density and fast electron density in a 2kHz (a) and a 15kHz (b) modulated discharge, the discharge current is 10A and source pressure 1mTorr. In the 2kHz case the electron temperature reaches 2.6eV during the discharge and decays after switch off with a decay time of 35μs. The electron density is $1.8*10^{11}/cm^3$ and the fast electron component is roughly 20% just at switch on and after about 30μs this drops to 8%. In the post discharge the fast electrons disappear and the electron density falls with t_e=30μs In the 15kHz case the same behaviour is observed with a high electron temperature and a n_f/n_e ratio of roughly 8%. Interestingly in both cases the fast electron density at switch on is a large fraction of the bulk density which results in the decrease in the H^- density seen when the discharge is switched on.

6.8. Control of the EEDF

In chapter 2 it was proposed that the time averaged electron temperature could be controlled by simply varying the duty cycle at a high modulation frequency, 15kHz. This can be determined from the I-V characteristic's for different duty cycles taken in 10A, 1mTorr discharge pulsed at 15kHz. Figure 6.9 shows the time averaged electron temperature as a function of percentage "on" time.

The time averaged discharge current in all the measurements is 10A. The control over the EEDF is clearly possible as figure 6.9 demonstrates. At 100%, continuous discharge the electron temperature is 2.1eV, as the duty cycle is decreased the time averaged electron temperature decreases correspondingly, at 50% it is 1.6eV and at a duty cycle of 25% kT_e is only 0.98eV. Note that the decrease in electron temperature is not a linear function of duty cycle in the lower part of the plot, this is due to the time required for the electron temperature to settle after switch on. Thus in a plasma with an average discharge current the time averaged electron temperature can be set at any value between a minimum, dependent upon the lowest duty cycle capable of delivering a current of $Id_{(avg)}$/duty cycle, and the electron temperature for a continuous discharge of similar current simply by varying the duty cycle of the modulation. This gives effective control over the discharge parameters within the

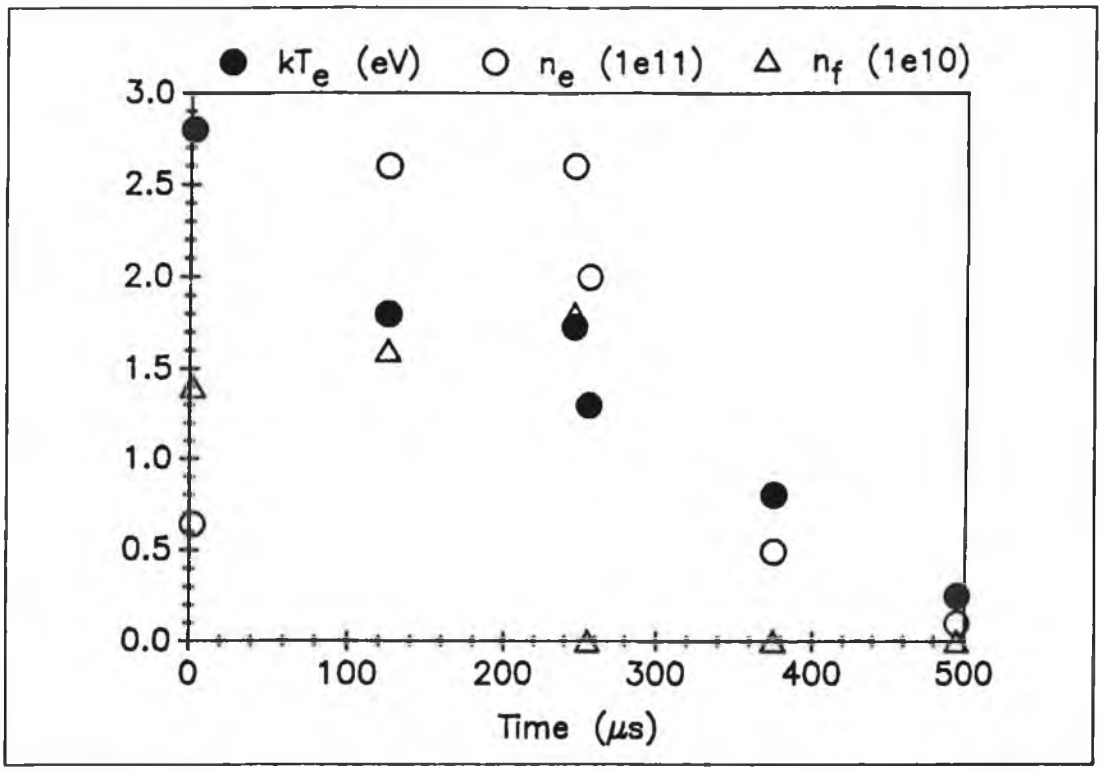

Figure 6.8.(a). **kT_e, n_e and n_f as a function of time in a 2kHz modulated discharge**

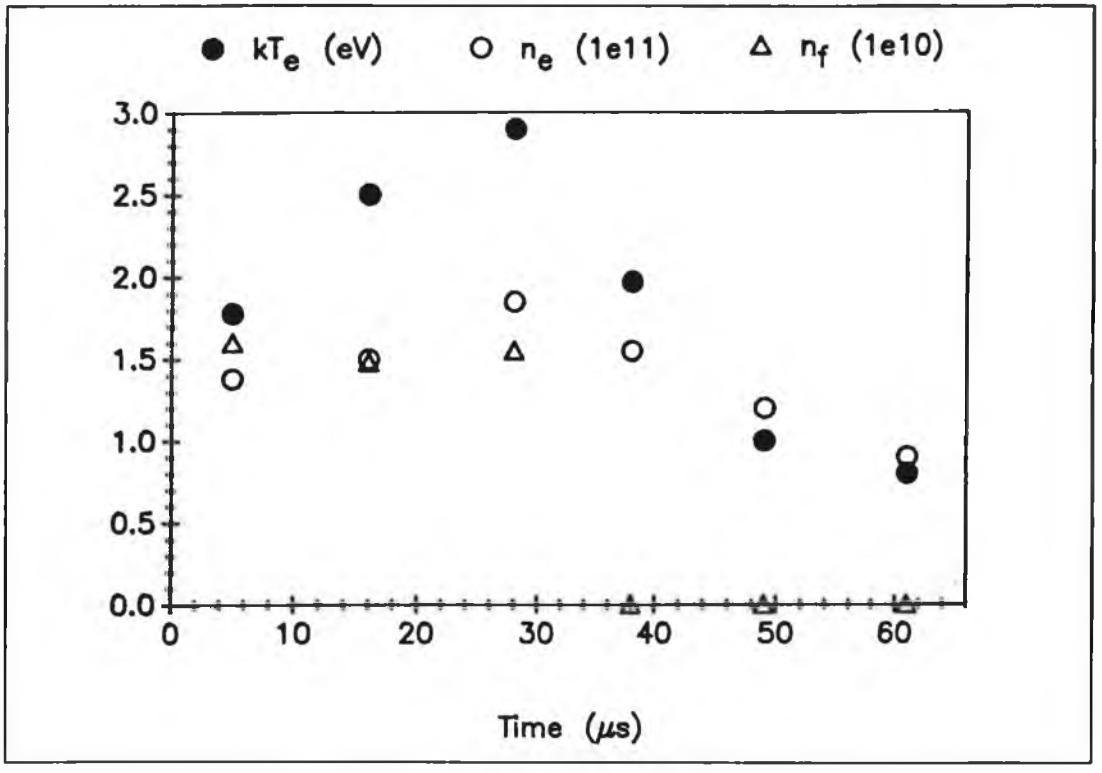

Figure 6.8.(b) **kT_e, n_e and n_f as a function of time in a 15kHz modulated discharge.**

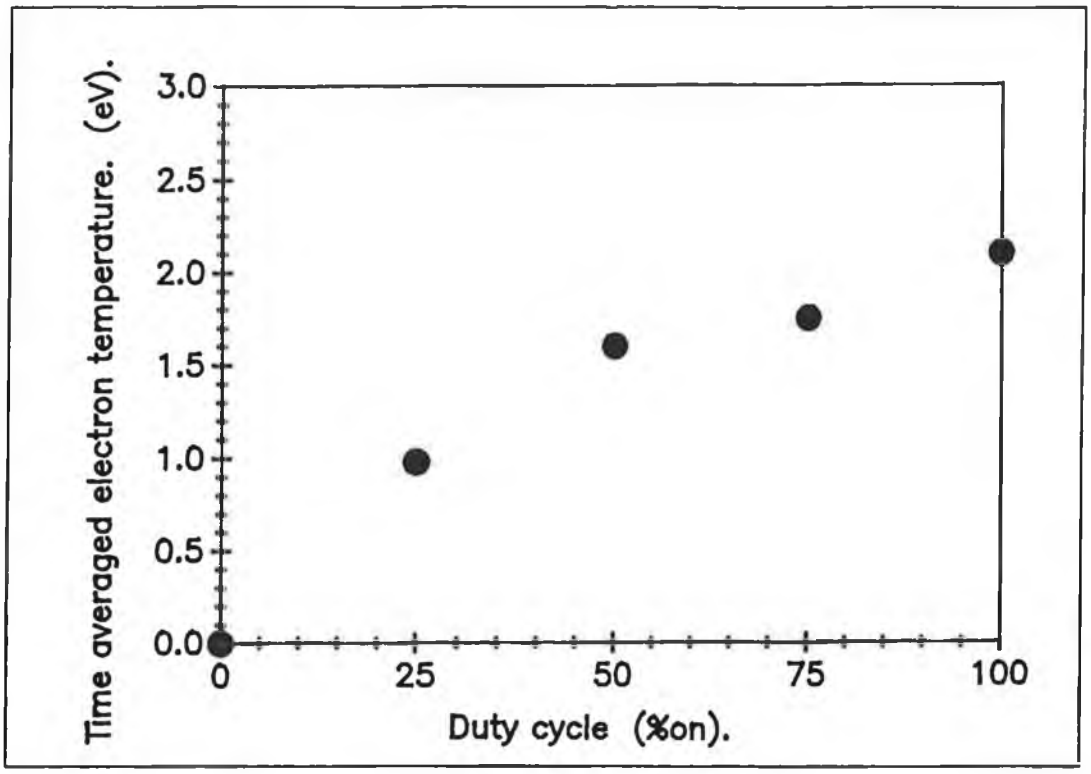

Figure 6.9. Time averaged electron temperature as a function of duty cycle in a 10A, 1mTorr, 15kHz modulated discharge.

range set by the continuous discharge regime.

6.9. Modelling the negative ion density.

In chapter 2 an outline of a model to predict the behaviour of the negative ion density in a modulated discharge was given and this model used typical parameters for a low pressure, high power discharge to show how an enhancement in the H^- density could be achieved by appropriate modulation of the discharge current. In the following chapters extraction and photodetachment measurements were used to confirm that these predicted increases do occur. Moreover these dramatic increases in negative ion density in the post discharge have been demonstrated experimentally on two different volume ion sources, both the D.C.U. source and the DENISE source at FOM in Amsterdam have shown time averaged increases in extracted current when modulated. In this section the probe measurements made on the D.C.U. source are used in a model to calculate the behaviour of the negative ion density in this source and are compared with the experimental data to assess the accuracy of the proposed

mechanism for temporal filtering of the negative ion density. A simpler model has already been described with regards to the FOM source [9], chapter 4, and this has shown a reasonable agreement with the extracted results from the source.

The six species considered are fast electrons, n_p, bulk electrons, n_e, positive ions, n_+, atomic density, n_h, the vibrationally excited density, n''. The time dependent equations for these are,

$$\frac{dn_p}{dt} = \frac{Id}{Ve} - \frac{n_p}{n_g<\sigma_\epsilon v_p>+\frac{1}{\tau_w}} \qquad \text{Eqn. 6.7}$$

$$\frac{dn_e}{dt} = n_g n_p<\sigma_{ion} v_p> - \frac{n_e}{\tau_e} \qquad \text{Eqn. 6.8}$$

$$\frac{dn_h}{dt} = n_g n_p<\sigma_{dis} v_p>+n_g n_{ij}<\sigma_{ij} v_{ij}> - \frac{n_h}{\tau_-} \qquad \text{Eqn. 6.9}$$

$$\frac{dn_+}{dt} = n_g n_p<\sigma_{ion} v_p> - \frac{n_+}{\tau_+} \qquad \text{Eqn. 6.10}$$

$$\frac{dn''}{dt} = n_g n_p<\sigma_{EV} v_p> - \frac{n''}{\tau''} \qquad \text{Eqn. 6.11}$$

$$\frac{dn_-}{dt} = n_e n''<\sigma_{DA} v_e> - \frac{n_-}{\tau_-} \qquad \text{Eqn. 6.12}$$

In the model several assumptions are made which allow easier computation of the H^- density but are not expected to have a major effect on the overall accuracy. It is assumed that the positive ion density is equal to the electron density, this is not strictly true but is a good approximation as [10],

$$n_+ = n_e + n_{ef} + n_- \qquad \text{Eqn. 6.13}$$

where n_-/n_e=1% to 2% and therefore in general n_+ can be approximated to $n_e + n_{ef}$. In the post discharge however n_-/n_e can reach 5% to 10% and may result in a slightly underestimated ion density. The rate co-efficients used are assumed constant

during the discharge and are time dependent in the post discharge, this dependency in the post discharge is due to the cooling of the electron temperature after switch off. This assumption is not exact as the electron temperature during the discharge will also vary as it builds up to steady state. This should not be a huge discrepancy for most reactions but the DA rate may be somewhat affected. It is further assumed that the dominant production mechanism is through the two stage process of EV and DA. Other possible mechanisms for production are discussed in chapter 1, however as EV and DA are assumed as the major production process [11] these are not included here.

The model used consists of first order ordinary differential equations for the species n_p, n_e, n_h, n_+, n'', n_-. To solve these numerically a fourth order Runge-Kutte algorithm was employed with a chosen step size of 10ns. This step size corresponded to the largest increment for which the solution was step size independent. The sets of equations are divided into a discharge regime where the electron temperature and the rate coefficients are assumed constant. In the post discharge the differential equations are solved for a time varying electron temperature with the appropriate rate coefficients being stored in a datafile. The algorithm solves the differential equations for the first discharge period with initial conditions set to zero. The post discharge equations are then solved using the last outputs from the discharge as initial conditions.In figure 6.6 I-V characteristics for the discharge and post discharge periods were plotted. In figure 6.10 the electron temperature and electron density are plotted as a function of time in the post discharge of a 10A, 1mTorr plasma. From this variation we can determine the rate co-efficients of the various processes. In this case the two most important processes are the dissociative attachment of H^- and the collisional detachment by fast electrons. The variation of these with time in the post discharge is plotted in figure 6.11.

The DA rate can be seen to increase from 1e-8cm^{-3}/s at switch off to almost $3*10^{-8}cm^{-3}/s$ after 20μs, it is this increase that is vital to the enhancement of the time averaged negative ion density when modulating at optimum frequencies. The ED rate decays by a almost two orders of magnitude as the post discharge progresses. The RCIP rate for $H_2(v^*)$ destruction, which may also be affected by the rapid decay of the fast electrons, is not shown in figure 6.11 and since the loss time for vibrational levels is long this is not a dominant factor.

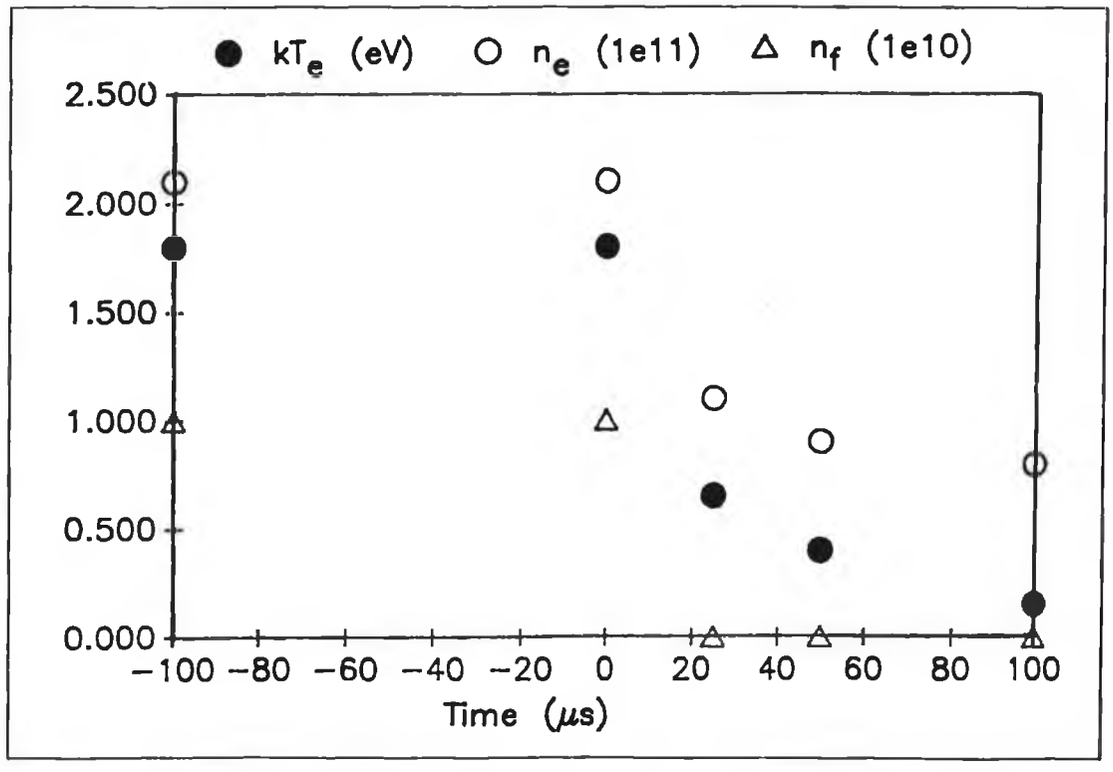

Figure 6.10. Electron temperature, electron density and fast electron density evolution in the post discharge of a 10A, 1mTorr plasma.

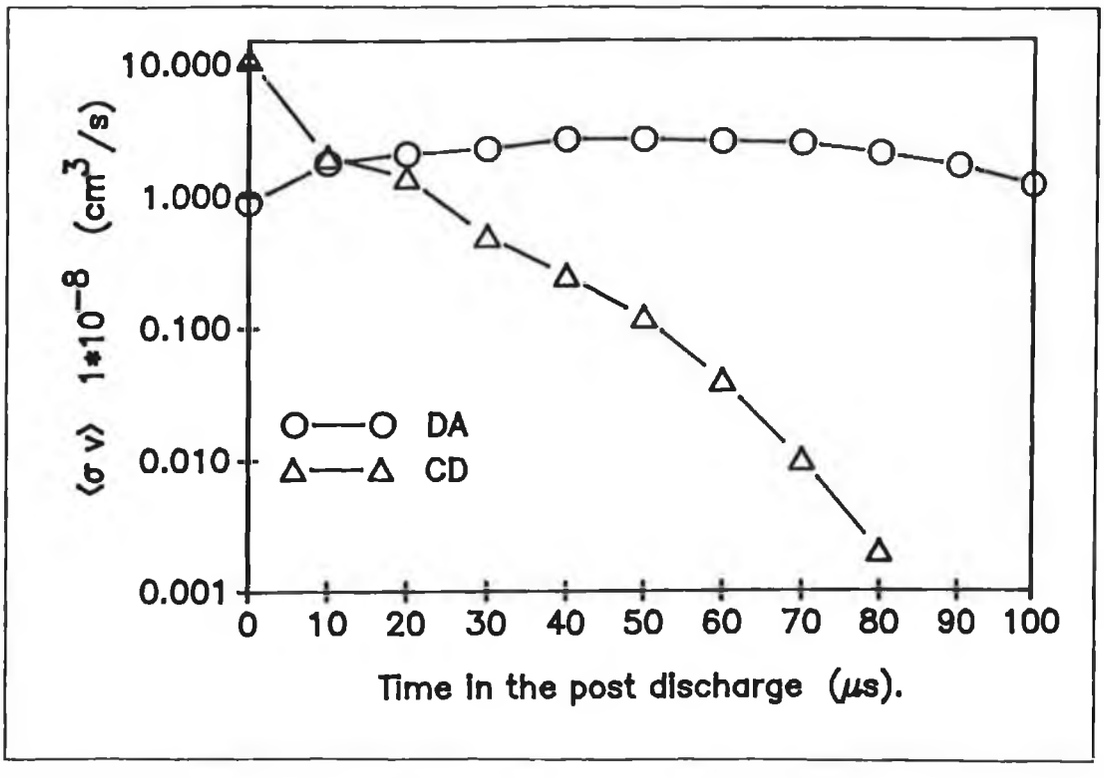

Figure 6.11. Evolution of the DA and CD rate coefficients in the post discharge of a 10A, 1mtorr plasma.

6.10. Calculated H^- densities and production and loss rates.

Figure 6.12 shows the calculated and experimentally determined H^- densities for a 10A, 1mTorr discharge at 20cm from the plasma electrode.

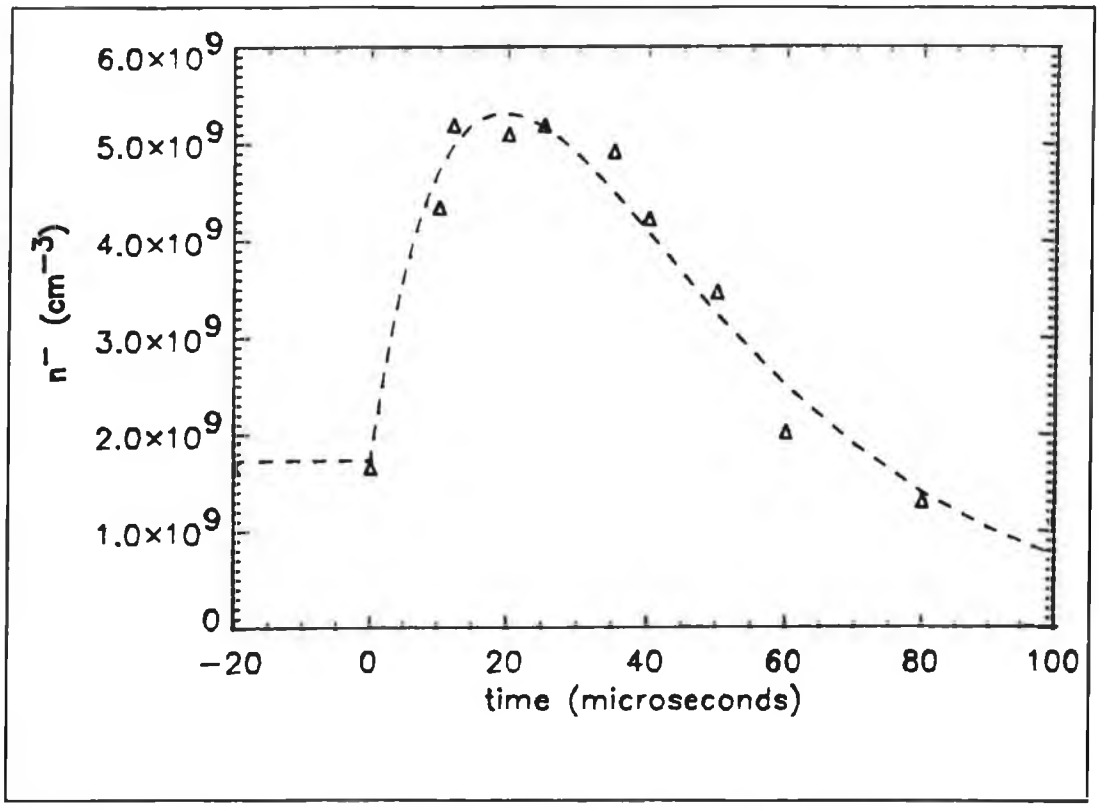

Figure 6.12. Calculated and experimentally determined H^- densities as a function of time in a pulsed 10A, 1mTorr discharge.

The calculated density is in good agreement with the measured data, showing the same rapid increase in the post discharge followed by an exponential decay. The production and loss rates for H^- in the post discharge are shown in figure 6.13. After switch off the production rate can be seen to increase rapidly while the loss rate decreases almost instantaneously, further into the discharge the interchange of the dominance of losses due to MR and AD with wall losses can be seen at roughly 100μs as the H^- decay rate decreases to 200μs. During the discharge the loss rates due to CD are by far the most dominant almost 60% while the other losses account for 40%. This is due to the high percentage of fast electrons present during the discharge. In contrast in the FOM source there is a much lower percentage of fast electrons in the range of operation, at 0.75pa and 10A, n_f/n_e is only 1% and therefore the CD losses are not as

dominant resulting in a much lower post discharge increase in H^- extracted current.

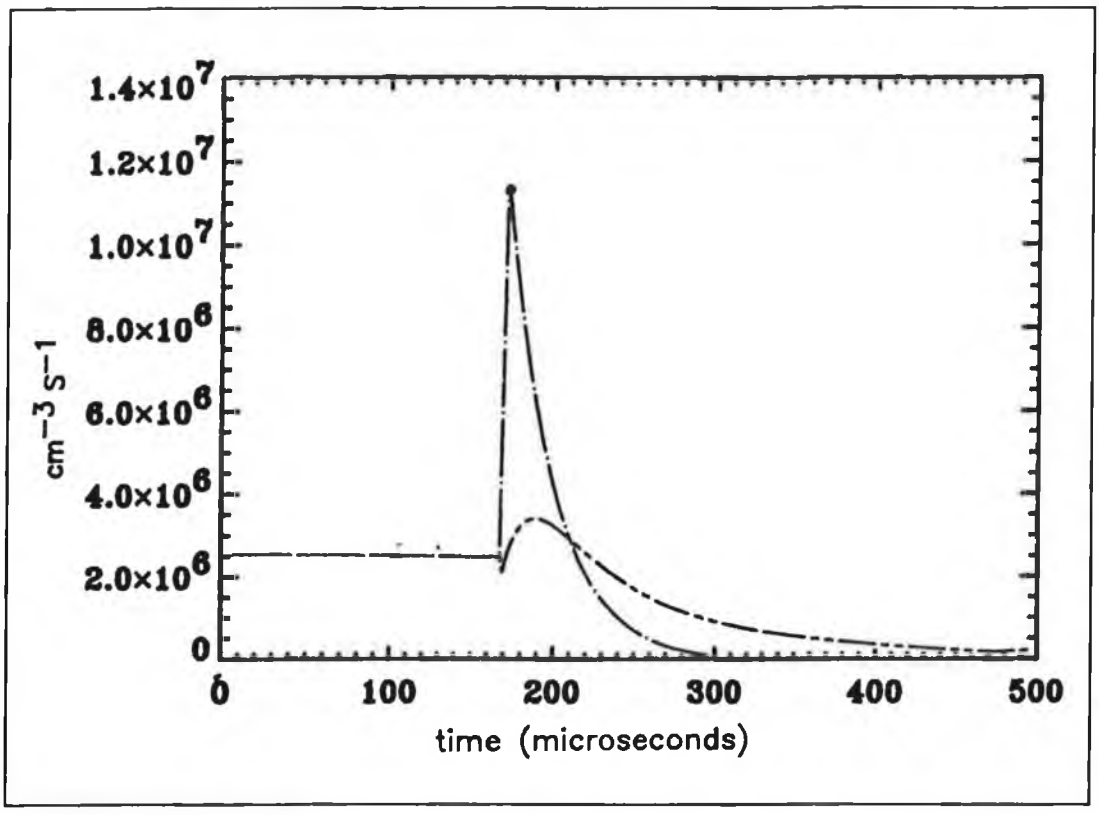

Figure 6.13. Calculated production and loss rates as a function of time in a pulsed 10A, 1mTorr discharge.

The correlation between the calculated densities and the experimental data supports the view that the mechanism responsible for the enhancement is the electron temperature cooling and reduced CD losses. An important note here is that the model shows a smooth increase to the peak and a smooth decay subsequently whereas the experimental data shows some scatter in the absolute H^- densities around the peak. This scatter may indicate that there exist some structure in the peak region. This has not been investigated but it may possibly be due to an interaction of the two processes responsible for the enhancement or due to some other effects not catered for in the model.

In figures 6.14 (a) and (b) the calculated H^- densities in a 2kHz (a) and a 15kHz (b) discharge are plotted. Here for the 2kHz case there is good agreement between the calculated and measured values of negative ion density. Both the experimental data and the calculated densities show a similar decrease after the discharge is switched on again. This has been explained by the rise time of the CD

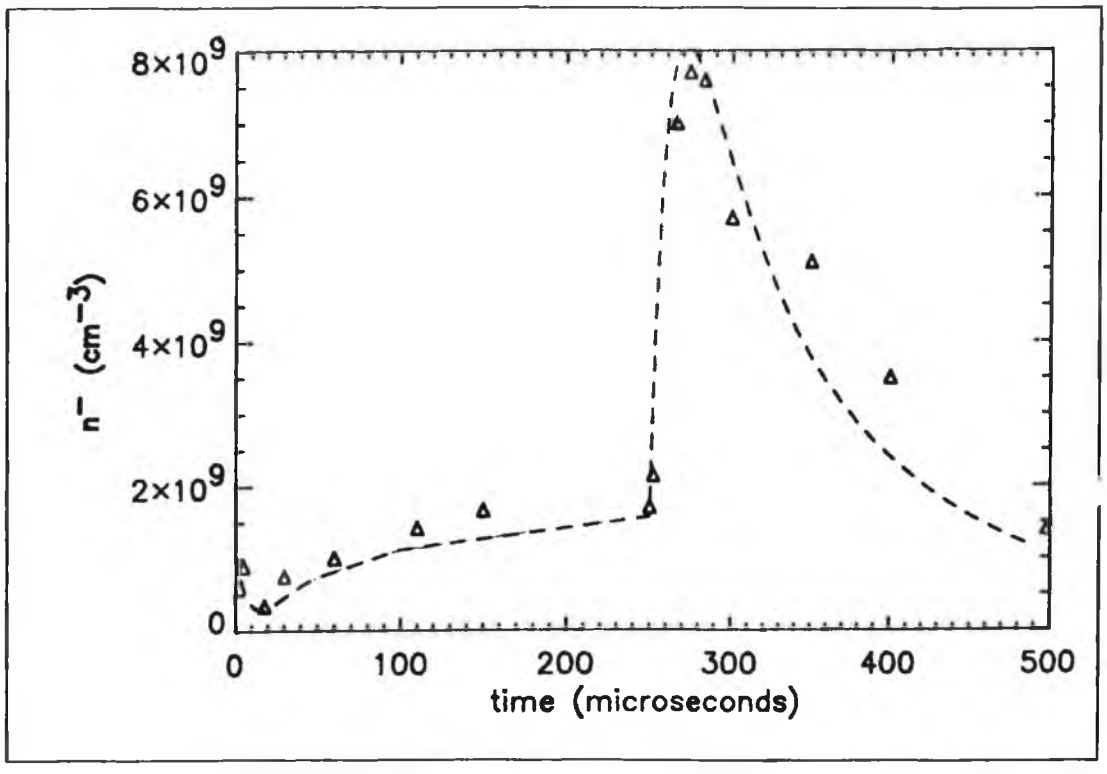

Figure 6.14.(a) **Calculated and experimental H^- densities in a 2kHz modulated discharge. Id=10A, P=1mTorr.**

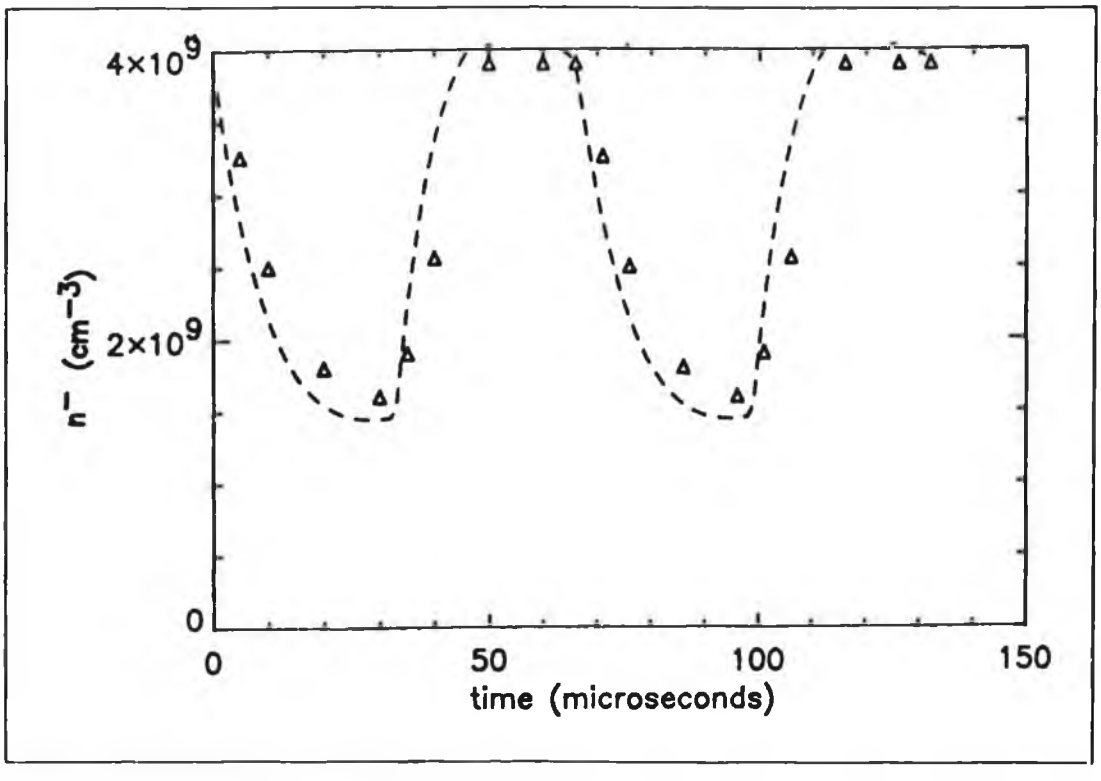

Figure6.14.(b) **Calculated and experimental H^- densities in a 15kHz modulated discharge. Id=10A, P=1mTorr.**

losses, >1μs, at switch on whereas the production rate evolves much more slowly. This is borne out by figure 6.15.(a) where the production rate and loss rate are plotted as a function of time. At switch off the production rate, enhanced by the cooling kT_e, far outstrips the decreased losses, this results in the H^- increase.

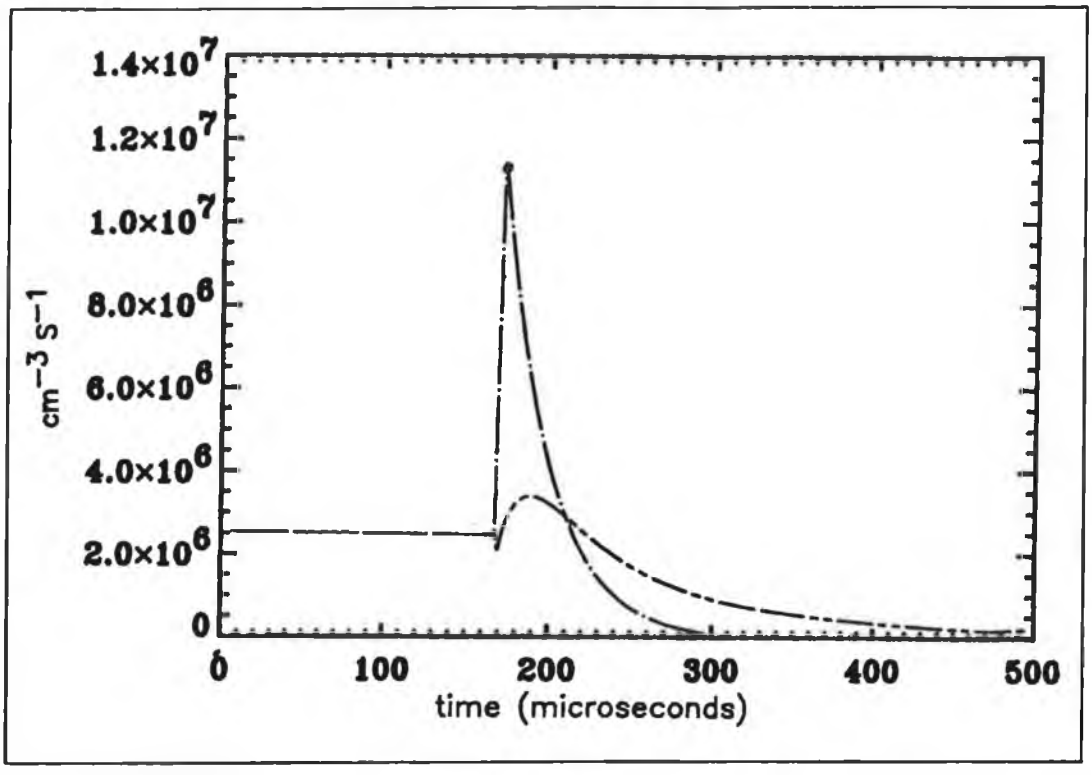

Figure 6.15.(a) **Calculated production and loss rates in a 2kHz modulated discharge.**

Further into the post discharge the losses over take the production and the density decreases. At switch on the loss rates increase rapidly as the fast electron density builds up but the production rate actually decreases as the electron temperature increases. These effects mean that the H^- density will remain highly modulated even at high modulating frequencies. This effect is in keeping with the extracted results from FOM and the photodetachment measurements on the D.C.U. source, but is at odds with the extracted results from the D.C.U. source. This discrepancy appears to be due to the accelerator configuration rather than to the physical phenomenon involved in H^- production and is discussed further in chapter 7. In the case of the modelling results for a 15kHz modulated discharge a similar behaviour is observed in the calculated densities with a rapid increase upon switch off and a decrease at switch

on which extends up to 20μs into the discharge before the density recovers. In this case an overall increase in the time averaged density is seen but the calculated densities are again very modulated. It can also be seen that the calculated densities are in good agreement with the experimental data.

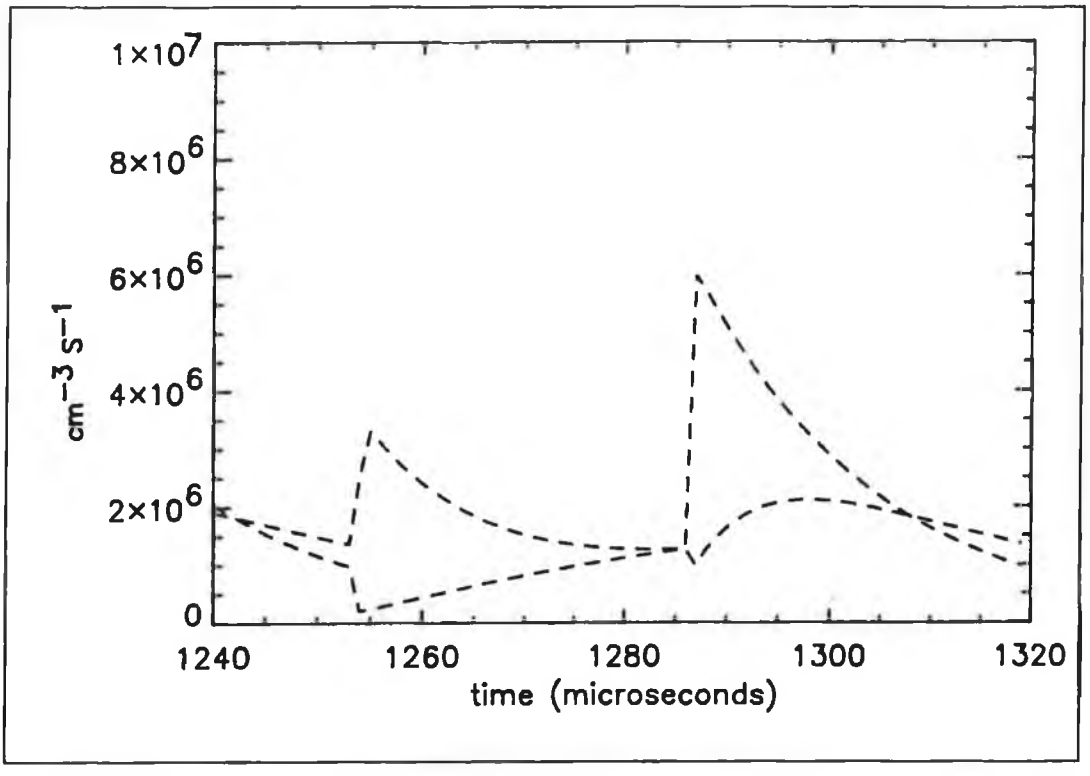

Figure 6.15.(b) Calculated production and loss rates in a 15kHz modulated discharge.

6.11. Conclusion.

The probe measurements presented in this chapter confirm that the cooling of the electron temperature and the reduction of losses in the post discharge for the basis of the mechanism responsible for enhancement of the negative ion density by modulation of the discharge current. The dependence of the electron temperature on pressure and current have been shown to behave in the manner used in previous chapters to explain the peak/dc ratio and the post discharge peak rise time dependence upon the same parameters. Also the high fraction of fast electrons required to account for the large CD losses have been confirmed, with n_f/n_e ratios of up to 10% in low pressure high power discharges. A model has been used to solve the time dependent

differential equations describing the species densities in both the discharge and post discharge periods. The calculated densities show a good agreement with the experimentally measured H^- densities and also provides an explanation for the temporal behaviour of the negative ion density in the source, especially the high modulation of the H^- which is seen in the photodetachment measurements at D.C.U. and in the extracted current from DENISE. This modulation is due to the rapid increase in CD losses at switch on which depletes the H^- density before the production has reached it maximum value.

References.

[1] Bacal, M, et al.
Journal of Applied Physics, 52, p1247, 1981.

[2] Hiskes, J.R, et al.
Journal of Applied Physics, 53, p3469, 1982.

[3] Scanlan. J.V.
PhD Thesis, Dublin City University, 1991.

[4] Chapman, B.
"Glow Discharge Processes"
Wiley and Sons, New York, 1980.

[5] Bernstein, I.B. and Rabinowitz, I.N.
Physics of Fluids, 2 (2), p112, 1959.

[6] Braithwaite, N.
Private Communication.

[7] Hopkins, M.B, Graham, W.G. and Griffin, J.J.
Review of Scientific Instruments, 58 (3), p143, 1987.

[8] Hopkins, M.B. and Graham, W.G.
"4th International Symposium on the Production and Neutralisation of Negative Ions and Beams.", Brookhaven, 1986.

[9] Heeran, R.M.A, et al.
Europhysics Letters, 17 (6), p503, 1992.

[10] Amemiya, M.

Journal of Physics D: Applied Physics, 23, p999, 1990.

[11] Bacal, M.

Nuclear Instrumants and Methods in Physics Research, B37/38, p281, 1989.

Chapter 7. Discussion of results.

7.0. Introduction.

In the preceding four chapters results have been presented on the measurement of negative ion density and extracted currents from a modulated volume ion source. This has been done in order to determine the effectiveness of a proposed temporally filtered source [1], and also to assess the ability of such a source to meet the demands of the next generation of neutral beam heating systems for fusion plasmas. Along with this much can be learned about the processes and reactions responsible for H^- production and loss in the volume source. This chapter discusses the results of extraction of negative ions, measurement of negative ion density and modelling of the behaviour which have been presented individually and tries to assimilate a coherent argument for the effects seen in each. The individual results show enough similar behaviour to support the underlying principle of enhancement as proposed in chapter 2. Moreover the differences observed between the experiments, especially between the extraction results from FOM and D.C.U. lead to important conclusions as to the most effective method of increasing the output from a volume ion source.

7.1. Summary of results.

The concept of increasing the negative ion density in the post discharge of a plasma has been verified by all the measurements and modelling presented to date. In each case these increases have been explained in terms of a combination of the two effects of the cooling of the electron temperature and reduction of losses after the plasma has been switched off. Increases of over three times the dc operated value have been shown to be possible. Appropriate pulse modulation of the D.C.U. source has shown time averaged increases of up to 300% in both the extraction and photodetachment measurements. The DENISE source has shown increases of over 40% in the time averaged extracted currents when modulated at 5.8kHz, this was however at low discharge currents, 20A, and high source pressures, >5mTorr. It is speculated that much larger increases are possible if the source is operated at high

power, >100A, and lower pressures, <1mTorr, with high modulation frequencies. Therefore it has been shown possible to vastly improve the power and gas efficiencies of the volume ion sources by temporal filtering.

The photodetachment and extraction measurements from the D.C.U source show the same pressure and current dependence of the post discharge enhancement, no enhancement is seen above pressures of 5mTorr and increasing peak to dc ratios are observed as the pressure is decreased. At source pressures of 0.5mTorr to 1mtorr post discharge peak values have been measured similar to the maximum values from a continuous discharge at higher pressure, thus indicating that the temporal filter could have advantages when operating the volume source at lower pressures as required by modern accelerators [2]. This pressure dependence is corroborated by probe measurements as being consistent with the mechanisms assumed responsible for temporal filtering, i.e the electron temperature and fast electron density increases with decreasing pressure leading to greater enhancement in the post discharge.

The current dependence has shown a similar trend in both the extraction and photodetachment measurements, as the peak/dc ratio has been shown to be a strong dependence of the discharge current and increases at higher power operation. The FOM extraction results show a similar pressure and current dependence, however the pressure dependence occurs over a larger range, i.e the peak continues up to higher pressures, approximately 13mTorr to 15mTorr. Again these are consistent with the probe measurements given by Eenhuistra [3]. Also the peak rise times from both diagnostics show good agreement, the peak rise time dependence with current and pressure is shown to be as a result of the variation of the electron temperature and n_f. The spatial dependent broadening of the peak rise time is explained by the movement of the negative ions throughout the source in the post discharge. The timescales of the FOM results are also within the range of those expected, these extraction results have shown a very strong dependence of the peak rise time with pressure and this is explained by the high power density of the source. However no spatial resolved measurements are available at present for this source. The dependence of the peak rise time on the electron temperature and fast electron density has been clearly shown in figure 5.13, where the magnetic field which cools the electron temperature and reduces n_f also reduces the peak rise time.

7.2. Differences between FOM and D.C.U results.

There are several differences between the various measurements made, i.e. peak rise time dependence on pressure, current and position, differences in the behaviour of the H^- density with discharge current at 20cm and 1cm from the plasma electrode and the higher pressure range of the FOM source. However one of the major differences between the results is the depth of modulation of the H^- density and extracted currents. The original extraction results from the D.C.U. source [4] show little or no modulation of the extracted beam when pulsed at high frequencies. However the photodetachment results and the extracted results from DENISE, along with the modelling of the discharge, show the negative ion density to be highly modulated [5]. This modulation of the density is important as it effectively limits the possible use of the modulated source in modern accelerators. In the FOM source this modulation resulted in an almost discontinuous beam output. Modelling and photodetachment results point to this modulation as being due to the rapid increase in H^- loss rate as the fast electron density build up immediately after switch on, $<1\mu s$. Why then do the extracted results from the D.C.U source not show the same modulation of the beam. It is proposed here that this is due to the presence of a magnetic field in the vicinity of the extraction aperture.

7.3. Effects of a magnetic field at the extraction aperture.

It has been previously been shown that a magnetic field can effectively remove the fast electron density and result in a cool maxwellian discharge. This magnetic filtering is responsible here for the depleting the n_f density close to the extraction aperture of the accelerator. In the FOM source, figure 4.1, the magnetic field of the electron trap is placed in the extraction electrode at a distance of 3mm from the plasma electrode. This small magnetic field will only extend across the electron trap and should have no effect on the plasma boundary near the aperture. In the D.C.U. source the accelerator had an electron trap with magnets placed in the plasma electrode resulting in a magnetic field across the aperture. It is believed that this field reduces the fast electron density in the area adjacent to the aperture. If this field were to operate as a tandem style region then we would expect a vast increase in H^- density

during the discharge with no increase occurring in the post discharge. It is proposed here that this area is too small for sufficient production and that the main production occurs in the driver regions outside this field and the negative ions subsequently drift into this region where losses are reduced, this is possible as the mean free path of H^- even during the discharge will be sufficient to travel across the short distance to the aperture, figure 7.1.

There is also the effect of the extraction voltage to consider, this will have the effect of drawing the negative ions into the field region from adjacent areas and also of removing those H^- ions that are produced in or drift into this region preventing a build up of the density.

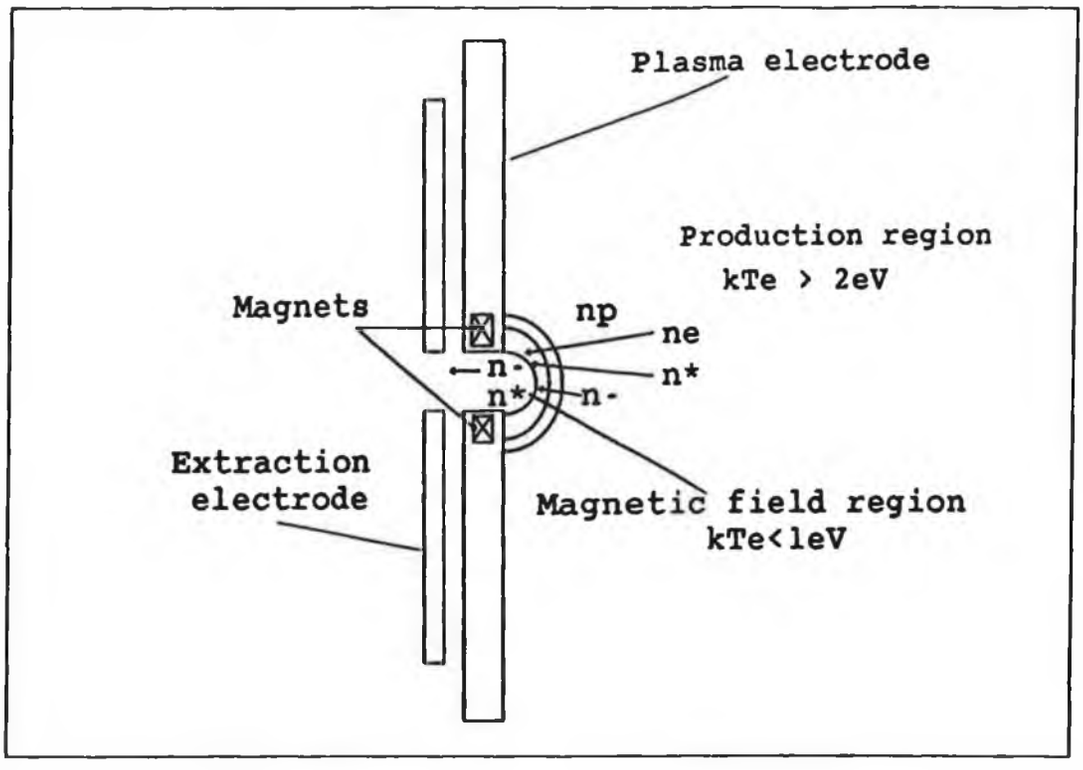

Figure 7.1. Representation of the effect of magnetic field on H^- ions near the aperture.

Figure 7.1 shows a representation of the possible effect of the magnetic field and extraction voltage near the extraction aperture. The field region is shown as extending a short distance into the plasma. The $H_2(v^*)$ states can drift into this region, while the negative ions can drift or be pulled by the extraction voltage towards the aperature. Once a H^- ion enters this region the losses are greatly reduced. Upon

switching off the discharge, the H^- density in the region close to the field increases rapidly, by up to a factor of 3 to 4, these H^- ions can then move into the aperture region where they are extracted. When the discharge is switched on again the fast electron density builds up, <1μs, and the H^- density in the adjacent regions decreases. However there are little or no fast electrons in the field region and thus the H^- density decays away with at a similar rate to the rest of the post discharge, ≈100μs, a much slower rate than outside this region. The density in the aperture region continues to decay slowly until the density in the adjacent area builds up again, 30μs, and starts to replenish the decaying H^- in the field region. Thus the extraction aperture sees less modulation of the negative ion density than the interior of the source. While the negative ions can be drawn into this region by the extraction voltage, those $H_2(v^*)$ that drift in can be affected in a similar manner as the losses due to fast electrons are reduced, this also leads to a higher density and less modulation at the aperture. The effect of the $H_2(v^*)$ will not be a major factor as the long lifetime, ≈1ms, means minimal modulation of the density occurs even in the interior of the chamber.

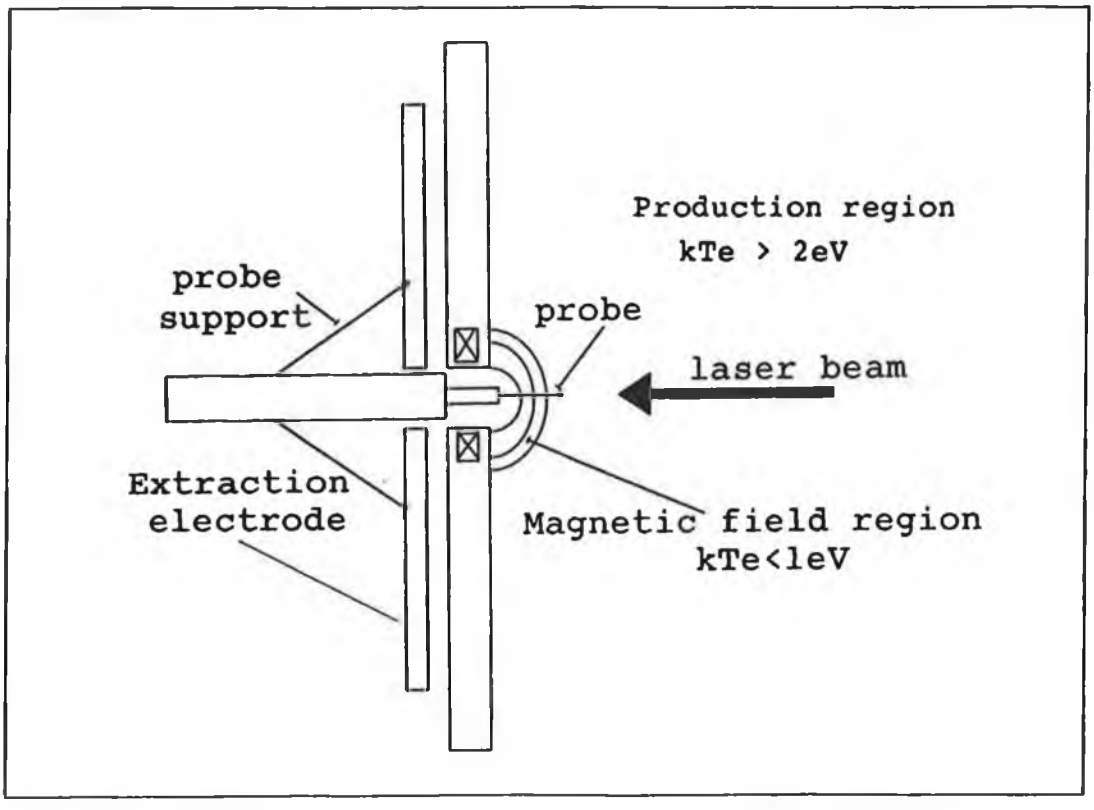

Figure 7.2. Experimental configuration used to determine the effect of the magnetic field on the H^- density near the aperture.

This was investigated by measuring the H^- density by photodetachment near the aperture with a magnetic field present, figure 7.2. Magnets are placed on the inside of the plasma electrode resulting in a magnetic field across the probe when placed in the aperture.

Figure 7.3 shows the time resolved photodetachment signal for a 2kHz modulated discharge taken at 1cm from the plasma electrode with a magnetic field present. Here we can see that upon switch off the density increases to almost twice that of the continuous level and then slowly decays away, t_{H^-}=50μs. At switch on the density shows no increase in the loss rate and starts to build up to the dc level as the electron density recovers.

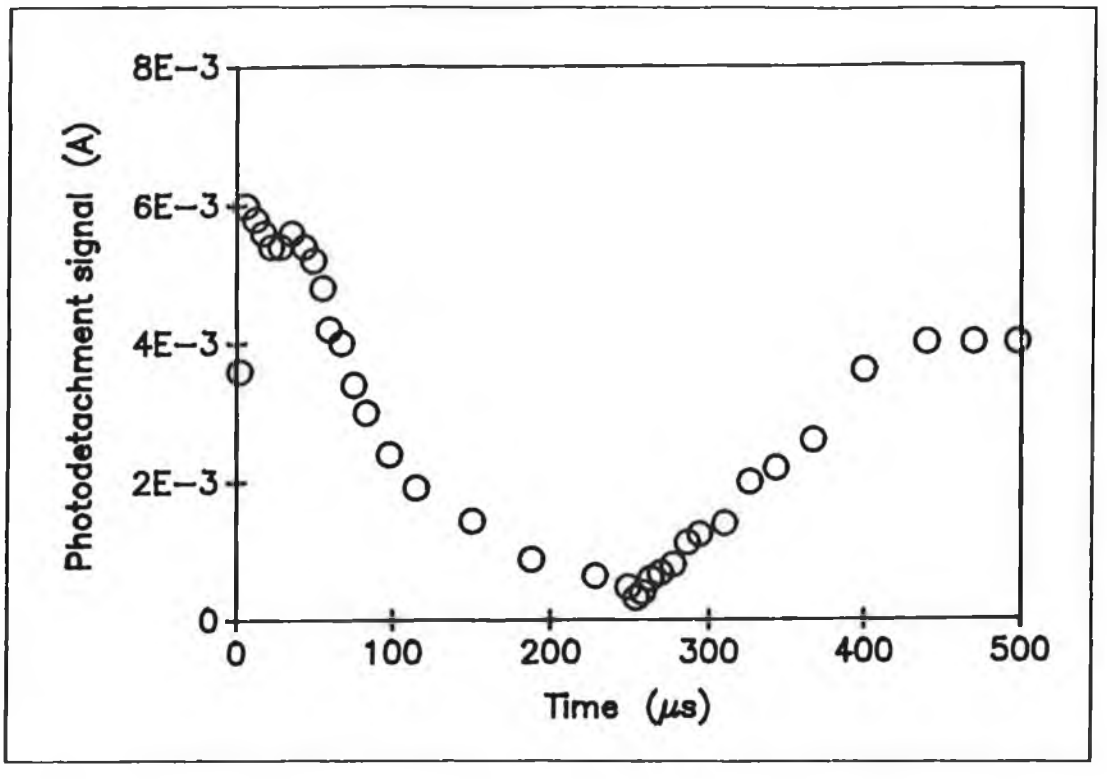

Figure 7.3. Photodetachment signal as a function of time for a 2kHz modulated discharge in the presence of a magnetic field.

In figure 7.4 the photodetachment signal in a 5kHz discharge taken at 0cm is plotted. Again at switch off the density increases to almost twice the dc level and then decays away, in this case a slight decrease is seen before the density starts to build up again. This decrease in H^- at switch off is less than that seen in the measurements taken earlier in the centre of the source.

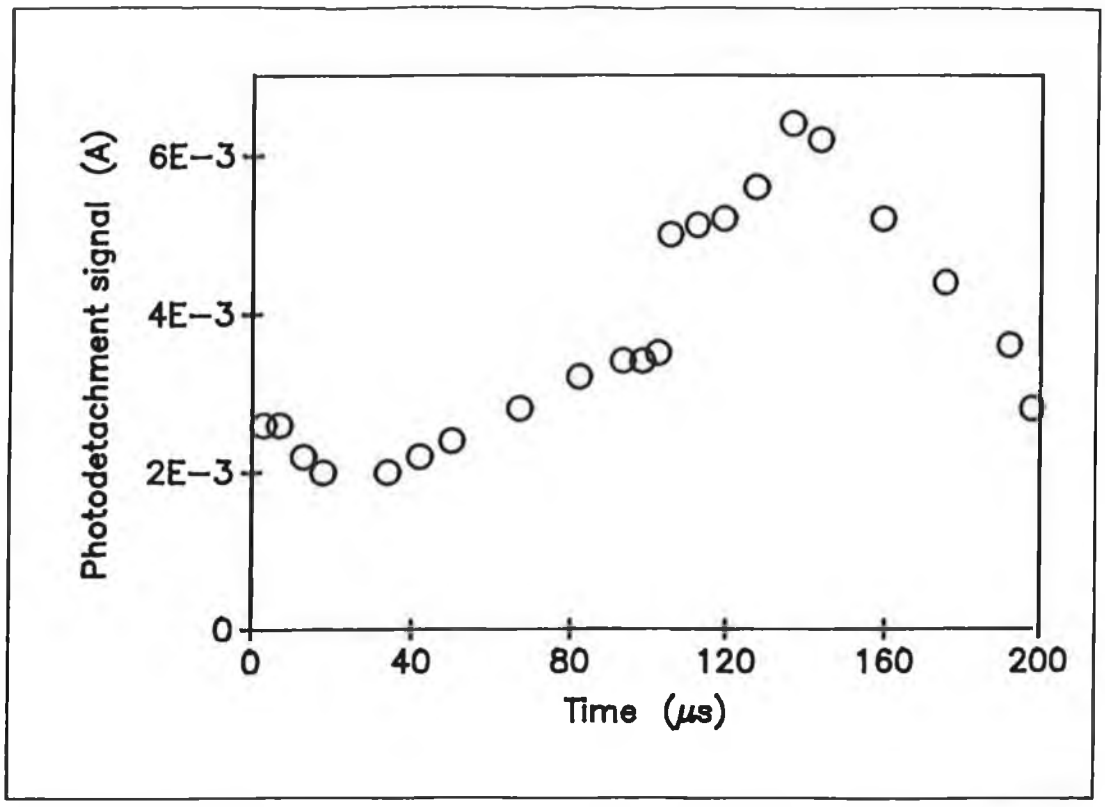

Figure 7.4. Photodetachment signal as a function of time in a 15kHz modulated discharge in the presence of a magnetic field.

These figures show in some respects the effects observed in the extracted results in chapter 3. However they do not replicate fully the behaviour of the H^- density needed for an unmodulated extracted current. In these the modulation is definitely reduced, but it is also obvious that some tandem effects are occurring here as the dc density can be seen to increase when entering this field region and the post discharge enhancement is not as large as that seen in the extracted currents or for photodetachment measurements with no magnetic field. Also note that the peak rise time has shortened considerably, a magnetic filtering effect, chapter 5. However there are some important differences between the conditions under which the two sets of measurements were taken. In the case of these photodetachment measurements the field area will be more substantial, as the aperture in the plasma electrode for the probe support is approximately 12mm in diameter and therefore the magnets are further apart than in the extraction results. This will have the effect of increasing the tandem style production region and thus the contribution of these negative ions to the measurements. Also there is no applied voltage behind the aperture, this would have

the effect of depleting the H^- near the aperture and pulling H^- ions into this region from adjacent driver region. Because of the tandem effect and with no extraction voltage the negative ion density in this region will be higher and therefore this will limit the drift of ions into the region from adjacent areas. Even so the measurements taken here do indicate that the magnetic field from an accelerator can have the effect of reducing the modulation which occurs at switch on in the rest of the source. Moreover this implies that for the temporal filtering concept to be effective then the magnetic field effect must be fully investigated to ensure minimal modulation of the extracted beam.

7.4. Peak rise times.

The peak rise times in the post discharge have been discussed in all the previous results, these rise times are important as they give much information about the processes and effects leading to the enhancements in the post discharge. Also they are a useful diagnostic tool as the relative broadening or sharpening of the peak is related to the electron temperature in the discharge and they can also give insights into movement of the ions throughout the chamber. In all cases the dependence of the peak rise time on pressure and current has been observed, more obviously in the FOM source, but the extraction and photodetachment results from D.C.U. also show this dependence. Probe measurements have verified that this dependence is due to the electron temperature and fast electron density variation with discharge parameters. More specifically the pressure dependence has shown the relative change of the peak rise time to be indicative of the efficiency of the source. As the pressure is decreased the efficiency of the two stage , via EV and DA, production process decreases, a result of the increasing kT_e and n_f and the peak rise time reflects this change. Moreover the peak rise times must be known to establish the criterion for effective enhancement of the negative ion density, as the peak is dependent upon the change in the loss rates from the discharge to the post discharge periods.

7.5. Comparison of the Temporally filtered source and the Tandem source.

Apart from the surface conversion and cesiated sources under investigation, the

tandem source is the most successful adaption of the volume ion source to date and the most likely to form the basis of the future neutral beam heating systems. Therefore it is against the tandem source that any new source must be compared. The source at D.C.U. has not been operated as a magnetically filtered source and therefore no absolute comparisons can be made with the results obtained on it. The FOM source has been characterised, for operation with and without a magnetic filter by Eenhuistra et al [3].

We have already observed, chapter 4, the enhancements in the time averaged extracted currents by modulation over the dc values of a source operated without a filter. At pressures of 5mTorr and discharge current of 20A, by modulating at 5.8kHz an enhancement of 40% was obtained in the time averaged extracted. However the extracted current from a 20A continuous discharge, operated with a filter, has been shown to be 0.9mA. This is a factor of 4 larger than the time averaged extracted current of the above modulated discharge, even for an optimised modulation frequency it will be at most around 30% of the tandem source current. However the temporal filtering is ineffective at higher pressures while it is the optimum pressure for the tandem source. At lower pressures the extracted current from the tandem source decreases dramatically and in the pressure range of 0.5mTorr to 1mTorr the extracted current has fallen to 0.2mA-0.3mA. It has been previously shown in extracted and photodetachment results from D.C.U. that the post discharge peak value at lower pressures, 0.5mTorr, is the same or greater than the dc value at higher pressures. This has also been indicated in the FOM results where the peak/dc ratio increases with decreasing pressure. Thus it can be speculated that the post discharge peak from an source without a filter will be similar to that obtained from a tandem source at the same pressure.

The discharge current dependence of the extracted current from an magnetically filtered source operated at optimum pressure, 5mTorr to 7mTorr, shows an almost linear increase in n^- with increasing discharge current. This is due to the dependence of both the production and loss rates on discharge current. However at lower pressures, <1mTorr, the extracted current appears to saturate as the current is increased. This may be explained by the large numbers of fast electrons which will be present at lower pressures which will increase with increasing discharge current.

Further the increasing kT_e will limit the production of H^- via DA. Thus the efficiency of a tandem source at low pressures and high powers is limited.

The peak/dc ratio in the pulsed experiments has been already been shown to increase with discharge current especially at high power, in the photodetachment measurements from the D.C.U. source peak/dc ratios of over five have been observed for discharge currents above 100A. In figure 4.5 the extracted currents from the FOM source have been observed to increase with increasing discharge current.

Thus while the post discharge peak at low pressures will be similar to the tandem source current for a 20A discharge, it is expected that for much higher power operation, 100's of amperes, at low pressures the pulsed discharge time averaged extracted current will be equal to or greater than that possible from a tandem source and it is this low pressure capability that is a major advantage for the temporally filtered source.

7.6. The temporal source and the requirements of NBI.

Neutral beam injection systems require high power, >1Mw, negative ion beams. One of the major losses of H^- in accelerators is due to the stripping of the negative ions by gas molecules. This loss is dependent upon the source pressure and thus a lower operating pressure is preferable. One of the limitations of the tandem source is that its optimum H^- output occurs at high source pressures, 5mTorr to 10mTorr. As has been shown the temporally filtered source is more efficient at lower pressures and will provide much larger enhancements at pressures below 1mTorr.

With the extraction of negative ions, electrons are also extracted and must then be dumped in the accelerator which can cause major heating and acceleration problems. In figure 3.11 the ratio of the extracted H^- to electron currents was shown to increase from 1/50 to less than 1/10 with high frequency modulation of the discharge current. Also the temporal source allows production of H^- and $H_2(v^*)$ to occur throughout the whole source, unlike the tandem source where the production of $H_2(v^*)$ is limited to the driver region.

The above effects point to the temporal source as having major advantages as a source of ions over other sources. Unfortunately this optimism must be tempered by it's one major possible disadvantage, i.e the modulation of the H^- density and extracted

current. In order to produce a high brightness nonmodulated enhanced H^- beam from a low pressure high power modulated source, the effect of the magnetic field in reducing the beam modulation must be fully understood to determine if it can be applied to a conventional accelerator on a volume source and produce an unmodulated output.

7.7. Conclusion.

The discussion of the results has compared the measurements, extraction and photodetachment, taken on two different volume ion sources and have indicated that large gains in the H^- density are possible in the post discharge of pulsed discharge. These enhancements show the temporal source to have several advantages over the tandem source, i.e lower operating pressures and increased negative ion to electron extracted currents. And with the possibility of RF generated plasma longer operating lifetimes are possible. However the results have not yet shown the temporal source to be a viable replacement for the tandem source. The main obstacle is the high modulation of the extracted currents and H^- density in the source and this may prove to be the limiting factor in the use of temporal sources in NBI systems. However the temporal source may other applications where modulation of the density is not as important, i.e the production of high intensity , short duration pulses of negative ions or large time averaged negative ion densities. The measurements presented all show a consistent behaviour with modulation of the discharge current and probe and modelling results support the proposed mechanisms assumed responsible for enhancing the negative ion density.

References.

[1] Hopkins, M.B.
"4th European Workshop on the Production and Application of Light Negative ions" 26-28 March, Belfast, 1991.

[2] Hemsworth, R.S.
"6th International Symposium on the Production and Neutralisation of Negative Ions and Beams.", Brookhaven, 1991.

[3] Eenhuistra, P.J, et al.
Journal of applied Physics, 67 (1), p85, 1990.

[4] Hopkins, M.B. and Mellon, K.N.
Physical Review Letters, 67 (4), p449, 1991.

[5] Heeren, R.M.A, et al.
Europhysics Letters, 17 (6), p503, 1992.

Chapter 8. Conclusions

8.1. Summary of Work.

The concept of a temporally filtered volume negative ion source for low pressure, high power operation has been investigated in this work. The negative ion density has been shown to increase dramatically in the post discharge of a low pressure, ≈1mTorr, plasma. Extraction measurements, photodetachment measurements and Langmuir probe analysis on the D.C.U. source along with extraction measurements at FOM in Amsterdam have been used to determine the effect of modulating the discharge current. In both sources the post discharge peak increase has been shown to be a strong function of the source pressure, at low pressures there are large peak/dc ratios, this ratio decreases as the source pressure is increased and at a sufficiently high pressure no post discharge enhancement is observed. In the D.C.U source this occurred at pressures above 5mTorr, however in the FOM source post discharge increases were observed at pressures up to 15mTorr, this is explained by the higher power densities of the FOM source. This post discharge increase is explained by the rapid decay of the fast electron density after switch off coupled with improved negative ion production through dissociative attachment as the electron temperature cools. At higher pressures there are few fast electrons and the electron temperature is cooler and no enhancement is observed after switch off. Probe measurements support this view showing the optimum conditions for negative ion production in the D.C.U. source to occur at 5mTorr and in the FOM source at pressures upto 15mTorr. The post discharge peak rise time is also dependent upon the source pressure, with the peak broadening at lower pressures. Photodetachment and probe measurements at D.C.U. have shown that the temporal behaviour is dependent upon position in the chamber, in regions where the cusp fields extend into the source and tandem style magnetic filtering occurs the peak/dc ratio is shown to decrease as the fast electrons are removed and the electron temperature drops. In regions close to the filaments the electron temperature is hot and there are large numbers of fast electrons, here large enhancements are seen, it is believed that these regions act as production regions for the vibrationally excited states. High frequency modulation of the source at D.C.U. has

shown enhancements of up to four times the continuous value, the extraction results have shown the extracted current density to increase with modulation frequencies up to 15kHz and the beam is unmodulated. However photodetachment measurements show the density in the source to be highly modulated and this is in line with the extraction results form FOM which shows time averaged increases in the extracted current but the beam is modulated. A model based on the time dependent species densities has been developed and correlates well with the measured densities in the source. This model predicts that the modulation of the density is due to the depletion of the negative ions by fast electrons as the losses due to CD evolve much faster than the production of negative ions when the discharge is switched on. The results accumulated support the two stage mechanism of E-V and DA as the dominant production mechanism in volume ion sources.

8.2. Suggestions for further work

The next stage of the development of this work is the investigation of the possibility of using radio frequency driven discharges instead of filament driven discharges. Filaments have a limited operational lifetime and for high power operation, as required for future negative ion sources, a source with reliable and sustainable long life is required. RF is the obvious choice for such a source, however RF driven discharges have a higher electron temperature and therefore a high optimum operating pressure. The temporal filtering of such a source is of much interest as large enhancements may be expected at the low operating pressures required. Also modulation of RF is easier than that of dc discharges.

The problem of the extracted beam modulation, as observed at FOM, must be addressed, it has been proposed here that the magnetic field in the accelerator of the D.C.U. source effectively removes this modulation. However more indepth work needs to be done in this area before the temporal filter can be considered as a replacement for the tandem source.

The spatial dependence of the extracted beam must be investigated to determine the optimum position of the accelerator in relation to the filaments, this spatial dependence may be lessened by the use of a symmetrical antenna in RF driven discharges.

Appendix 1: Listing of the program used to model the negative ion density in the D.C.U. volume ion source.

```
#include  < stdio.h >
#include  < stdlib.h >
#include  < math.h >

void grinit();
void rate();
void calc();
void plot();

FILE *fb;
FILE *fh;

double Cp1,Cp2,Ce1,Ce2,h;
double i;
double ng,pressure;
double Id;
double rr[20][20];

int g,ST;
long int on,dur,cycles,j,I,Time;
int repeat;
double test;
char datafile[15];
char datafile1[15];
char ch;

                    /***MAIN PROGRAM***/

main()
{
 char stg[40],stg1[40],stg2[40],stg3[40],stg4[40],stg5[40],stg6[40],
          stg7[40],stg8[40],stg9[40],stg10[40];

  printf("INPUT FILENAME\n");
  scanf("%s",&datafile1);
     strcat(datafile1,".dat");
     fh=fopen(datafile1,"r");

  j=0;
        while(fscanf(fh," %s %s %s %s %s %s %s %s %s %s %s\n",stg,stg1,
              stg2,stg3,stg4,stg5,stg6,stg7,stg8,stg9,stg10) !=EOF)
         {
         rr[j][1]=atof(stg);rr[j][2]=atof(stg1);
         rr[j][3]=atof(stg2);rr[j][4]=atof(stg3);
        rr[j][5]=atof(stg4);rr[j][6]=atof(stg5);
        rr[j][7]=atof(stg6);rr[j][8]=atof(stg7);
        rr[j][9]=atof(stg8);rr[j][10]=atof(stg9);
        rr[j][11]=atof(stg10);

         printf("%5.2e %5.2e %5.2e %5.2e %5.2e %5.2e %5.2e %5.2e %5.2e
         %5.2e %5.2e\n",rr[j][1],rr[j][2],rr[j][3],rr[j][4],rr[j][5],
         rr[j][6],rr[j][7],rr[j][8],rr[j][9],rr[j][10],rr[j][11]);
```

```
            j=j+1;
        }

    calc();
  printf("FINISHED");
}



                    /***CALCULATION OF DENSITIES***/
void calc()
{

int n;
double dI=1.0;
double nenew,npnew,nhnew,nvnew,nmnew;
double np,ne,nh,ni,nm,nv,nr,nl,lr;
double k11,k12,k13,k14,k21,k22,k23,k24,
       k31,k32,k33,k34,k41,k42,k43,k44,
       k51,k52,k53,k54;

      printf("OUTPUT FILE NAME");
      scanf("%s",&datafile);
      strcat(datafile,".dat");
      fb=fopen(datafile,"w");

printf("INPUT DISCHARGE CURRENT AND PRESSURE\n");
scanf("%lf%lf",&Id,&pressure);

      ng=pressure*3.5e13;
      cycles=5;
      on=50;
      dur=100;
      g=1;

      np=0;
      ne=0;
      nh=0;
      nv=0;
      nm=0;
      I=0;


function(np,ne,nh,nv,nm,&nr,&nl,&k11,&k21,&k31,&k41,&k51);


      for(j=1;j<=cycles;j++)
    {

          for(i=1;i<dur*100;i++)
           {
```

```
nmnew = nm + ( (0.1667)*(k51 + 2*(k52 + k53) + k54) );


}


        if(i > on*100)
        {

         dI = (double)I;

     /*CALCULATE Kii VALUES*/
 function(np,ne,nh,nv,nm,&nr,&nl,&k11,&k21,&k31,&k41,&k51);

    /*CALCULATE Ki2 VALUES*/
 function( (np + (0.5*k11)), (ne + (0.5*k21)), (nh + (0.5*k31)), (nv + (0.5*k41)),
(nm + (0.5*k51)),&nr,&nl,&k12,&k22,&k32,&k42,&k52);

    /*CALCULATE Ki3 VALUES*/
 function( (np + (0.5*k12)), (ne + (0.5*k22)), (nh + (0.5*k32)), (nv + (0.5*k42)),
(nm + (0.5*k52)),&nr,&nl,&k13,&k23,&k33,&k43,&k53);
```

```
if(i < =on*100)
 {
  dI = (double)I;

/*CALCULATE Kii VALUES*/
function( np,ne,nh,nv,nm,&nr,&nl,&k11,&k21,&k31,&k41,&k51);

/*CALCULATE Ki2 VALUES*/
function( (np + (0.5*k11)), (ne + (0.5*k21)), (nh + (0.5*k31)), (nv + (0.5*k41)),
(nm + (0.5*k51)),&nr,&nl,&k12,&k22,&k32,&k42,&k52);

/*CALCULATE Ki3 VALUES*/
function( (np + (0.5*k12)), (ne + (0.5*k22)), (nh + (0.5*k32)), (nv + (0.5*k42)),
(nm + (0.5*k52)),&nr,&nl,&k13,&k23,&k33,&k43,&k53);

/*CALCULATE Ki4 VALUES*/
function(np + (0.5*k13),ne + (0.5*k23), (nh + (0.5*k33)), (nv + (0.5*k43)),
(nm + (0.5*k53)),&nr,&nl,&k14,&k24,&k34,&k44,&k54);


npnew = np + ( (0.1667)*(k11 + 2*(k12 + k13) + k14) );

nenew = ne + ( (0.1667)*(k21 + 2*(k22 + k23) + k24) );

nhnew = nh + ( (0.1667)*(k31 + 2*(k32 + k33) + k34) );

nvnew = nv + ( (0.1667)*(k41 + 2*(k42 + k43) + k44) );
```

```
        /*CALCULATE Ki4 VALUES*/
     function(np + (0.5*k13),ne + (0.5*k23), (nh + (0.5*k33)), (nv + (0.5*k43)),
    (nm + (0.5*k53)),&nr,&nl,&k14,&k24,&k34,&k44,&k54);


              npnew = np + ( (0.1667)*(k11 + 2*(k12 + k13) + k14) );

              nenew = ne + ( (0.1667)*(k21 + 2*(k22 + k23) + k24) );

              nhnew = nh + ( (0.1667)*(k31 + 2*(k32 + k33) + k34) );

              nvnew = nv + ( (0.1667)*(k41 + 2*(k42 + k43) + k44) );

              nmnew = nm + ( (0.1667)*(k51 + 2*(k52 + k53) + k54) );
}
                                  lr = nl + nr;

              if(fmod(dI,1000.0) = = 0.0)
                {

                Time = (int) (dI/100.0);

                printf("%ld %e %e %e %e %e %e %e %e\n",Time,np,ne,nh,
                        nv,nm,lr,nr,nl);

                fprintf(fb,"%ld %e \n",Time,nm);
                }

        np = npnew;
        ne = nenew;
        nh = nhnew;
        nv = nvnew;
        nm = nmnew;

if(np < 1)
{
np = 1;
}

if(ne < 1)
{ne = 1;
}
if(nh < 1)
{nh = 1;
}
if(nv < 1)
{nv = 1;
}
if(nm < 1)
{
nm = 0;
```

```
}
I=I+1;

        }
      }

      fclose(fb);
}

function(double np,double ne,double nh,double nv,double nm,double *nr, double
*nl,double *x1d,double *x2d,double *x3d,double *x4d,double *x5d)
  {
    int pd1,step;
    double ni3,nh3,Ch1,Ch3,th,Cv1,Cv2,Cm1,Cm2;
    double RCDA,RCEV,RCAD,RCVT,RCED,RCMR,RCG,RCION,RCIN,RCDIS,RCIP;
    double prod;
    double x, C0,C1,C2,C3;
    if(i < (on)*100)
    {
    ST=0;
    RCDA=rr[ST][1];RCED=rr[ST][2]; RCEV=rr[ST][3]; RCVT=rr[ST][4];
    RCMR=rr[ST][5];

    RCAD=rr[ST][6]; RCIP=rr[ST][7]; RCG=rr[ST][8]; RCIN=rr[ST][9];
    RCION=rr[ST][10]; RCDIS=rr[ST][11];

    h=1e-8;
    Cp1=Id/(2e-16); /*  Id/eV */
    Cp2=ng*RCIN/1.2;
    Ce1=ng*RCION;
    Ce2=8.45e4;
    ni3=ne/0.5;
    nh3=ni3;
    Ch1=nh3*3e-5;
    Ch3=  3e4;
    Cv1=RCEV*ng;
    Cv2=1.3e4;
    Cm1=.8e-8*nv*ne;/*RCDA*/
    Cm2=(7e4)+(nh*3e-9)+(ne*5e-9)+  (np*6e-6);

   }

   if(i>=(on)*100)
    {
    pd1=(int)(i);
    floor(pd1);
    step=((pd1/100)-on)+1;

    if(fmod(pd1,2000.0)==0)
     {
     ST=((step/10)/2)+1;
     }
```

```
    RCED=rr[ST][2]; RCEV=rr[ST][3]; RCVT=rr[ST][4]; RCMR=rr[ST][5];
    RCAD=rr[ST][6]; RCIP=rr[ST][7]; RCG=rr[ST][8]; RCIN=rr[ST][9];
    RCION=rr[ST][10]; RCDIS=rr[ST][11];

C0=1.02;
C1=5.114e-2;
C2=3.9e-4;


x=step;
C3=C0 + (C1*x) + (C2*x*x);
RCDA=C3*1e-8;
     h=1e-8;
     Cp1=0;
     Cp2=ng*RCIN*0.8;
     Ce1=ng*RCION;
     Ce2=3e4;
     ni3=ne/0.5;
     nh3=ni3*3e-8;
     Ch1=nh3;
     Ch3= 1e4;
     Cv1=ng*RCEV;
     Cv2=2.7e4;
     Cm1=2.7e-8*nv*ne;/*RCDA*/
     Cm2=(7e4)+(nh*3e-9)+(ne*2e-9);

     }
test=*x2d;


    *x1d=h*(Cp1-(np*Cp2) );
    *x2d=h*( (np*Ce1)-(ne*Ce2) );
    *x3d=h*( (np*Ch1)-(nh*Ch3) );
    *x4d=h*( (np*Cv1) -(nv*Cv2 ));
    *x5d=h*( (Cm1) -(Cm2*nm) );
         *nr=h*( (Cm2*nm) );
         *nl=h*( Cm1);

}


void rate()
{
int j,i,x;
char ch;
char stg[40],stg1[40],stg2[40],stg3[40],stg4[40],stg5[40];
char stg6[40],stg7[40],stg8[40],stg9[40],stg10[40];
char rfile[40];
FILE*fh;
scanf("%d",&x);
printf("INPUT REACTION RATE FILE NAME");
```

```
printf("HELLO");
strcat(rfile,".dat");
fh=fopen(rfile,"r");
j=0;

while(fscanf(fh,"%lf %lf %lf %lf %lf %lf %lf %lf %lf %lf %lf\n",
   rr[j][1],rr[j][2],rr[j][3],rr[j][4],rr[j][5],rr[j][6],rr[j][7],
   rr[j][8],rr[j][9],rr[j][10],rr[j][11])!=EOF);

    {

    j=j+1;

     for(i=1;i<=j;i++)
      {
      printf("%d%15d\n",i,j);

      printf("%lf %lf %lf %lf %lf %lf %lf %lf %lf %lf %lf\n",
      rr[j][1],rr[j][2],rr[j][3],rr[j][4],rr[j][5],rr[j][6],
      rr[j][7],rr[j][8],rr[j][9],rr[j][10],rr[j][11]);

      }
  }
```